Corrosion and Fretting Corrosion Studies of medical grade CoCrMo implant material in a more clinically relevant simulated body environment.

By

OCRAN Emmanuel Kofi

A Thesis submitted to the Faculty of Graduate Studies of the

University of Manitoba

In partial fulfillment of the requirements of the degree of

Master of Science

Department of Mechanical and Manufacturing engineering

University of Manitoba,

Winnipeg, Manitoba

Abstract

In modular hip implants, micro-motion, which leads to fretting corrosion at the head/neck and neck/stem interfaces, has been identified as a major cause of early revision in hip implants, particularly those with heads larger than 32mm. It has been found that the type of fluid used to simulate the fretting corrosion of biomedical materials is crucial for the reliability of laboratory tests. Therefore, to properly understand and effectively design against fretting corrosion damage in modular hips, there is the need to replicate the human body environment as closely as possible during in-vitro testing and validation. In this work, corrosion behavior of CoCrMo in 0.14 M NaCl, phosphate buffered saline (PBS) and clinically relevant simulated body fluid (*sbf*) is carried out. Also, fretting corrosion studies of the CoCrMo alloy in a clinically relevant novel simulated body fluid *(sbf)* environment is studied. The presence of phosphate ions in PBS accounted for the higher corrosion rate when compared with 0.14 M NaCl and *sbf* environment. Despite the low and comparable corrosion rates in 0.14 M NaCl and *sbf*, the nature of the protective passive film formed in *sbf* shows the suitability of the novel *sbf* for future corrosion and fretting corrosion analysis. Finally, the influence of micro-motion at the modular head/neck and neck/stem interfaces on the concentration of metallic ions that goes into the synovial fluid and surrounding tissues is reported.

Acknowledgments

The respect and appreciation I have for Drs. Olanrewaju Ojo and Urs Wyss remains unparalleled. These great supervisors not only have provided mentorship, support, and guidance, but also funded this project and my stipend through their research grant. To both of you, I say thank you for affording me the opportunity to work on this innovative research study under your supervision. Indeed, your advice was timely and informing. I am grateful.

To the Orthopedic Innovation Center (OIC) in Winnipeg, Manitoba, I would like to thank Dr. Jan-M Brandt, for support and advice in carrying out the wear simulation tests. I would like to acknowledge the assistance of Leah Guenther, Trevor Gascoyne, Richard Dyrkacz, Sean O'Brien, Alexander Vecherya and Matthew Gale for the laboratory assistance and technical conversations.

To Dr. Michael Freund and Michael McDonald, the discussions I had with your research team at the initial stages of this research provided the much needed background information required to see this project through. I say thank you for your assistance.

The effective use of the research facilities at the materials characterization laboratory of the University of Manitoba may not have been possible without the assistance of Dr. Abdul Khan, Mike Boswick, and Trevor Smith. I say thank you. To my friends, Nana K. Baafour, Johnson Aina, Ziyuan Wang, Jianqi Zhang, etc., thank you all for your support.

Last, I honor the source of life and wisdom, the Almighty God, without whom this work would have been impossible. I truly consider myself blessed to have had the opportunity to undertake this research.

Dedication

This MSc. thesis work is dedicated to:

my mum: *Elizabeth Adjoa Ocran,*

my siblings: *Ebenezer Yaw Ocran, Paul Kwesi Ocran and Faith Afua Ocran,* and

the loving memory of my dad, *Mathew Kojo Ocran (1954-2006).*

Table of Contents

List of Tables

List of Figures

List of Copyrighted Material

No copyrighted material was used throughout this thesis.

Author's Declaration

I, *Emmanuel Kofi Ocran*, hereby declare that the entire result presented in this thesis is the sole product of my work, under the supervision and approval from my supervisors and examiners.

I am aware that my thesis may be made electronically available to the public.

List of Symbols and Abbreviations

CoCrMo	Cobalt-chromium-molybdenum alloy
MoM	Metal-on-metal
CoC	Ceramic-on-ceramics
MoP	Metal-on-polyethylene
CoM	Ceramic-on-metal
CoP	Ceramic-on-polyethylene
sbf	Simulated body fluid
THA	Total hip arthroplasty
TKA	Total knee arthroplasty
XPS	X-ray photoelectron spectroscopy
AES	Augur electron spectroscopy
PBS	Phosphate buffered saline
BCS	Bovine calf serum
EDX	Energy-dispersive X-ray spectroscopy
SEM	Scanning electron microscope
BSE	Back scattered electron
NaCl	Sodium chloride
nm	Nanometers
AsDL	Activities of daily living
TJR	Total joint replacement
UHMWPE	Ultra-high molecular weight polyethylene
CPH	Closed-pack hexagonal
FCC	Faced center cubic
wt%	Percentage weight
g/L	Grams per liter
$\boldsymbol{i_{app}}$	Applied current
$\boldsymbol{\beta_a}$	Tafel slope for anodic reaction
$\boldsymbol{\beta_c}$	Tafel slope for cathodic reaction
$\boldsymbol{\Delta E}$	Electrode potential

ICP-MS	Inductively coupled plasma mass spectroscopy
η	Absolute viscosity, Pas
$\boldsymbol{\omega}$	Rotational speed, rps
$\boldsymbol{p}$	Pressure
$\boldsymbol{h_{min}}$	Minimum film thickness
$\boldsymbol{S_{q1}^2}$	Surface roughness for pin
$\boldsymbol{S_{q2}^2}$	Surface roughness for disc
$\boldsymbol{\lambda}$	Film parameter
$\boldsymbol{H}$	Hersey number
OCP	Open circuit potential
PoD	Pin-on-disc
$\boldsymbol{E_{corr}}$	Corrosion potential
$\boldsymbol{i_{corr}}$	Corrosion current density
$\mathbf{i_{pass}}$	Primary passive current density
$\mathbf{i_{crit}}$	Critical anodic current density
$\boldsymbol{E_{pp}}$	Primary passive potential
TEM	Transmission electron microscope
Ra	Average surface roughness
Mc	Million cycles
R	linear correlation coefficient
$\boldsymbol{\mu g/l}$	Milligrams per liter
ppb	Parts per billion
EIS	Electrochemical impedance spectroscopy
BSA	Bovine serum albumin
DMEM	Dulbecco's modified Eagle's medium
BEI	Backscattered electron imaging
SEI	Secondary electron imaging
ESCA	Electron spectroscopy for chemical analysis
BEC	Backscattered electron composition

1 INTRODUCTION

1.1 Background Information

Cobalt-chromium-molybdenum (CoCrMo) alloys have been successfully used in orthopedic implants, such as those for hip and knee joint replacements. Their use is due to their good abrasion resistance and high corrosion resistance in the synovial fluid environment of human joints [1], [2]. Synovial fluids are the natural joint lubricants of the human body that help the joint parts effortlessly move together. The presence of synovial fluids in human joints enhances the formation of a thin protective film (1-4 nm) on the surface of the CoCrMo alloy [3]–[5], which mostly contains oxides of chromium [6]–[8]. These protective oxides make implants even more biocompatible with the human body environment. Generally, the development of passive films on active-passive metals (which CoCrMo is an example) is not a simple process. Factors such as the type of alloy, synovial fluid composition, implant-fluid interface potential and implant exposure time have been proven to influence the nature and kinetics of the passive film formed on active-passive metals [3].

Yan et al. [9] reported enhanced lubrication effects due to the formation of complex organometallic/oxides by interactions between amino acids (used to model proteins in synovial fluids) and the implant surface. Also, Valero Vidal and Igual Muñoz [2] showed that AISI 316L and CoCrMo alloys may exhibit different passive behaviors when exposed to the same type of solution. Their work also showed that while albumin reduces the corrosion resistance of AISI 316L, it increases the corrosion resistance of the CoCrMo alloy, despite the fact that it is adsorbed on the surface of both alloys. Therefore,

in truly understanding the behavior of an implant material in its service environment, the need for laboratory testing in a clinically relevant fluid environment is crucial.

The use of modular hip ahead of monoblock hip is due to surgeon's intraoperative choice of neck version, neck length, stem size etc. Also, in modular hips, the surgeon can adjust the femoral offset and correct the patients leg length to achieve a better hip stability [10]. However, despite the advantages of modular components, fretting corrosion, a synergetic effect of wear and corrosion, has been identified as a major cause of early revision. This is because the effects of micro-motion at the head/neck and neck/stem interfaces of modular prostheses can lead to the breakdown and depassivation of the protective passive film, and hence, the release of metallic ions and particles from the substrate alloy into the surrounding tissues, causing adverse tissue reaction. The rate of intermittent passivation and depassivation due to mechanical interaction influences the contribution of corrosion and corrosion related damage to the fretting corrosion synergy.

Furthermore, the nature of the protective passive film formed onto the CoCrMo alloy in a synovial fluid environment contributes to its effectiveness, and hence, can influence the rate of film passivation and depassivation. Therefore, in the design and testing of orthopedic biomaterials, only clinically relevant synthetic fluids, which are a close substitute for the real biological environment, can produce a passive film that will be a replica of what is to be expected in the human body. Also, since tissue inflammation, aseptic loosening, osteoarthritis etc., have been linked to the release of ionic species from metallic implants, only a clinical replica of the passive film formed in the human body environment can truly predict the relative concentration of ions that will be released into

the human body. Hence, there is the need for in-vitro testing of future implants in a clinically relevant environment with a novel simulated body fluid (*sbf*).

Furthermore, the type of synthetic fluid used during laboratory electrochemical and fretting corrosion testing influences the electrochemical and fretting corrosion behaviors [11]. Therefore, the proximity of these synthetic fluids to the actual synovial fluid in the joints is of paramount importance. To properly understand existing implants and effectively design future implants, there is a need to replicate the human body environment as closely as possible during in-vitro testing. Various synthesized fluids are being used in the experimental testing of orthopedic biomaterials. However, most of these synthesized fluids are less stable and more prone to protein degradation. This may be due to at temperatures up to and above 69^0C, microbial contamination, and mechanical shear during testing [12], [13]. These degraded proteins can affect how the moving parts of an artificial joint interact, thereby affecting the accuracy of in-vitro predictions [12], [14], [15].

1.2 Problem Definition

Recently, a novel and more clinically relevant *sbf* has been developed [15]. This fluid has the relevant composition of constituent elements and additives that enhances the stability of the proteins present. The corrosion properties and the fretting corrosion behavior of the CoCrMo alloy in this novel fluid had not been studied prior to this research. This work carried out a detailed study on the corrosion and fretting corrosion behavior of the CoCrMo alloy in the novel fluid environment, as compared to pre-existing fluids (0.14 M NaCl and PBS) already being used for corrosion and fretting corrosion testing.

This work will aid future research on tribocorrosion. One major criterion for selecting the solution for the laboratory simulation of tribocorrosion experiments is a low corrosion rate that is comparable with the human body environment. However, the 'corrosion rate' as the only criterion can be misleading. Despite the fact that low corrosion rates have been reported in the literature for some of the existing simulated fluid (e.g. 0.14 M sodium chloride (NaCl)), the nature of a passive film that replicates clinical expectations is still yet to be fully reported in the literature. In this work, by using a clinically relevant novel *sbf*, a more relevant and clinically acceptable passive film that will have direct influence on fretting corrosion behavior at the modular head/neck and neck/stem interfaces will be studied. In reality, during fretting in metal-on-metal (MoM) implants, only the passive film formed is in direct contact, not the CoCrMo alloy substrate material itself. Therefore, the identified passive film will be invaluable for future analyses of the corrosion properties and fretting corrosion behavior (modeling and experimental) of the CoCrMo alloy in a more clinically relevant *sbf*.

1.3 Research Objectives

This thesis work aims to achieve the following objectives:

- to characterize the corrosion properties of the CoCrMo alloy in 0.14 M NaCl, PBS and a more clinically relevant novel simulated human body fluid, and

- to study the fretting corrosion behavior at the head/neck and neck/stem interface of modular CoCrMo alloy in a more clinically relevant novel simulated human body fluid.

1.4 Major Findings

In spite of the success enjoyed by modular hip implants, fretting corrosion at the modular head/neck and neck/stem interfaces still remains a source of concern to researchers and biomedical engineers. This is because the wear particles and metal ion release from micro-motion at these interfaces have been a major cause of adverse tissue reactions. However, by using a clinically relevant novel fluid, this study has made some progress towards the understanding of fundamental corrosion properties and fretting corrosion behavior of the CoCrMo alloy in the human body environment.

First, although the CoCrMo alloy in *sbf* and in 0.14 M NaCl shows low corrosion rates comparable to that in the human body environment, the nature of the surface film formed is different. The film composition and film formation kinetics in both solutions are different. Therefore, by using a more clinically relevant fluid, this work has experimentally characterized the most predictable passive layer comparable to the human body environment. The results from this work confirm that protein compounds and organometallic complexes in clinically relevant synovial fluids adsorb onto the surface of the material.

Second, this work shows that there is an increase in the ion release concentration in the presence of micro-motion. This finding makes it very important to focus the design of future implants against causes of micro-motion..

Third, hydrodynamic or elastohydrodynamic separation reduces wear particle generation. Under optimized conditions in a clinically relevant fluid, a lubrication regime that totally

(or partially) cause direct separation between contacting surfaces can be achieved in patients. This condition can reduce wear particle generation though mechanical damage

1.5 Thesis layout

This dissertation contains seven chapters. The organization is as follows,

- Chapter 1 provides detailed background information on the use of Cobalt-chromium-molybdenum (CoCrMo) in orthopedic applications; success and limitations of modular hip prosthesis; objectives of and major findings from the study,
- Chapter 2 provides a detailed review of the literature under the following sub-headings; human bones, joint anatomy, cobalt based alloys in orthopaedic applications, the implant service environment, corrosion, tribology and tribocorrosion of CoCrMo in the human body environment,
- Chapter 3 provides the experimental plan, materials used, preparation procedure, testing equipments and methods used to carry out the research work,
- Chapter 4 provides the results obtained from the study,
- Chapter 5 provides a detailed discussion of the results and how these results contributes to the state of knowledge,
- Chapter 6 summarizes major findings, conclusions of current work and suggestions for future work,
- Chapter 7 lists all the literature referenced in writing this dissertation.

2 LITERATURE REVIEW

2.1 Human bones and joint anatomy

The human body is connected together by a network of coupled parts called the skeleton. The skeleton is made up of bones, cartilages and connective tissues that function to provide shape and support in humans. For example, the skull protects the brain, ribcage protects the heart and lungs, and pelvic girdle protects the digestive tract and reproductive organs. The human skeleton also facilitates movement of the body parts because the muscles are attached to the bones to give them leverage. Generally, bones are not a uniform solid material. Rather, they have spaces between the hard elements. There are two types of bone tissues, which are compact (cortical) and trabecular (cancelous).

The hard outer layer of bones is made of cortical bone tissues due to their minimal gaps and spaces, and they are 5-30% porous. These give bones their smooth white and solid appearance and account for up to 80% of the total bone mass. The interior of the bone, on the other hand, is filled with trabecular bone tissue. Trabecular bone tissues are lighter and usually allow room for blood vessels and marrow. They account for the remaining 20% of the total bone mass, but have nearly two times the surface area of cortical bone tissues with porosity from 30-90%. Cartilages are the flexible connective tissues usually found in joints between bones, the rib cage, ears, nose, bronchial tubes and intervertebral discs. They are softer and less rigid than bones. Their main function is to reduce friction in the bone joints. They can also serve as attachment of two or more bones in a joint, for example, the ribs.

2.1.1 Joint replacement

Joint replacement, also known as replacement arthroplasty, is a surgical procedure in orthopedic surgery in which a dysfunctional joint surface is replaced with an artificial prosthesis. This surgical technique has enjoyed a good success rate over the last 50 years and has been considered a good treatment for joints where severe pain has been experienced as well as where joint functionality has been a concern [16]. A typical hip replacement implant is shown in Figure 2.1. The hip is essentially a ball and socket joint with up to three degrees of freedom and three pair of principal directions. They are, flexion and extension around a transverse axis (left-right); lateral rotation and medial rotation around a longitudinal axis (along the thigh); and abduction and adduction around a sagittal axis (forward-backward). This multiaxial motion is constrained by the bony and ligamentous structures of the joint. These functional constraints have generally defined the goals for the design of hip implants over the past half-century.

The artificial hip is divided into three components: the femoral stem and head, which may be integrated or modular, and the acetabular cup. The combination of the femoral head and the acetabular cup provide the bearing surface for the joint. The femoral stem transfers the load to the femur and provides resistance to the bending moment caused by the anatomy of the joint. Due to increasing incidents of osteoarthrosis and similar disabling conditions, total artificial replacement of human joints has become a widely used treatment [17]. Total hip replacement (THR) and total knee replacement (TKR) are two of the most popular total joint replacements (TJRs) in patients. TJRs were normally only performed on patients who were over 60 years old.

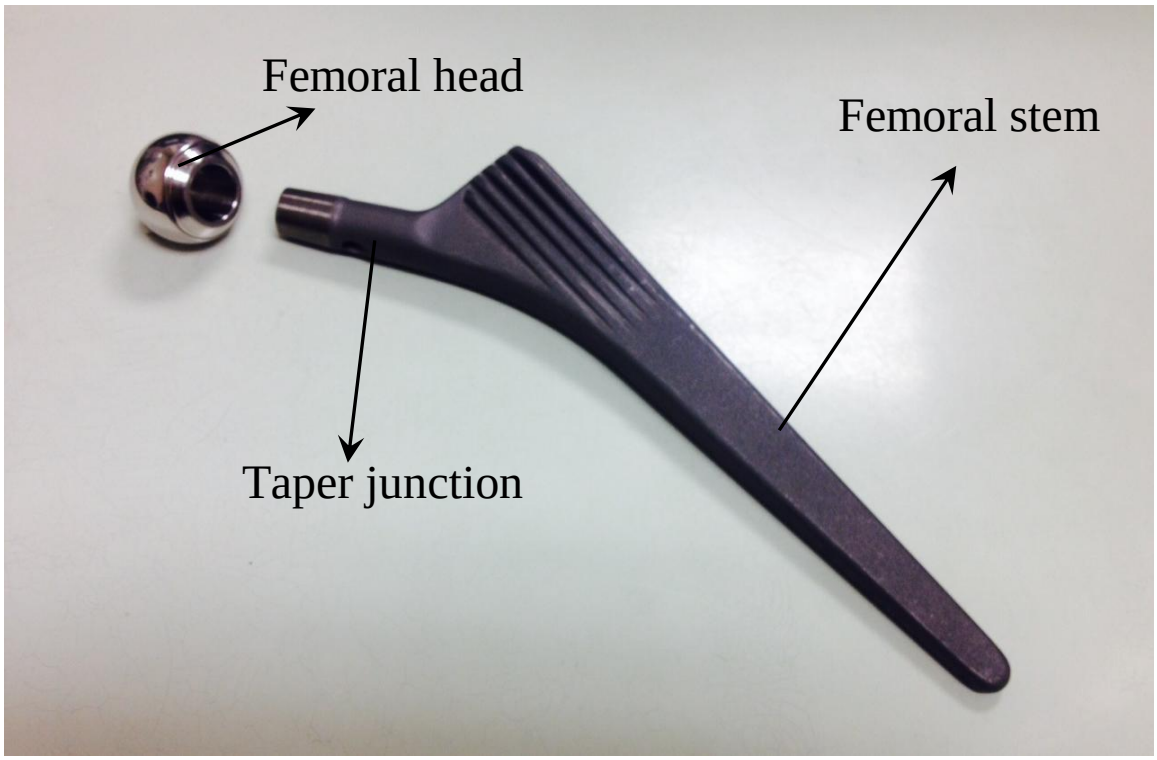

Figure 2.1: Modular hip implant

However, nowadays, more and more young and active patients require TJR surgery. Kurtz *et al*. [18] recently projected more than 50% increase in total hip and knee replacements in patients in less than a decade from now. Therefore, the improvement and development of safer, longer lasting and better functioning implants are anticipated for such applications [17]. Generally, the activities of daily living (AsDL) expose human joints to different contact forces and stress conditions. For example, walking and jogging may expose the hips to cyclically repeated loading conditions by gravity and muscular action [17], [19]. Therefore, mechanical properties, such as strength, elasticity, toughness and ductility, are relevant factors to consider in the design of artificial hips and knees. Table 2.1 shows the mechanical properties of a typical bone.

It has been reported that the peak load on the hips during a walking cycle is up to 4 times the body weight [17]. Other researchers believe that the weight on the hips may be higher (up to 8 times the body weight) when AsDL, such as jogging, walking up the stairs, etc. are being carried out [17]. Most researchers believe that the material degradation process (primarily wear) aggravates artificial prostheses when increased loads are applied onto them. Therefore, the correct material combinations, surface finish, diameter of the femoral head and clearance are important aspects in minimizing the effects of friction, wear, as well as corrosion. Low friction and wear rate, and good biocompatibility are desirable characteristics for a lasting prosthetic material. The evolution of hip arthroplasty has over the years seen many material combinations in strive for improvements. Table 2.2 shows different femoral head and acetabular cup material combinations and their resulting pros and cons.

Table 2.1: Mechanical properties of a typical bone.

Bone	Tensile modulus (GPa)	Yield strength (MPa)	UTS (MPa)	% elongation	Young's Modulus (GPa)
Cortical	18	80	100-300	1-2	10-20
Cancelous	0.2-0.5	5-30	10-20	5-7	

Table 2.2: Pros and cons of femoral head and acetabular cup material combinations

	Pro	Con	Remark
MoP	• Most commonly used, longest experience and follow up • Most economical device	• High wear volume • High susceptibility to aseptic loosening • Suitable only for older patients	• Wear rate ≈0.1 mm/year • Wear rate ≈0.01-0.02 mm/year (crosslinked UHMWPE)
MoM	• Low volumetric wear rate • Improved joint stability due to larger femoral head • Low rate of aseptic loosening	• Risk of metallosis, metal allergy and hypersensitivity • Unknown long-term effects of exposure to metal ions	• Wear rate ≈0.005 mm/year • Renewed interest in its use up until about 2008. • Decreasing use due to metal ion/particles release leading to adverse tissue reactions
CoP	• Wear rate reduced compared to MoP • Elasticity of UHMWPE mitigates fracture risk of ceramic femoral head	• Residual polyethylene wear with late risk of aseptic loosening	• Wear rate ≈0.03-0.1 mm/year
CoM	• Improved joint stability and range of motion due to larger femoral head size • Low volumetric wear rates	• Catastrophic fragile fracture of ceramic component	• Reduced in-vitro wear rates • CoCrMo acetabular cup components provide stability for larger ceramic femoral heads
CoC	• High wear resistance and lowest wear rate • Weak tissue interaction with ceramic wear debris • Low risk of aseptic loosening • High scratch resistance • Very low surface roughness • Good lubrication conditions • High wettability	• Catastrophic fragile fracture of ceramic components • Tiny fracture debris may cause third body wear after revision • Squeeking effect may occur • Most expensive device	• Wear rate ≈<0.003 mm/year

Clearly, MoM and ceramic-on-ceramic combinations have the lowest wear rate while combinations with polyethylene have the highest wear rate [20]. Although ceramics are proven to be a good material, its brittleness under impact loading conditions may be a limitation for its continual use. Therefore, proper material selection is an integral part of the design of prosthetic implants.

2.1.2 Historical evolution of hip replacement

Historically, total hip arthroplasty (THA) has enjoyed a long standing success rate [21]. According to the 10th International Medical Conference, the earliest recorded attempts at hip replacement occurred in Germany in 1891 [1], and ivory was used to replace the femoral heads of patients whose hip joints had been destroyed by tuberculosis. This continued to the 19th and early 20th century. Sometime in 1925, the use of glass was introduced by an American surgeon called Marius Smith-Petersen. Although glass is compatible, the hollow hemispherical prosthesis which is fitted over the femoral head failed to withstand the forces and stresses associated with the hips, and as such, it shattered.

The first to use an MoM prosthesis on a regular basis was English surgeon George McKee [1]. In 1953, a cemented hemi-arthroplasty was first experimentally used for the treatment of femoral neck fractures with a one-piece cobalt-chrome socket as the new acetabulum. This prosthesis had a good survival rate, with one study that recently showed a 28 year survival rate of 74%. However, due to the local effects of metal particles seen during revision surgery, this prosthesis became less popular by the mid-1970s. Sir John Charnley, an English surgeon who worked at the Manchester Royal Infirmary, is

considered the father of the modern THA. In 1962, he replaced an arthritic hip socket with a plastic cup and the femoral head with a metal prosthesis. This THR procedure was the first of its kind. The implant survival rate of around 85% in his patients for 20-25 years was astounding. The method of allowing the metal femoral head component to smoothly slide onto the plastic cup surface worked out rather well, thus becoming the standard in THR surgery. This was called 'low friction arthroplasty' as Charnley advocated the use of a small femoral head which reduces wear due to its smaller surface area. Since the successful operation performed by Charnley over fifty years ago, THR surgery has greatly improved. Today, there are a multitude of different components, which allow for a variety of options based on the specific needs of patients.

2.1.3 Implantable biomaterials

Any natural or synthesized material that can interact with biological systems without having adverse effects is a biomaterial. Biomaterials cover all classes of materials for various needs (e. g. orthodontic, orthopedic and cardiovascular). The choice of biomaterials for specific applications can be complex. When selecting a material for use in medical applications, some considerations are usually taken into account.

First, the functional requirements of the implant must be met. The function of the implant includes the physiologic role that it will replace, as well as the length of time that it is designed to fulfill that role. Second, the ways that the implant will interact with the body need to be considered. The interaction can be influenced by either the effect of the biological environment on the material properties or that of the material, and degradation may occur on the local and systemic physiology of the body. In modern design

engineering, factors such as corrosion and wear resistances, biocompatibility, fatigue, fracture, etc., have shifted the research focus onto biomaterials that possess physical properties such as high modulus, yield point and ductility. In recent times, the primary materials used include stainless steels, cobalt based alloys, pure titanium and titanium based alloys, polymers, ceramics, etc. In the subsections below, these biomaterials are discussed with a focus on their applications as biomedical implant materials.

2.1.3.1 Cobalt and its alloys

Cobalt is a very strong metal with good wear resistance. Two major alloys of cobalt used in biomedical applications are CoCrMo and cobalt-nickel-chromium-molybdenum (CoNiCrMo). In the last 50 years, hip and knee prostheses, fracture fixation plates, etc. have predominantly used the CoCrMo alloy. This alloy is preferred in articulations due to its low wear rates. However, excessive cobalt ions or particles release into the human body can lead to allergies or even toxic effects. As such, cobalt has to be alloyed with 26-30% chromium, which builds the Cr_2O_3 passive layer. The second most important alloying material is molybdenum, which is used with a percentage between 5 and 7%. The maximum values of the rest of the elements are: 1% manganese (Mn), 1% silicon (Si), 0.75% iron (Fe), and a maximum of 0.35% carbon (C).

2.1.3.2 Titanium and its alloys

Titanium and its alloys have good biocompatibility and show excellent electrochemical properties especially in static conditions [22], [23]. Ti-6Al-4V has long been the primary titanium alloy used in the medical field of implants. However, for permanent implant applications, the alloy has a possible toxic effect that results from released vanadium and

aluminum. For this reason, vanadium- and aluminum-free alloys have been introduced for implant applications, based on Ti-6Al-4V implants. These new alloys include Ti-6Al-7Nb, Ti-13Nb-13Zr and Ti-12Mo-6Zr [22]. Although titanium and its alloys have mechanical properties acceptable for most biomedical applications, they have relatively poor shear strength and are less resistant to wear when compared to cobalt-based alloys. This makes them less desirable for implants that require high loads and shear stresses, e.g. hip and knee prostheses. Alloying elements such as Iron (Fe) and niobium (Nb) have been shown to slightly improve the fatigue strength of conventional titanium alloys.

2.1.3.3 Stainless steel 316L

Stainless steels were the first set of metallic alloys to be used for orthopedic applications. Type 316L stainless steel (SS) is the medical grade alloy commonly used. Chromium is added to the alloy for enhanced corrosion resistance and formation of a resistant passive film [24]. Nickel and carbides and other alloying elements also affect the strength and wear resistance of stainless steels through the alteration of their microstructures. Molybdenum is a ferrite stabilizer. To counter this tendency to form ferrites, nickel is added to stabilize the austenitic phase, which enhances the passive layer formed. However, one major limitation of the 316L SS is its susceptibility to pitting and crevice corrosion. Therefore, 316L SS is preferred for temporary biomedical applications. The 'L' in 316L stands for low percentage of carbon. This reduced percentage of carbon minimizes the formation of $Cr_{23}C_6$, which has been reported to cause intergranular corrosion at the crystal borders of the alloy [24].

2.1.3.4 Ultra-high molecular weight polyethylene

Polymeric materials are widely used as biomaterials due to their compatibility and close resemblance to natural polymeric tissue components. Ultra-high molecular weight polyethylene (UHMWPE) is a high-modulus polyethylene that is commonly used in this type of application. Due to its covalently bonded long chain atoms, they can withstand more loads and are tough in nature. UHMWPE is odorless, tasteless, nontoxic and resistant to corrosion. However, because of the biochemical and mechanical factors in the body environment, polymers suffer a large amount of degradation that results in ionic attacks, thus leading to tissue irritation and decreased mechanical properties [17]. The major limitations of polymeric materials are their aggravated deterioration under cyclic loading and increase in wear volume produced when compared to other materials. This polymeric wear debris has been reported to cause osteolysis and loosening of devices [25].

2.1.3.5 Ceramics

Alumina, zirconia, calcium phosphates, bioactive glasses, and porcelain are all inorganic materials classified as ceramics. They generally have good resistance to electrochemical degradation and can retain their properties even at elevated temperatures. They are inert in nature and have low volumetric wear rates when used as articulating surfaces. Their major limitation is low tensile strength and brittle nature under impact loading. These can lead to catastrophic failure of prosthesis in the event of sudden loading.

2.2 Cobalt-based alloys in orthopaedic applications

Cobalt-based alloys are non-magnetic alloys that exhibit high strength, good corrosion resistance, and excellent wear resistance. Due to their minimal residual porosity, good hardness and microstructural properties, the CoCrMo alloy (a major cobalt-based alloy used in orthopedic applications) has in recent years emerged as the most popular material used as second generation MoM implant material [17], [26]. Cobalt-based alloys have two possible crystal structures. At temperatures below 417^0C, they exhibit a close packed hexagonal (CPH) crystallographic structure while at temperatures above 417^0C, they can transform into a face centered cubic (FCC) structure [27].

Depending on the carbon content added into their alloying elements during the casting process, CoCrMo alloys can be either 'high carbon' (up to 0.35 wt%) or 'low carbon' (below 0.05 wt%) [27]. It has been established that high carbon content in CoCrMo alloys favors the formation of carbides which increases the wear resistance and reduces the volumetric wear loss of the articulating surfaces [28], [29]. Irrespective of their carbon content, all CoCrMo alloys have a balance of cobalt, which can be as low as 60 wt%. There is approximately 28% chromium which forms a chromium rich passive oxide film (Cr_2O_3) that spontaneously forms on the surface of the metal [30]. This gives good corrosion resistance by separating the metal from the air and aqueous environments [31]. Typically 5-7 wt% molybdenum is used to improve the mechanical properties of the alloys as it provides solid solution strengthening and good localized corrosion resistance [32]. CoCrMo alloys can either be cast or wrought depending on their production route. Cast alloys, usually used for the femoral part of knee joints, are often used for complicated shapes that cannot be machined quite easliy, though when used as

acetabular cup of THRs, they are easier to machine. However, this process has its limitations, such as the development of inhomogeneous microstructures as a result of unequal cooling rates. This can lead to wrought alloys being a favorable alternative whereby large castings are hot forged and thermo mechanically processed, and reworked into a smaller size [33].

2.3 Implant service environment

Implanted biomaterials do not function in isolation. Rather, they function in the human body environment which can be very dynamic in nature. Therefore, to design and utilize metallic biomaterials in the body, it is useful to have a clear understanding of the environment in which these alloys operate. For the purpose of discussion, the service environment has been divided into three main categories, namely, the electrochemical, biological and mechanical environments.

2.3.1 Electrochemical nature of human body environment

When metallic biomaterial devices are placed into the human body environment, they are immediately surrounded by synovial fluid which may be aggressive and cause interactions between the implant and its environment and vice versa. These interactions may lead to the electrochemical degradation of the implant material and/or ionic contamination of the body fluid, which is called corrosion. Typically, the human body environment is an oxygen rich saline solution with a salt content of about 0.9%, pH of roughly 7.4, and temperature of 37±1°C. Bodily fluids consist of water, complex compounds, dissolved oxygen, and large amounts of sodium and chloride ions. Bodily fluids also consist of other electrolytes, such as bicarbonate and small amounts of

potassium, calcium, magnesium, phosphate, sulfate, amino acids, proteins, plasma, lymph, etc., [34]. All of these constituents make the human body service environment electrochemically aggressive to metallic biomaterials. There are many causes that accelerate the electrochemical interaction between metallic biomaterials and the service environment. For example, infectious microorganisms and crevices formed between components can reduce oxygen concentration, both of which contribute to the corrosion of an implant. Electrochemical degradation is a surface degradation mechanism; therefore, the environment to which the metallic biomaterial is exposed is of paramount importance in the experimental study of implant materials.

During in-vitro testing, efforts have always been made towards the employing of lubricants that are approximate substitutes to the real biological environment. Usually, in approximating the inorganic species present in the body solution, 0.9% (0.154 M) NaCl at pH 7.4 is the most simplified approximation used in acceptable testing. More complex solutions include phosphate buffered saline (PBS), Ringer's and Hank's solutions, *sbf*, and several others [34]. In incorporating organic species, compounds such as amino acids, single protein solutions (e.g., albumin), cell culture media, and media with serum can be added to the lubricant. All of these additions attempt to replicate a more relevant body environment, yet there is still room for improvement. It has been established that some of these species present may (or may not) participate in electrochemical reactions. In fact, all of these additions not only increase the complexity of possible electrochemical reactions, they also make interpretation more difficult. For example, species such as hydrogen peroxide, when present in a solution, may not participate in the electrochemical reaction, but rather, adsorb on the metal surface and may (or may not) influence the

electrochemical potential at the metal/solution interface. Therefore, as of today, there is no clear definition to the electrochemical behavior of metallic implants in a clinically relevant human body environment.

2.3.2 Biological nature of the human body environment

The biological nature of the human body environment is highly complex, and dynamic with variation in location. The human body environment contains living entities that can interact with metallic biomaterial. Aside from this, it is important to note that the implant material is placed into the wound site. Literally speaking, surgical intervention creates a zone of damage around the metal where the wound healing process must occur. Researchers have reported that after surgery, the pH surrounding an implant can be reduced to 2, typically due to the trauma of surgery and acute inflammation [35]. This condition can alter the interaction between the implant material and the body environment. Many of the cellular and biochemical constituents in a wound site can produce redox processes [34]. As mentioned, species like hydrogen peroxide, hypochlorous acid, peroxynitrite, and other enzymes are redox active and can create local conditions that can alter electrochemical interactions. For example, albumin (used to model proteins) has been reported to adsorb on the surface of CoCrMo alloys, thus forming organometallic complexes that can alter the nature of the passive film formed on the material surface [36], [37].

2.3.3 Mechanical nature of human body environment

Mechanical interactions at an implanted site can affect the behavior of the implant. For example, an artificial hip joint is typically loaded by cyclic stresses acting onto the

implant material. It has been established that the presence of cyclic loading under electrochemical degradation can lead to fatigue corrosion failure [38]. Also, proper functioning of the implant entails the accommodation of bearing loads that may be associated with AsDL. This can lead to surface interactions that include wear against articulating surfaces. Electrochemical degradation in the presence of wear can lead to fretting corrosion, one of the causes of implant failure in artificial prostheses. Generally, most oxide film abrasion is caused by mechanical interactions and may lead to increased corrosion attacks.

2.4 Corrosion in bio-environments

Corrosion in bio-environments refers to the reaction between biomaterials and their service environment. This electrochemical process includes charge transfer across the electrode-electrolyte interface, which takes place on electrode surfaces. These electrode reactions can either be by oxidation or reduction. In oxidation, the metal atoms on the metal surface go into the metal ions in a solution, and a positive charge moves from the electrode to the electrolyte, while in reduction, a positive charge moves from the electrolyte to the electrode surface, and a negative current is produced. In all electrochemical systems, there is no external source or sink of charge, and the two half cell reactions take place in a closed system. Therefore, the sum of the anodic currents balances out the sum of the cathodic currents and the electrode-electrolyte interface adjusts its voltage to attain a condition where both anodic and cathodic currents are equal. This is called the 'mixed potential theory'. Some typical oxidation and reduction half cell reactions are presented in Equation 2.1-7:

Oxidation:

$$Co \rightarrow Co^{2+} + 2e^{-} \quad (2.1)$$

$$2Cr + 3H_2O \rightarrow Cr_2O_3 + 6H^{+} + 6e^{-} \quad (2.2)$$

Reduction:

$$O_2 + H_2O + e^{-} \rightarrow HO_2^{\cdot} + OH^{-} \quad (2.3)$$

$$HO_2^{\cdot} + H_2O \rightarrow H_2O_2 + OH^{\cdot} \quad (2.4)$$

$$H_2O_2 + 2e^{-} \rightarrow 2OH^{-} \quad (2.5)$$

$$O_2 + 2H_2O + 4e^{-} \rightarrow 4OH^{-} \quad (2.6)$$

$$O_2 + 2H_2O + 2e^{-} \rightarrow H_2O_2 + 2OH^{-} \quad (2.7)$$

For cobalt-based alloys, Equations 2.1-2.2 are oxidation reactions that represent the ionic dissolution of cobalt and protective oxide film formation of Cr_2O_3in CoCrMo implant material. Some possible reduction reactions that may be present at the implant surface are presented in Equations 2.3-2.7 [34]. Generally, these reactions involve oxygen, water, and their reactive oxygen by-products, including hydroxide radicals and hydrogen peroxide. These intermediate species that may arise from reduction processes may have effects on the biological system. Generally, there may be more than one half-cell reaction at the electrode-electrolyte interface. When this occurs, all reactions (both oxidation and

reduction) balance out to establish a potential at the electrode interface; this is called the equilibrium potential. However, which of the reaction occurs depends on the potential of the electrode relative to the equilibrium potential of the half cell. In the case where there exist multiple half-cell reactions on a single implant surface, the electrode potential is automatically adjusted until all oxidation processes balance with all of the reduction half-cell reactions. This potential is called the open-circuit potential (OCP) and it is the potential that defines where all half-cell reactions balance out to a net zero current. [34]. The relative magnitude of the OCP and equilibrium potential give insight into the direction of the redox reaction. Specifically, if the OCP is above a particular half-cell equilibrium potential, then that half-cell reaction will be an oxidation reaction, whereas if the OCP is below the half-cell potential, then the reaction will be a reduction reaction. The rate of the specific reaction will be governed by the magnitude of the voltage difference between the OCP and the equilibrium potential, availability of the species, and voltage–current characteristic behavior that governs the kinetics of the reaction.

2.4.1 Types of corrosions

Having established the human body as a corrosive environment, the question remains, what kind of effect can we expect this environment to have on CoCrMo alloys as an implant material? Generally, we can expect metals and alloys to experience pitting, crevice, galvanic, intergranular, stress-corrosion cracking, corrosion fatigue, and fretting. However, of all these forms of corrosion, only pitting, crevice and fretting are pronounced with the use of the CoCrMo alloy in total joint arthroplasty [39]. Hence, they will form the core basis of this discussion.

2.4.1.1 Pitting corrosion

Pitting corrosion is a localized type of corrosion caused by the dissolution of the passive film and the formation of cavities surrounded by an intact passivated surface [39]. Pitting corrosion usually occurs in halide environments, in which chloride ions are the most aggressive [40]. It is also associated with the formation of small cavities or holes on the surface, which are called pits. These pits tend to form in areas of the bio-film surface where there are defects or the film formed is weak in nature. The extent to which a metal will form in these pits is highly dependent on the strength of the surface film that forms on the metal [41]. The mechanism of pitting depletes oxygen in areas where the surface film is weak and this is associated with the formation of free acids (H^+ and Cl^-), as shown in Figure 2.2. The resistance to the pitting corrosion of CoCrMo alloys is attributed to the oxides and hydroxides of chromium and molybdenum in the composition of the formed passive film. According to Virtanen *et al.* [39], the pitting corrosion of CoCrMo alloys is seldom observed since they typically fail due to transpassive dissolution, thus leading to the activation of the surface as a result of oxidation of the insoluble Cr (III) oxide layer to soluble Cr (VI) species. Even though pitting does not necessarily lead to a complete and immediate deterioration of the CoCrMo alloy implant, it does indicate that the metal is not completely stable in its environment. Moreover, it increases the release of metal ions into the surroundings. One major problem that comes from pitting corrosion is that the pits formed enable stress-corrosion cracking and corrosion fatigue to propagate more easily throughout the material, which can cause catastrophic failures to occur [42]. These pits can be hard to detect, as most of them are not visible with the naked eye.

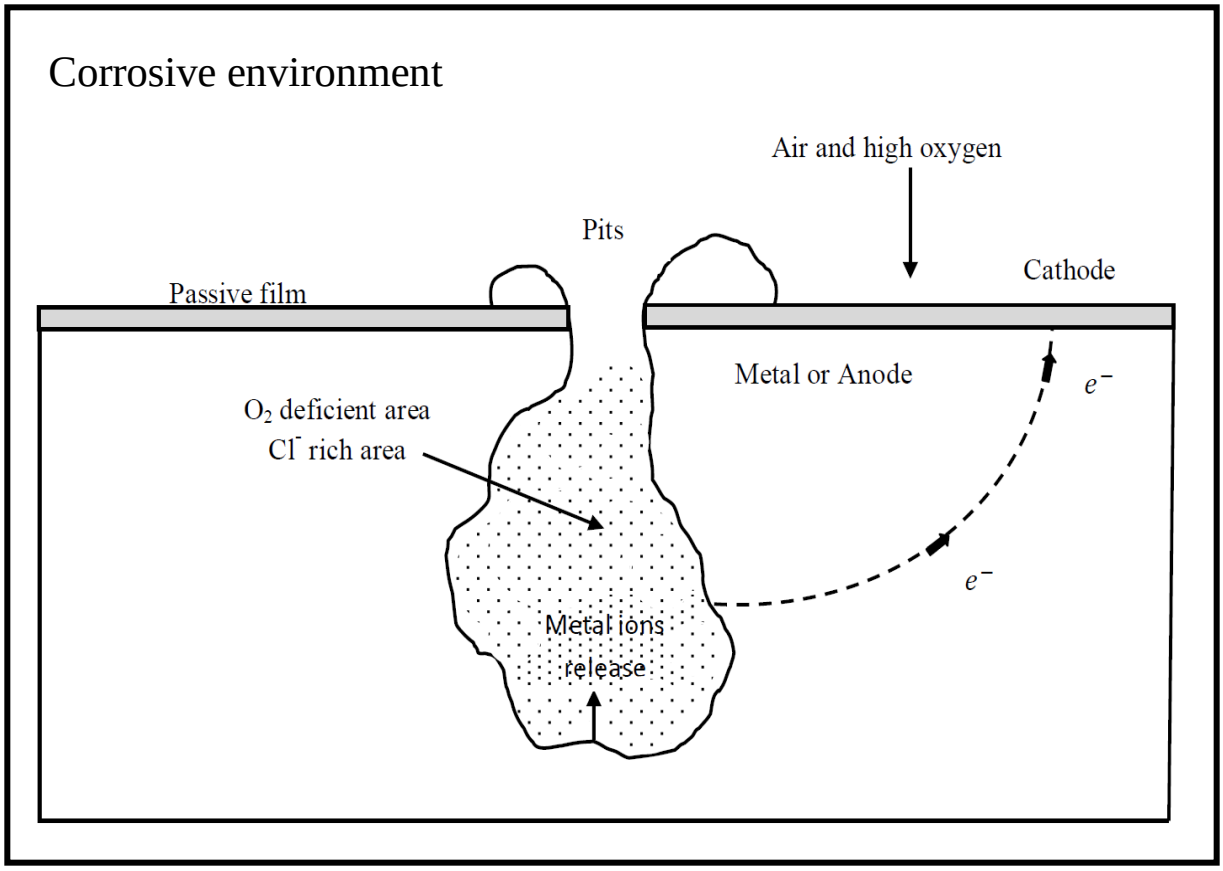

Figure 2.2: Mechanism of pitting corrosion.

In CoCrMo implant material, the effect of pitting is greatly reduced by adding a small amount, typically about 2-3%, of molybdenum to the alloy, which somewhat contributes to the passive film formed on the alloy surface.

2.4.1.2 Crevice corrosion

Crevice corrosion, just like pitting, is also a localized form of corrosion which preferentially occurs in regions on the metal surface where mass transfer is limited [39], e.g. in crevices, narrow openings, cracks and under deposits. In these occluded areas, the concentration of aggressive chloride ions, decrease in pH value and depletion of oxygen can rapidly lead to activation of the surface, see Figure 2.3. The high chromium content and the contribution of molybdenum in the passive film of a CoCrMo alloy make the alloy more resistant to crevice attacks in the human body environment. Virtanen *et al*. [39] studied the effect of pH on the dissolution rate of a CoCrMo alloy in 0.14 M (0.9% volume) NaCl, and the results showed that for a number of pHs, there is no change in the dissolution rate of the alloy, which is a characteristic behavior of the alloy in its passivity region. This is in agreement with the Pourbaix diagram shown in Figure 2.4.

2.4.1.3 Fretting corrosion

Fretting is the conjoint action of mechanical wear and corrosive attack on the material surface. It occurs at the interface of two closely fitting surfaces when they are subjected to slight oscillatory actions of split and joint corrosion in the presence of load (Figure 2.5). The damage is mostly restricted to local sites and the generated debris (mostly oxide) is usually accumulated locally, thus leading to an increase in stress.

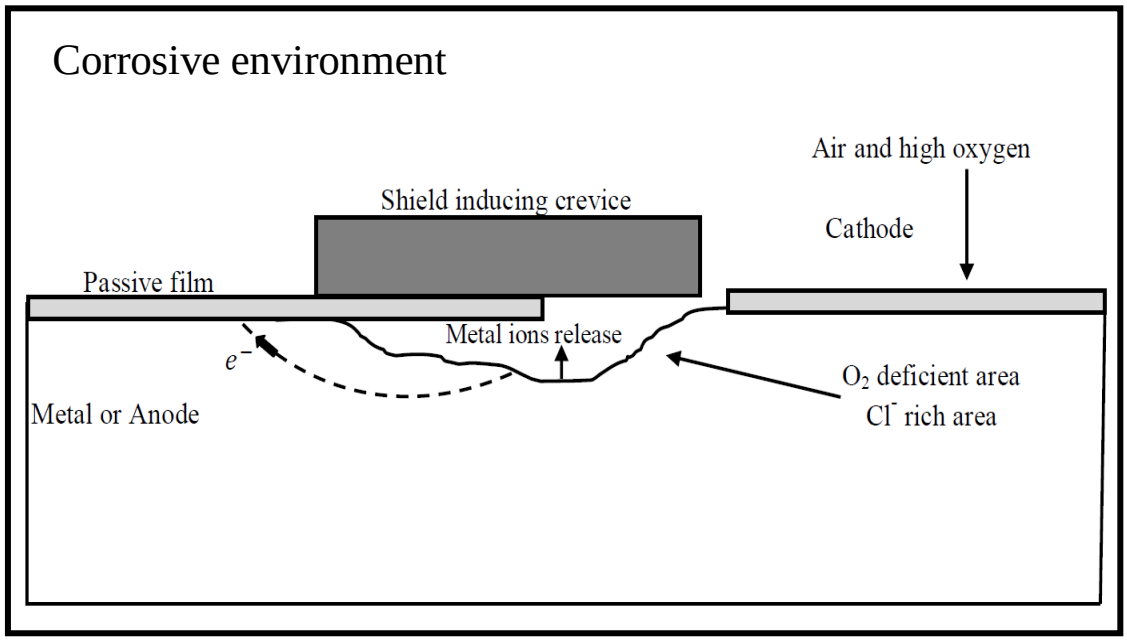

Figure 2.3: Mechanism of crevice corrosion.

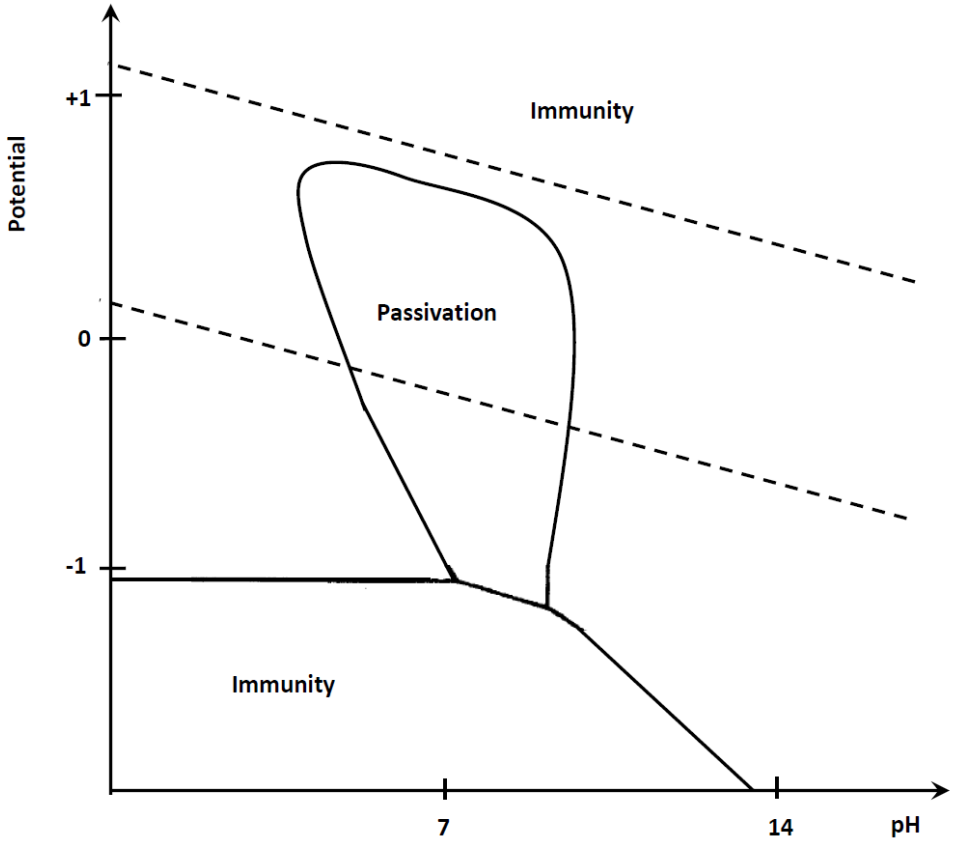

Figure 2.4: Pourbaix diagram of chromium in saline solution.

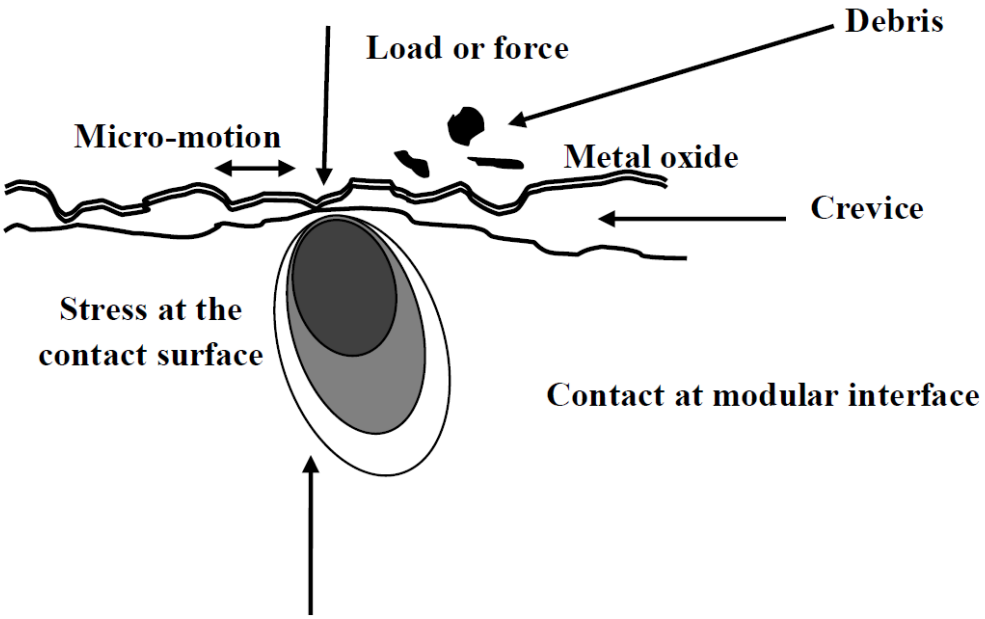

Figure 2.5: Asperity contact on metal oxide interface.

This has been reported in the neck/stem interfaces of modular THA [43], and a schematic representation is shown in Figure 2.6. An increase in hardness generally leads to a reduction in fretting wear behavior. It is worthwhile to note that on articulating and fretting surfaces (e.g. hip and knee arthroplasty), passivation, depassivation and repassivation may exist due to the effects of load and mechanical disruption of the film. When this occurs, the oxide film covered surface may be abraded and will see its OCPs shift to more cathodic potentials. As the potentials shift to more negative values, the corresponding reduction reactions will increase until the excess electrons are removed and the potentials slowly move more positively back to their starting OCPs.

These shifts in the OCP's are important to understand because they: (1) change the structure of the oxide film, (2) alter the reactions that are taking place, and (3) can result in propagating electric fields that may affect biological processes in the adjacent tissue [34]. Fretting corrosion can drastically alter the corrosion behavior by mechanically destroying the passive film [44]. Consequently, the ability of the material to repassivate, i.e. to rebuild the passive layer, becomes crucial. Fretting corrosion, alone or in combination with crevice corrosion, has been identified as one of the leading causes of implant degradation [39].

2.4.1.4 Other types of corrosions

Galvanic corrosion occurs when two dissimilar metals have electric contact while in the same corrosive or conductive environment.

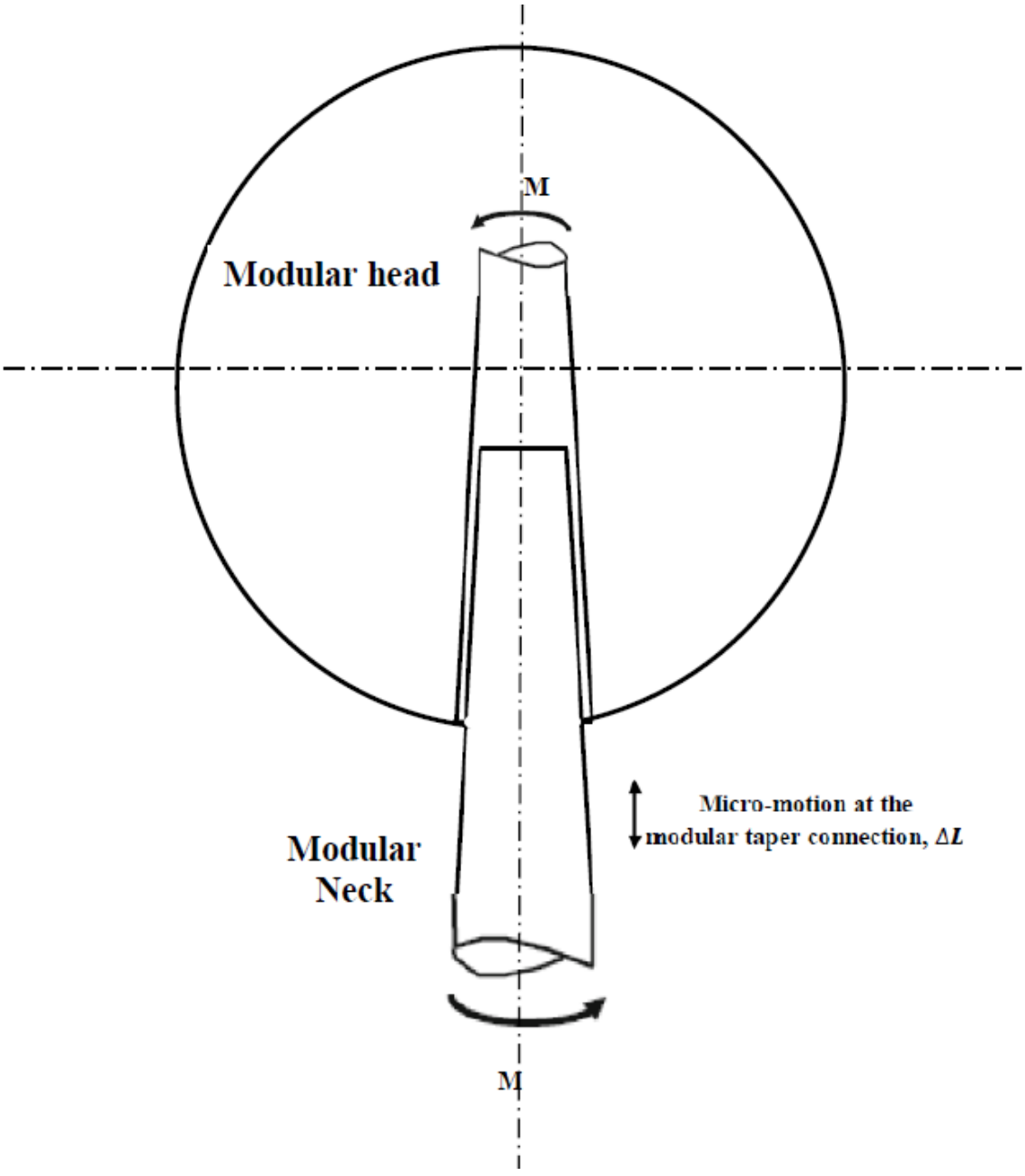

Figure 2.6: Modular neck-step interface that shows crevices and micro-motion.

This usually occurs when potential differences exist between two dissimilar metals. These potential differences produce an electron flow between them. Galvanic corrosion may be an issue for modular prostheses, in places where components made of different metals come into contact with one another, e.g. at taper junctions between the stem and femoral head. Galvanic corrosion has been reported on the tapered interface between the head and neck of mixed-metal (CoCr head/titanium alloy stem) prostheses [34], whereas no corrosion was observed in combinations that used these same alloys. Therefore, implant modules made of different material combinations galvanically accelerate corrosion which can play a major role in the failure of modular prostheses.

Intergranular corrosion occurs as a result of the reactive nature of the grain boundaries of implant materials. Generally, most engineering materials undergo heat treatment processes, mechanical actions, welding, etc. These processes involve heat and the heat affected zones of these materials can be very sensitive and reactive, thus leading to intergranular corrosion. Intergranular corrosion can be an extremely dangerous form of corrosion because it is very difficult to detect. The most common scenarios of intergranular corrosion in engineering materials is the depletion of chromium in the grain boundary regions of SS. Although this form of corrosion is rare in CoCrMo alloys and most implant materials, some researchers, see [5], [45], have noted that the massive precipitation of chromium carbides near the grain boundaries could conceivably decrease the amount of chromium locally available in a passive layer and thus there is the inclination to accelerate intergranular corrosion in alloys where chromium is the main element responsible for passivation ability.

Stress corrosion cracking (SCC) refers to the electrochemical degradation that causes cracking by the simultaneous presence of tensile stress and a specific corrosive medium. Usually, when this form of degradation occurs, the implant material is essentially unattacked over its surface, but fine cracks progress through the alloy [24]. Factors such as environment temperature, corrosive nature of the environment and corrosion products have been established as factors that accelerate the susceptibility of engineering materials to SCC. Also, the role of tensile stress has been shown to be important in rupturing protective films during the initiation and propagation of cracks. For instance, pitting corrosion can make SCC more intense, as stress-corrosion cracks usually form on the bottom of holes created by pitting corrosion.

Corrosion fatigue is the reduction of fatigue resistance due to the presence of a corrosive medium. Generally, AsDL expose human joints to different contact forces and cyclic stress conditions. AsDL, such as walking, squatting, bending, jogging, etc., may expose the hips and knees to cyclic loading conditions. When this occurs in the presence of a corrosive medium, the fatigue resistance is reduced because corrosion products and pits can increase stress and initiate cracks. Corrosion pits and fatigue striations have been reported on retrieved CoCrMo alloys used in bone plates and screws [46]. The research work reported that it is not only the design of the CoCrMo implant devices that influences the fatigue behavior of implants, but rather, their microstructure is also of prime importance. Some important considerations in reducing the susceptibility of implant materials to corrosion fatigue is to design implants with less stress components, use stress relieving heat treatments or shot-pen the surface to induce compressive

stresses. These stress relieve processes are already being used in the design of many artificial joints [32].

2.4.2 Passivation of CoCrMo alloys in bio-environments

The resistance to electrochemical degradation in active-passive bio-implantable materials (with CoCrMo alloys an example) is due to the formation of a thin protective bio-film layer [35], through a mechanism called 'passivation'. Passivation is the creation of a protective oxide or hydroxide layer on the surface of a metal. These layers are formed from initial corrosion products which further react to form protective films that adhere onto the surface of the implant material. The development of these films is not a simple process. Factors such as the type of alloy, synovial fluid composition, implant-fluid interface potential, pH and implant exposure time have been established to influence the nature and kinetics of these protective films [47].

It is important to note that on real metallic biomaterial surfaces, the OCP of the surface can undergo changes depending on the reactive species present and how they affect the overall balance of the reactions. For example, increased concentrations of hydrogen peroxide (a by-product of inflammation) typically results in a more positive OCP for a particular alloy surface, while additions of proteins to the electrolytes will typically decrease the OCP of the surface. Specifically, CoCrMo alloys owe their applicability as a biomaterial to their ability to form a protective passive layer of Cr_2O_3. Although the thickness of these passive films is typically only a few nanometers [45], [48], they act as a highly protective barrier between the metal surface and the aggressive service environment.

Consequently, the passive film kinetically retards the rate of dissolution by many orders of magnitude. The protectiveness of the passive film is determined by the rate of ion transfer through the film, as well as the stability of the film against dissolution. Figure 2.7 shows a schematic representation of the ion transfer mechanism across an oxide layer interface. The thermodynamic tendency to form a passive film on an active-passive metal can be predicted by using a Pourbaix diagram.

A Pourbaix diagram is a potential versus pH diagram developed based on theoretical chemical relationships. Figure 2.4 (previously shown) is a Pourbaix diagram of chromium which shows the anticipated corrosive behavior of the CoCrMo alloy in a saline solution (a simplified version of the human body environment) as a function of pH and the potential at the interface. This Pourbaix diagram shows that three general behaviors can exist for CoCrMo alloys in an ionic environment: corrosion (dissolution of the CoCrMo alloy), passivation (Cr_2O_3 layer protects the alloy from further dissolution), and immunity (a region where minimum oxidation occurs as the equilibrium concentration of metallic ions is low). At an acidic pH, cobalt and chromium oxidize, which gives bivalent aqueous ionic Co(II) and Cr(II) as the primary oxidation products while the cathodic partial reaction is the hydrogen evolution reaction [49]. At an alkaline pH, cobalt and chromium originate the oxide species CoO and Cr_2O_3 while oxygen electronation reaction supplies the oxidation current [49].

Two broad theories describe the tenacious nature of passive films in active-passive metals [50]; The first suggests that the passive film is always a diffusion-barrier layer of reaction products such as metal oxide or other compounds which retard the anodic dissolution.

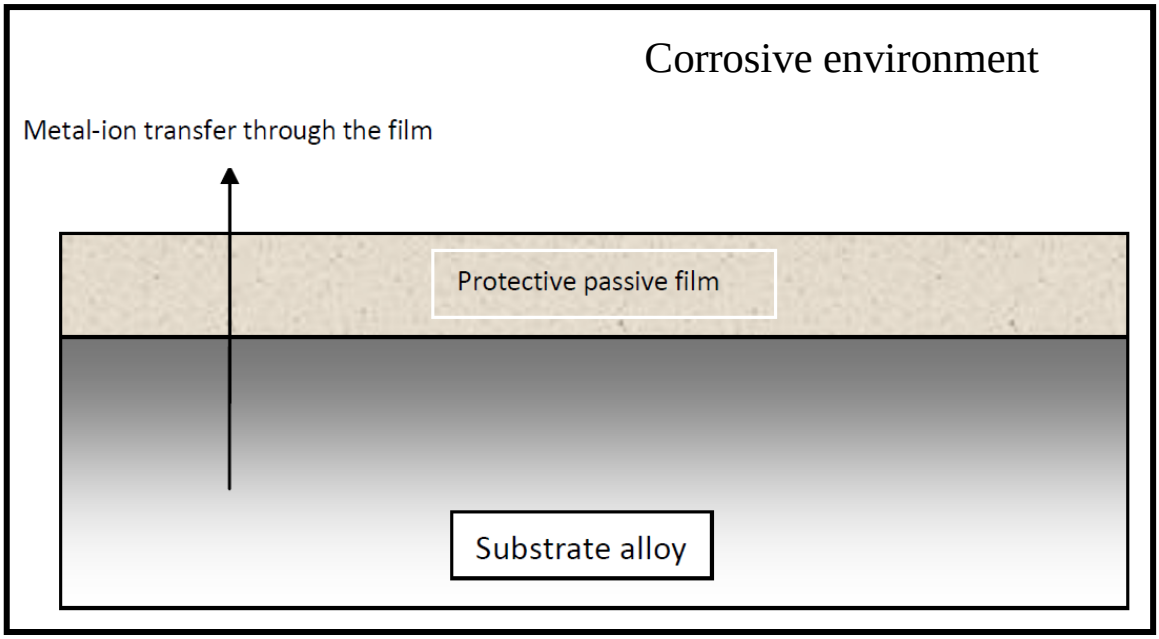

Figure 2.7: Schematic representation of ion transfer mechanism across oxide layer interface.

The second theory suggests that generally a monolayer or so of a chemically adsorbed film of oxygen imparts passivity [50] by displacing the normally adsorbed water molecules and thus slowing down the rate of anodic dissolution which involves the hydration of metal atoms. This theory is based on the fact that most of the metals that exhibit or impart passivity to an alloy are transition metals with electron vacancies or uncoupled electrons in the d-shells of atoms. These uncoupled electrons form strong bonds with oxygen which also contains uncoupled electrons, thus resulting in electron-pairing or covalent bonding hat supplement ionic bonding [50].

2.4.3 Influence of proteins - formation of organometallic complexes

Among other constituents, human synovial fluid contains an average total protein concentration of 34 g/L [15]. This can be harsh to metals in terms of corrosion and tribocorrosion. In fact, the role played by in-vivo proteins (which are essential components of the synovial fluid) varies, and can be difficult to predict [9], [51]. With focus on the articulating surface of MoM implants for example, Valero Vidal and Igual Munoz [2] reported the absorption of proteins and amino acids on the surface of AISI 316L and CoCrMo. Their work showed that protein and amino acid absorption decreased the corrosion resistance of AISI 316L and increased the corrosion resistance of CoCrMo alloy.

Generally, when an implant is placed in the human body environment, the implant surface and initial tribocorrosion products (particulate debris and ions) can combine with the proteins in the synovial fluid to form a proteinacious or organometallic layer that adsorbs on the bearing surfaces, usually called a bio-film [13]. Some researchers have

reported the beneficial and detrimental effects of bio-film formation on MoM bearings. Contu *et al*. [52] reported a diffusion controlled mechanism that causes anodic dissolution of the alloy by inhibiting the hydrogen evolution reaction in the presence of protein containing calf serum fluid. In his work, the bio-film which forms a diffusion barrier prevents chloride ions and other aggressive species from accelerating the metal ion release of the implant material. On the other hand, Yan *et al*. [9] reported an enhanced ion release and passive film breakdown of a CoCrMo alloy under static corrosion in the presence of proteins. This observation was associated with a reduced passive film region following protein adsorption to the sample surface. Many researchers have reported the formation of a boundary lubrication regime in synovial fluids containing protein [36], [53]. This effect has been reported to be beneficial for tribology studies on the human joints, possibly due to reduced coefficients of friction [53], [54].

As already stated above, while the presence of proteins has been established to favor the formation of organometallic complexes on the passive layer, a thorough understanding of the interactions is still yet to be fully elucidated. Researchers have attributed the dynamic behavior of proteins and protein compounds to their susceptibility to denaturation under in-vivo and in-vitro conditions [37], [55]. Denaturation is the process of altering the native/low free energy conformation of a protein complex. Denatured proteins do not retain their original properties or biological functions and this implies that the specific conformation of proteins may be altered. Generally, the peptide bonds in these protein complexes remain intact and the proteins usually retain their original primary structure. Therefore, in principle (although rarely in nature), denatured proteins can return to their native state and resume their specific biological activity. Proteins have specific

parameters for denaturation. These parameters are usually ranges of pH, relative humidity and temperature, organic solvents, applied stresses, etc.

Proteins and their complexes can cause major differences between the corrosion and tribocorrosion behavior of CoCrMo alloys (and other implant materials) in-vitro and in-vivo. Generally, the properties of the bio-film formed on the implant can change with time. This is because both thermodynamic and kinetic factors are involved in protein adsorption and the adjacent cells are actively involved in protein synthesis [51]. To this end, the effects of proteins on CoCrMo alloy corrosion in-vivo and in-vitro can be said to be complex and may increase or decrease the corrosion rate [2]. A review of the corrosion studies on CoCrMo alloys reveals that there may not be a straight cut prediction of the behavior, especially under varying electrochemical, material and service conditions. This is because human joints can be characterized by dynamic, constantly changing chemical and physiological processes, mechanical loading patterns, and bioelectric potentials which can alter the bio-film properties with time.

2.4.4 Corrosion testing and corrosion rate measurements

Corrosion and corrosion assisted degradation have always been of particular concern in a wide range of areas where metals and alloys find applicability. In the biomedical industry, the use of metals as bio-implantable devices will continue to necessitate the need for corrosion testing and corrosion rate measurements for the design of future bio-implantable materials. Irrespective of the nature of the environment, corrosion is always an insidious process and often difficult to recognize until deterioration is well advanced. For example, corrosion and corrosion products have been reported to cause physiological

defects, such as infections, osteolysis and aseptic loosening in some patients who have been implanted with artificial prosthesis [56]. These and other physiological effects are related to the type of corrosion products and their release rate. Therefore, when the corrosion process is left untested and its rate is left unmeasured, it will not only destroy implant materials, but can also lead to loss of life. Thus the need for corrosion testing and corrosion rate measurement in biomedical applications cannot be over emphasized due to the following reasons.

- Corrosion testing and corrosion rate measurement provide valid information for predicting the useful life of biomaterial in vivo.

- Corrosion testing and corrosion rate measurement provide valid information/data suitable for the design of new implants.

- Information derived from experimental testing can be used to better understand the cause of failure of retrieved implants.

- Information from experimental testing can be used to predict the concentration of ion release, i.e. to assess levels of contamination of body fluids (synovial fluid, blood, etc.).

Clearly, it is very difficult to simulate the complex conditions that exist within living organisms via laboratory in vitro experiments. Despite the challenges in achieving this, the galvanostatic polarization measurement technique and potentiostatic anodic

polarization measurement have been successfully employed in the in-vitro testing of biomedical implant materials.

2.4.4.1 Galvanostatic polarization measurement

The mixed potential theory forms the basis for galvanostatic polarization measurements. This technique employs the data obtained from cathodic and anodic polarization measurements by applying a current and measuring the resulting potential. Tafel extrapolation and linear polarization are the two major methods used for corrosion rate measurements.

Tafel curves and slopes are determined by applying currents that usually range from 0.1 μA to 10 mA in small uniformly spaced increments and recording the steady-state potential over a period of time. When the potential of the electrode is plotted against the logarithm of the applied current; A potentiodynamic polarization plot is obtained. A schematic potentiodynamic polarization plot is presented in Figure 2.8. The curve obtained is nonlinear at low currents, but at higher currents, the curve becomes linear on the semi-logarithmic plot, usually at approximately 50 mV more active than the corrosion potential [24]. The straight-line portion of the curve is the Tafel slope. The linear portion of the curve can be extrapolated and will intersect at E_{corr}. Further extrapolation of these lines brings them to the potentials for the reversible anodic and cathodic reactions. These reactions determine the polarity of the corrosion cell, with the anode being negative and the cathode positive. The extension of the anodic line to the reverse potentials brings it to a potential at which the metal is in equilibrium with its ions, and the extension of the cathodic line brings it to the reversible potentials for the cathodic reaction.

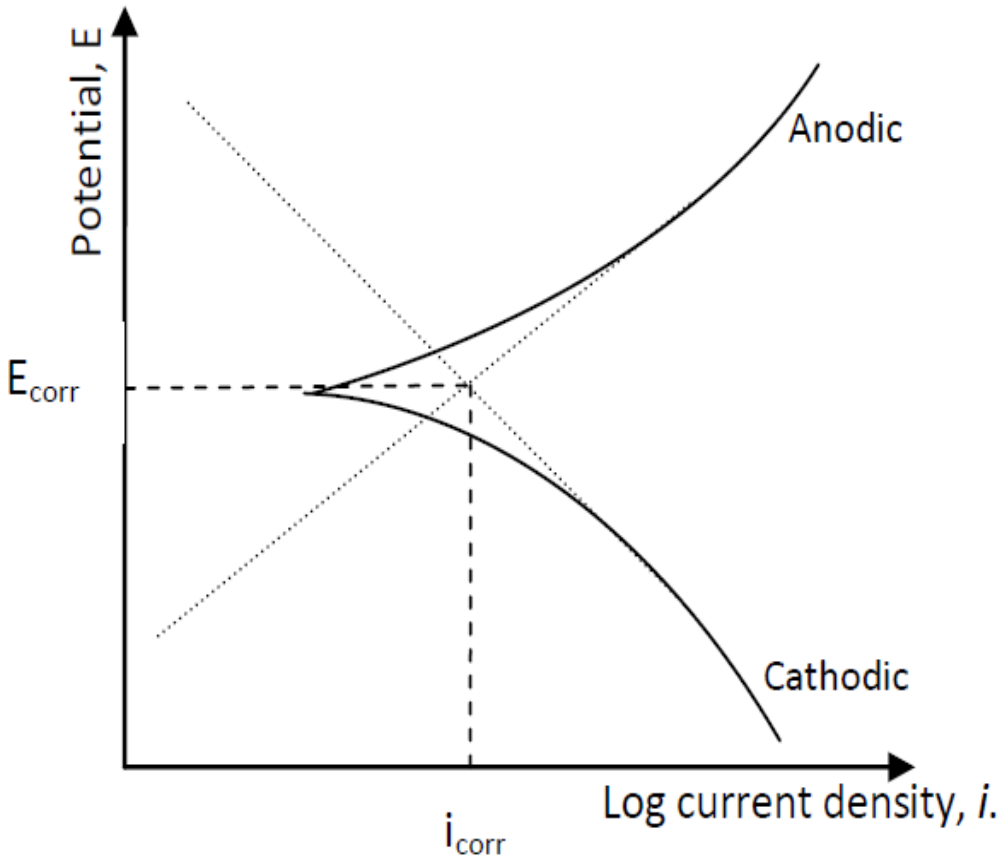

Figure 2.8: Schematic of the potentials vs. log density curve for anodic and cathodic galvanostatic polarization curves

The linear polarization technique can be used to determine the corrosion rate of a material within 10 mV nobler or more active than the corrosion potential of a material in a solution. It is observed that the applied current density is a linear function of the electrode potential within this interval. The slope of the linear polarization curve is related to the kinetic parameters of the system, as follows:

$$\frac{\Delta E}{\Delta i_{app}} = \frac{\beta_a \beta_c}{2.3 i_{corr}(\beta_a + \beta_c)} \tag{2.8}$$

where β_a and β_c are the Tafel slopes of the anodic and cathodic reactions respectively. Since the slope of the linear polarization $\Delta E/\Delta i_{app}$ is relatively insensitive to changes in beta values, a reasonable approximation reduces Equation 2.8 to Equation 2.9

$$\frac{\Delta E}{\Delta i_{app}} = \frac{0.026}{i_{corr}} \tag{2.9}$$

Equation 2.9 may be used to calculate the corrosion rate of a system without knowledge of its electrode-kinetic parameters. Among its advantages is the fact that it permits rapid corrosion rate measurements and accurately predicts very low corrosion rates.

2.4.4.2 Potentiostatic anodic polarization measurements

Potentiostatic anodic polarization measurements are performed by applying a potential and measuring the resulting current. The applied voltage increment should be small. A recommended rate of applying the potential is 0.006 to 0.012 V/min [24]. These measurements are especially suitable for measuring the corrosion of biomedical implant devices; this is because they behave as active-passive metals. These measurements will

show the length of the passive region in potentials, and the magnitude of the current in the passive regions. The variables of the environment, such as pH and organic constituents, can be studied with the use of this method. Another application of anodic polarization measurements involves the study of repassivation kinetics. Figure 2.9 shows a schematic of an anodic polarization curve.

2.4.4.3 Other corrosion testing methods

In modern terms, corrosion rates can be measured from chemical analyses of corroding solutions through atomic absorption. Also, the surface analysis of corroded surfaces can be made with several techniques, including x-ray photoelectron spectroscopy (XPS) and Auger analysis. Chemical analyses can provide data on the quantity of metal ions released. Leslie *et al.* [57] measured the rate of corrosion of a CoCrMo alloy by using inductively coupled plasma mass spectroscopy (ICP-MS) to measure the concentration of ions in the solution and quantifying the wear rate by considering the bedding in stage and the steady state condition in-vitro. Also, Pourzal *et al.* determined the wear rate of a CoCrMo alloy under sliding wear conditions by determining the chemical composition of the particles generated by using energy dispersive x-ray spectroscopy (EDS) [4]. From the above examples, these methods are shown to also give a reliable measure in the measuring of the corrosion rate of implant materials.

2.5 Tribology

Tribology is a branch of mechanical engineering that deals with the friction, wear and lubrication of interacting surfaces in relative motion.

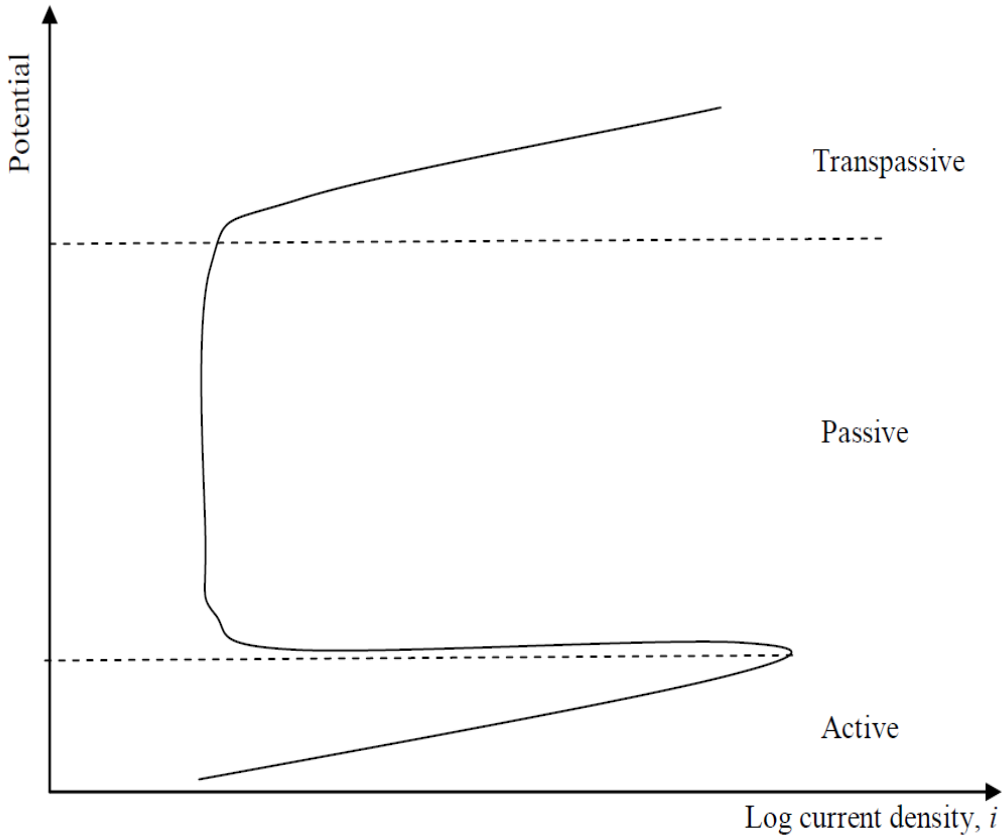

Figure 2.9: Potentiodynamic anodic polarization scan

2.5.1 Conforming and non-conforming contacts

Surfaces that are in contact are considered to be conforming when two bodies geometrically fit well into each other in a way that the area of contact is large. When this happens, the load carried is distributed over a large contact area. On the other hand, surfaces that are in contact may be non-conforming when the two surfaces do not fit well into each other. When contacting surfaces are non-conforming, the load between the bodies is carried by a relatively small area. Figure 2.10 shows diagrams of conforming and non-conforming contacts. Classification of the conforming and non-conforming contacts can be made by the geometry and loading condition of the contacts between the mating surfaces [58]. The geometry of an artificial hip is highly conforming, due to its large contact area and low contact stress under loading conditions. Artificial knees, on the other hand, are less conforming. They have a different range of motions, low contact area and higher contact stresses, and Cr(II) high susceptibility to fatigue that may lead to crack initiation, propagation and ultimately delamination, wear and fracture. This is why fractures are not much of an issue in the hips as they are in the knees.

2.5.2 Hydrodynamic and elasto-hydrodynamic lubrication

Hydrodynamic lubrication generally occurs in conformal contacts through positive pressure build-up in the fluid film due to a converging gap, where fluid is dragged in and pressurized. The pressurized film creates the possibility of applying a load which is carried by the fluid film. The pressure build-up is usually inadequate to cause elastic deformation of the contacting surfaces.

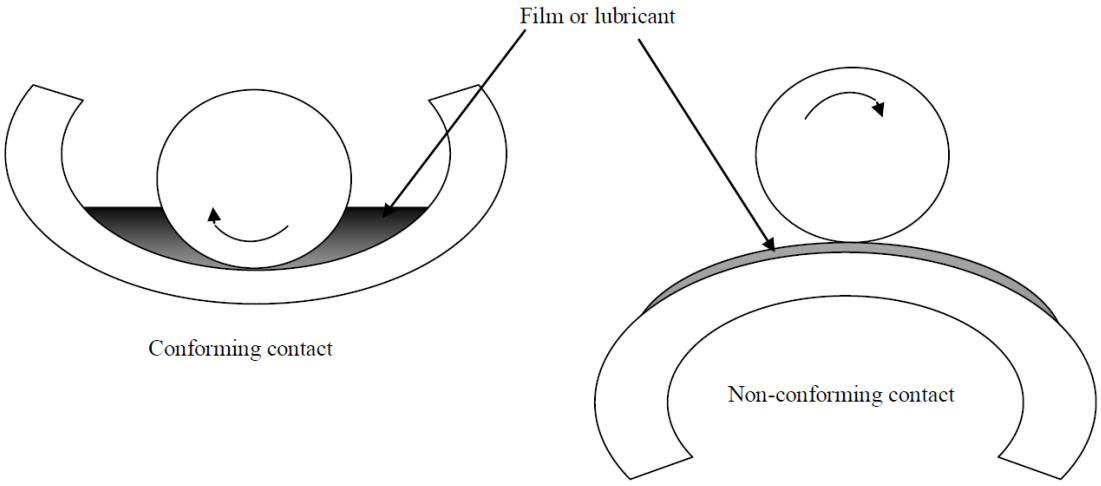

Figure 2.10: Conforming and non-conforming contacts.

Non conformal contacts are often associated with elasto-hydrodynamic lubrication where elastic deformation of the surfaces becomes pronounced. The elastic deformation creates a gap for the lubricant to pass through. Also, an exponential increase in viscosity with pressure keeps the lubricant from flowing out of the contact. Although systems that operate under elasto-hydrodynamic lubrication greatly increase their load bearing capacity, both hydrodynamic and elasto-hydrodynamic lubrication systems run with a fluid that is thick so that there is no contact between the solids. A system operating under these conditions experiences virtually no wear at all, and the friction coefficients are generally low and only attributed to shearing in the lubricant [58].

2.5.3 Lubrication regimes

Ideally, artificial hips and knees are designed to utilize hydrodynamic or elasto-hydrodynamic lubrication. This usually favors the formation of a fluid film that is thick enough to prevent direct contact between the surfaces in contact. This design method is usually geared towards reducing wear rates and friction coefficients to clinically acceptable values. Even though hydrodynamic and elasto-hydrodynamic lubrication have been reported to reduce wear rates and volumes, very low relative motion between articulating surfaces and high contact pressure have been reported that lead to the penetration of wear asperities through the lubrication film to the contacting surfaces [58]. Surface treatment plays an important role here since smoother surfaces will allow for higher loads or lower speeds without breaking of the fluid film by the asperities. A common approach is to divide the mode of a lubricated system into three regimes: boundary, mixed and hydrodynamic lubrication.

2.5.3.1 Boundary lubrication

Boundary lubrication is characterized by asperity interactions that carry all of the contact force. In this regime, the asperity interactions become more severe; the shear properties of the film on the solid surface become pronounced. With boundary lubrication, the physical properties of the bulk lubricant, such as density and viscosity, are not as important as the properties of the surfaces in contact. It has been reported that some artificial hip joint replacements experience boundary lubrication [17]. When this occurs, the contact friction and wear performance are governed by the physical and chemical properties of thin lubricating films formed on the surfaces in combination with the properties of the bulk material or material surface [58].

2.5.3.2 Mixed lubrication

Mixed lubrication is also known as the partial elasto-hydrodynamic lubrication regime. In this regime, the contact force is carried by both asperity interactions and the hydrodynamic and/or elasto-hydrodynamic effects of the lubrication film, which provide partial separation between the surfaces. The contact load is shared between the contacting asperities and the film when mixed lubrication prevails. Depending on the operating conditions, the coefficient of friction in the mixed lubrication regime can widely vary depending on how much of the load is carried by asperity interactions and hydrodynamic actions, respectively. Since there are still asperity interactions, the chemical effects of the lubricant are important.

2.5.3.3 Hydrodynamic lubrication

In the full film or hydrodynamic lubrication regime, there are no asperity interactions and the contact force is fully carried by hydrodynamic effects. When the pressures in the contact zone are so high that the material is elastically deformed, the mode of lubrication is called elasto-hydrodynamic lubrication (EHL). In hydrodynamic lubrications, the film is thick and the traction or friction force will be a function of the bulk rheological properties of the lubricant in the appropriate operating conditions of load, temperature, shear rate and so on. Fluid film lubrication is the most desirable form of lubrication. In this case, the surfaces are not in contact so resistance to their tangential motion, the friction force, is primarily dependent on the viscosity of the lubricant [17]. Also, since there is essentially in theory no contact between surfaces, no wear should occur.

2.5.4 Film parameter

The film parameter, lambda (λ), is a common way to predict the lubrication regime in which a system uses to run. This dimensionless number is the ratio of the film thickness to the surface roughness. Generally, when $\lambda < 1$, the system is running in the boundary lubrication regime, $1 < \lambda < 3$, the mixed lubrication regime, and $\lambda > 3$, the hydrodynamic lubrication regime [58]. The mathematical relation for the λ ratio is presented in Equation 2.10:

$$\lambda = \frac{h_{min}}{\sqrt{S_{q1}^2 + S_{q2}^2}} \tag{2.10}$$

where

h_{min}= Minimum film thickness, m

S_q = Composite surface roughness, m.

2.5.5 Stribeck curve

According to Yan [17], in 1902, Stribeck demonstrated that the coefficient of friction is directly proportional to the lubricant viscosity and the difference in speed of the contact surfaces, and inversely proportional to the pressure which is exerted onto the contact surfaces. Figure 2.11 shows a typical Stribeck curve with the three regimes of lubrication: boundary, mixed and hydrodynamic. The y-axis is the coefficient of friction and the x-axis is a dimensionless number, often referred to as the Hersey number (*H*) given by Equation 2.11. Generally, a small Hersey number indicates a thin lubricant film, and consequently a high Hersey number indicates a thick lubricant film.

$$H = \frac{\eta\omega}{p} \tag{2.11}$$

where

η = absolute viscosity, Pas

ω = rotational speed, rps

p = pressure, Pa.

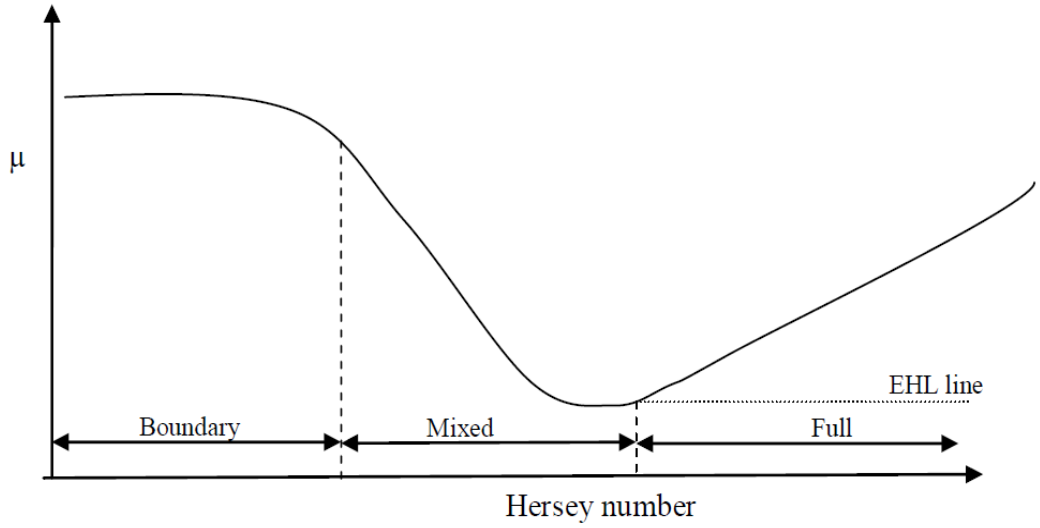

Figure 2.11: Stribeck curve that shows the boundary, mixed and hydrodynamic lubrication regimes.

2.5.6 Friction

Friction is a measure of the reluctance or resistance of a body when it moves over another body during direct contact.

2.5.7 Wear and wear mechanism

The wear of a metal is a measure of its hardness, i.e., its resistance to indentation or damage to the material surface, which generally involves the loss of material due to relative motion between that surface and a contacting substance. In artificial hips and knees, wear and wear related damage continue to be the major causes of revision surgery in implanted patients, hence the need for proper characterization of the wear particles is of importance [59], [60].

Generally, four different modes of wear have been associated with failure in artificial hip design [61]. They are:

- Mode 1: articulation between intended surfaces. E.g. articulation between the femoral head of the hips and acetabular cup,

- Mode 2: articulation of primary bearing surface and a material that was never intended to be a bearing surface. E.g. articulation between the femoral head and metal backing (a UHMWPE acetabular lining that was worn through to its metal backing),

- Mode 3: articulation between intended surfaces, but in the presence of third body particles. These third body particles could be poly(methyl methacrylate) (PMMA), bone, metal debris, etc. E.g. fretting wear particles, corrosion debris, and

- Mode 4: articulation between two non-bearing secondary surfaces. Backside wear is an example – micro-motion between the back of a polyethylene insert and its metal backing.

Five primary wear mechanisms have been directly linked to orthopedic medicine. They are adhesive, abrasive, third body, fatigue and corrosive wear. However, there are also other forms of wear, such as cavitation, fretting and diffusive wear.

2.5.7.1 Adhesive wear

Adhesive wear occurs when the atomic forces that occur between two materials in contact are stronger than the inherent properties in either material – the bonding or fracture of asperities creates wear debris. Adhesive wear involves the transference of material from one surface to another during relative motion. When this occurs, wear particles that are removed from one surface are either permanently or temporarily attached onto the other surface. The surface roughness of the contact affects adhesive wear. It is usually associated with plastic strain and a ‘’plasticity induced damage layer’’, due to multi-axial loading conditions at the hips.

2.5.7.2 Abrasive wear

Abrasive wear occurs between surfaces with different levels of hardness. Asperities on the harder surface plough through the softer material. Thus, the surface roughness of the bearing surface is important when it articulates against material with a different hardness value. The mechanisms of abrasive wear can comprise micro-cutting, fracture, ploughing or grain pull-out.

2.5.7.3 Third body wear

Generally, third body wear is usually regarded as a form of abrasive wear. Here, hard particles become embedded into the soft surface. An example is bone cement in UHMWPE. This can damage both surfaces and lead to polymer and metal debris.

2.5.7.4 Fatigue wear

Fatigue wear conditions are determined by the mechanics of crack initiation, crack growth and fracture of implants. Fatigue wear is the removal of particles detached by repetitive cyclic stress variations on the implant surface. This occur when the fatigue limit of the material is exceeded or subsurface shear and contact stresses lead to subsurface crack growth. Researchers have reported rim cracking in explanted hips and tibial components due to large cyclic contact stress onto these prostheses [56].

2.5.7.5 Tribochemical wear

Tribochemical wear is a wear process in which chemical or electrochemical reaction with the environment predominates. If a material (metal) is corroded to produce a film on its

surface while it is simultaneously subjected to a sliding contact, then one of the three following phenomena may occur [17].

- A durable lubricating film may be formed which inhibits both corrosion and wear.

- A weak film which has a short life-time under a sliding contact may be produced and a high rate of wear may occur.

- The protective surface films may be worn (e. g. by pitting) and galvanic coupling between the remaining films and the underlying substrate may result in the rapid corrosion of the worn area on the surface.

2.6 Tribocorrosion

Tribocorrosion can be defined as a degradation phenomenon that is derived from the irreversible transformation of material surfaces (wear, cracking, corrosion, etc.) subjected to the combined action of mechanical loading (friction, abrasion, erosion, etc.) and corrosion attacks caused by the environment (chemical and/or electrochemical interactions [46], [62]. A good example is the case of artificial hip replacement joints, where implant metals are constantly exposed to tribological events (joint articulations) in the presence of corrosive solutions (synovial fluids). While tribocorrosion involves the synergetic interaction between wear and corrosion, it is not simply the sum of corrosion and wear taken separately [27], [63], [64].

This synergism can have positive or negative effects depending on the specific reaction products formed on the surface of the materials, which can protect the surface as in the

case of self lubricating and/or self healing layers or aggravate the material degradation process and cause more material removal [62], [65]. Indeed, previous researchers [66], [67] have shown that surface films may influence the mechanical response of contacting metals while the scraping off of protective films can accelerate corrosion.

A recent review [62] of the significance of tribocorrosion in biomedical applications has categorized the factors that affect the process and mechanism of this subject matter into three major groups. They are: the properties of the contacting material, mechanics of the tribological contact, and physiological properties of the environment. While each category has direct influence on the tribocorrosion behavior of artificial prostheses in service, a combination of these factors can either be synergetic or antagonistic, which can be beneficial or deleterious to the overall performance of the implant material.

2.6.1 Influence of interfacial material properties

The interfacial properties of tribological material in contact are of paramount importance in understanding the tribocorrosion behavior of implant materials in service. While most implant materials rely on relatively thin surface oxide films, in the absence of corrosion, the wear resistance of a material depends on properties such as hardness, rigidity, ductility and yield strength, although the explicit relationship between these properties on the tribocorrosion rate is not very clear [62]. The microstructure of the material, presence of defects, grain size, inclusions, segregations, dislocation density, etc., are critical for the mechanical behavior of a material. Material surface topography, e.g., surface roughness, plastically deformed surface layers due to rubbing or impacts, nature of oxide film formed, etc., also play crucial roles in tribocorrosion [68]–[70].

2.6.2 Influence of mechanical and tribological contact conditions

The rate of tribocorrosion for a given metal-environment combination depends on the applied forces and the type of contact - sliding, fretting, rolling or impact. The other factors include sliding velocity, type of motion (or micromotion), shape and size of contacting bodies, alignment, vibration, frequency [38] and so forth. For example, it has been demonstrated that by applying a load to the surface of materials, the corrosion potential shifts from a passive region to a more active region [27]. This is the result of the physical removal of the passive film during sliding under load, thus allowing corrosion to proceed at an accelerated rate [71].

2.6.3 Electrochemical aspects and physiological properties of environment

Electrochemical conditions, such as interfacial surface potential and film growth rate at the tribological interface, have been reported to influence the tribocorrosion behavior of implant alloys [72]. Usually, when tribocorrosion experiments are performed at applied potentials that differ from the OCP, the thickness of the passive layer measured changes in accordance with the potential applied. Diomidis *et al*. [72] reported friction wear coefficients of similar experiments conducted at OCP and a specified applied potential under the same conditions. Their results showed that lower friction wear coefficients can be observed at OCP as opposed to an applied potential. The reason may be attributed to the fact that the wear promoting effect of passive films is largely due to the continuous depassivation and repassivation of surface oxide films. Since thicker passive films were recorded at the applied potential, the material loss due to depassivation/repassivation may have been lower under OCP condition, thereby promoting wear accelerated corrosion at

higher potentials. Aside from the potential and the film growth rate, other solutions and/or environment properties like viscosity, conductivity, pH, and temperature, may also play a vital role in the tribocorrosion behavior of implant materials.

2.7 Review of in-vivo and in-vitro studies of metal-on-metal implants

MoM articulations gained popularity in the 1960s and 1970s [73], [74]. However, in the mid 70s, MoM combinations were phased out and replaced with metal-on-polyethylene bearing combinations because of higher loosening rates, inflammatory response with MoM hips and concerns over biological reactions [75]–[77]. There has, however, been a resurgence of interest in MoM articulation due to concerns over osteolysis attributed to polyethylene wear debris [73]. In order to design against higher metallic ion release and loosening rates in MoM implants, focus in recent times has been on hip implants with larger femoral head sizes and optimized head-cup clearance that generates a reduced volumetric bedding in wear and lower ion levels in the steady state wear [57]. In the design of second generation MoM hip implants, a critical review of the major in-vivo and in-vitro observations of some of the hip implants is discussed below.

Biological response to wear particles and ion release - The systemic effects of wear and corrosion debris have been reported in the literature. Some researchers [78]–[81] have documented elevated serum and urine metal levels in patients who were undergoing total joint replacement, particularly in those with MoM bearing devices. Presumably, these metals are in the ionic form, bound to serum proteins. The biological effects of wear particles and metallic ion release have been reported to cause synovitis, periprosthetic bone loss, osteolysis, aseptic loosening of implants, etc. [56]. Wear

particles that cause biologic responses have been categorized into size, composition, shape and concentration [61]. Results from similar researchers [4], [56], [61] showed that particles of phagocytosable sizes (i.e. micrometer and sub-micrometer particles) influence bio-reactivity by inducing susceptibility to inflammatory responses as compared to nano-sized wear particles. Also, higher concentrations of Cr_2O_3 particles in cells and tissues could induce a decrease in the total cell number and increase in cell necrosis [4], [73], [82]. Despite multiple reports of implant debris in the body tissues, body cells, serum, urine, and end organs, the clinical implications of the systemic distribution of implant debris remain unclear [4], [61], [83].

Influence of protein containing lubricants on metallic ion release - Despite the low dissolution rate of CoCrMo alloys, the effects of tribocorrosion in the biological system over time have been reported to lead to an increase of metal ions in-vivo. This can cause adverse physiological effects, such as toxicity, carcinogenicity, genotoxicity and metal allergy [84]. In the presence of negatively charged protein compounds, cobalt and chromium ions bound to proteins and the resulting organometallic compounds formed are systematically transported and either stored or excreted. Cobalt has been reported to have fewer health risks to patients because when transported from the tissues to the blood, it is usually eliminated in the urine [75]. Chromium, on the other hand, has been reported to lead to physiological effects, such as osteolysis and metallosis because it is not easily excreted and builds up in the tissues and red blood cells.

Interaction between wear and corrosion in the presence of proteins - To truly understand the synergy between wear and corrosion on MoM bearings, a proper

elucidation of tribochemical reactions that take place on the bearing surfaces cannot be overemphasized. Pourzal *et al*. [4] studied the interaction between wear and corrosion in the presence of proteins. The study revealed that the tribomaterial generated from the bearing surface is progressively formed by mechanically mixing of the uppermost nano-crystalline zone of metals with proteins from the synovial fluid. This, they concluded, governs the wear rate and influences the corrosive behavior of the bearing surface, thus indicating that the tribolayer has some beneficial effects on the wear rate.

In-vivo studies of degradation in CoCrMo implants through wear and corrosion - After an implantation period of 8.5 months, a study of the surface degradation in CoCrMo implants through wear and corrosion was carried out on 12 sheep [85]. A chemical analysis of tissue samples from the interface region was also carried out for evidence of cobalt, chromium and molybdenum contents. From the results, clear evidence of wear and corrosion were observed [85]. The results supported other work which indicated that the modes of metal transport through poly (methyl methacrylate) bone cement play an important role in the surface degradation mechanism of the metal [86].

Effect of sliding conditions and friction on degradation – Researchers [65], [87] have studied the effect of sliding conditions and friction on the degradation of CoCrMo alloys and other bio-implantable materials, with the aim to understand the correlation behind corrosion degradation, wear accelerated corrosion degradation in biomedical materials, and sliding conditions. One of the major conclusions showed that the co-efficient of friction may change between the bearing surfaces, and varying corrosion current densities

can be measured at different co-efficient of friction, thereby altering the performance of biomaterials.

Effect of albumin used to model proteins - The contribution of albumin, which is used as to model protein, to the corrosion behavior of two bio-implantable materials has been reported by Valero Vidal and Igual Muñoz [2]. The results from their work showed that the influence of albumin on the corrosion properties of biomedical materials depend on the nature of the alloy. Albumin reduces the corrosion resistance of AISI 316L, but increases the corrosion resistance of the CoCrMo alloy. Despite the fact that the albumin adsorbed onto the surface of both alloys, the properties of the passive layer modified the effect of the albumin.

Effect of albumin and phosphate ions - Muñoz and Mischler [3] studied the interactive effect of albumin and phosphate ions on the corrosion behavior of a CoCrMo implant alloy. Their results showed that although phosphate ions act as anodic inhibitors and albumin acts as a cathodic inhibitor, the two species competitively adsorb onto the surface of the alloy, and form a metal/oxide/electrolyte interface.

Effect of metallic ions, exposure time and applied potential - The nature of the oxide film developed is dependent on factors such as the potential of the implant, nature of the electrolyte, time of exposure, etc. [88]. Hodgson *et al*. [89] characterized the nature of passive films formed on a CoCrMo alloy by studying the effect of exposure time and presence of ions in an *sbf*. Their results showed that passive film composition and the thickness of the CoCrMo alloy change with exposure time and potential. Also, the passive and transpassive behaviors of the alloy are dominated by chromium

(approximately 90% chromium oxides). Also, Hodgson *et al*. [89] reported that in the transpassive region, the change in oxide film composition is associated with an increased dissolution rate and all of the alloying elements dissolve according to the percentage composition of the alloy. The active dissolution behavior was dominated by cobalt (the base metal) under cyclic variations of applied potentials due to intermittent activation/repassivation cycles.

Effect of pH, chemical composition and aeration - The human body environment can be dynamic. Valero Vidal and Igual Muñoz [8] recently studied the behavior of a CoCrMo alloy under different experimental conditions in terms of the pH, chemical composition (PBS with and without bovine serum albumin (BSA)), and aeration (presence and absence of oxygen in the solution). The results from their work showed that general corrosion behavior depends on the pH because pH values above neutral exhibit a wide potential range of passivation. Also, the effects of the BSA and the aeration conditions are related to pH. Even though the negligible influence of BSA on the electrochemical behavior was observed at low pHs (about pH 3), an influence was observed at about pH 10, especially in the oxygenated solution. In terms of the effect of the PBS, $H_2PO_4^-$ favored the formation of passivating compounds which improved the resistance of the CoCrMo alloy to passive dissolution, thus indicating higher polarization resistance at higher phosphate ion concentrations. The effect of oxygen depended on the pH of the PBS solution, but reduced the passive dissolution resistance of the alloy in the studied condition.

Effect of carbide inclusions - High and low carbon CoCrMo alloys are the two cobalt based alloys mainly used in hip and knee prostheses. Lewis and Heard [90] studied the effect of carbides on the corrosion and dissolution of a CoCrMo alloy by immersing samples into PBS, synovial fluid and water respectively at 37^{o}C for 35 days. The findings in their work primarily showed that synovial fluid produces a thin oxide/hydroxide layer. Also, exposure of the CoCrMo alloy to synovial fluid produces the highest concentration of chromium and lowest concentration of cobalt. However, carbide inclusion did not have an effect on the corrosion and dissolution mechanisms, although the carbides were features on the metal surface.

Effect of corrosion on wear degradation - The release of ions through a corrosion process and nanoscale debris can seriously affect joint integrity [91]. An integrated study of the corrosion-wear interactions of high and low carbon CoCrMo alloys in serum, Dulbecco's modified Eagle's medium (DMEM) and 0.3% NaCl was carried out by Yan *et al*. [91]. In their approach to achieving the isolation of the wear components of degradation, cathodic protection (CP) was employed to completely stop charge transfers between the electrodes and the electrolyte. The work by Yan et al. [91] demonstrated that the biological nature of fluids affect the total degradation of CoCrMo alloys. More specifically, the effect of corrosion on tribocorrosion depended on the percentage of carbide inclusion and presence of proteins/amino acids in the CoCrMo alloy.

Effect of load and proteins - Some of the previous work have shown that increased load and articulations can increase the corrosion rate and metal ion release [92]–[94]. Mathew *et al*. [95] evaluated the corrosion and tribocorrosion behaviors of a low-carbon CoCrMo

alloy as a function of protein content and normal applied load in PBS and bovine calf serum (BCS). Their results showed that the presence of proteins improve corrosion resistance and passive behavior due to their generation of a protective boundary layer. However, in the presence of mechanical solicitation, there was an increase in passive film destruction. Therefore, when proteins and high normal loads are simultaneously present, they have a negative effect on the tribocorrosion behavior and increase the amount of material loss.

Effect of pH - Contu *et al*. [6] studied the influence of pH on the passive film formed on a CoCrMo alloy before, during and after mechanical disruption with a tribo-electrochemical cell in both serum and inorganic buffered solutions. Their results showed that irrespective of the solution type under consideration, the corrosion current density (and in turn, corrosion rate) measured is higher at an acidic pH than in a neutral pH. More importantly, the corrosion current recorded in the serum is lower than that observed in inorganic solutions at pHs of 4 and 7 respectively. Furthermore, the repassivation rate in the serum is higher at pH 7 than pH 4 in contrast to that in the inorganic solutions. According to their work, this explains the suppression of cobalt-oxide precipitation in the serum, which allows the undisturbed formation of the protective chromium -oxide film on the alloy surface [6].

Effect of solution chemistry, sliding conditions and applied potential - Gil and Muñoz [96] recently immersed an as-cast high carbon CoCrMo alloy into 100% PBS and 50% PBS + 50% BSA, with the aim to study the influence of the solution chemistry, sliding velocity (between 6 and 60 mm/s) on articulating surfaces and applied potential on the

corrosion and tribocorrosion behaviors of the CoCrMo alloy. Their results showed that anodic current density increases with sliding velocity, but the wear rate does not change at the applied potential. On the other hand, the BSA modifies the wear behavior (by agglomerating the debris formed by mechanical removal of particles), thus increasing the mechanical wear volume. Under cathodic conditions, the cathodic current density also increases during mechanical contact while the wear rate decreases with sliding velocity, and the BSA lubricates the contact, thus reducing the total wear volume with respect to the non-containing BSA solution. The work showed how electrode potentials critically affect corrosion and tribocorrosion rates by increasing the wear coefficients at applied anodic potentials due to severe wear accelerated corrosion.

Effect of solution type on thickness of oxide layer - In order to understand the influence of solution type on the thickness of the passive film formed, Lewis and Heard [97] immersed a CoCrMo alloy into human serum, fetal bovine serum (FBS), synovial fluid and a water solution for 5 days. Their results showed that the measured oxide/hydroxide layer is varied with solution type, an indication that solution type plays a role in the thickness of the passive film formed.

Influence of head size (28 & 36 mm) and production route – A retrieval analysis of an explanted artificial hip prosthesis was used for macroscopical assessment by eye with the aim of studying the influence of head size on corrosion and fretting damage at the head-neck interface [98]. It was observed that larger head sizes suffer more corrosion damage. It was reported that larger head sizes create larger torques that act along the taper joints, and lead to greater micro-motion between the head and the neck. It was also reported that

this micro-motion contributes to the deterioration of oxide films along the taper joints. Also, the same production route (source) has similar corrosion and fretting damage.

In the concluding remarks of this review, it can be said that continuous research and improvements in wear, corrosion and wear-corrosion synergy give a clear indication that an ideal artificial hip is still yet to be created. This is because CoCrMo alloys as a metallic bio-implantable material release potentially harmful ions; ceramic implants are susceptible to fractures; and polyethylene implants yield high amounts of wear debris that can lead to adverse tissue reactions [56]. With the ever increasing need for a longer lasting artificial hip, especially in younger patients, more long term studies need to be conducted and the bio-functionality and bio-compatibility of new materials need to be assessed to improve the success rate of artificial hips. To this end, a multidisciplinary research approach that involves material, biomedical and mechanical engineers, medical experts, etc. who can study the phenomena at the macroscopic, microscopic and nano-levels, will give more insight into the holistic understanding of this subject.

3 MATERIALS AND METHODS

3.1 Experimental plan

In this work, the three lubricants (0.14 M NaCl, PBS and novel *sbf*) used were prepared in accordance with ASTM F732. An electrochemical study was conducted by using potentiodynamic polarization and potentiostatic polarization scanning. In characterizing the nature of the passive film formed, EIS and XPS were carried out. The dissolved ionic species were analyzed by using ICP-MS. Film thickness was characterized by using Augur electron spectroscopy (AES). The study on fretting corrosion was performed by using a pin-on-disc (PoD) wear simulator while post experimental surface imaging and wear particle analysis were carried out by using a scanning electron microscope (SEM) and transmission electron microscope (TEM).

3.2 Materials

3.2.1 Test specimens

The material investigated in this thesis work is a medical grade CoCrMo alloy which conforms to ASTM F1537 and was obtained from Firth Rixson Metals Ltd. The average nominal composition of the alloy corresponded to ISO 5832-12, with an average grain size of 5 µm. In the case of the pure corrosion tests, all of the samples used were 8 mm in thickness and embedded into a bakelite mount so that only 0.713 mm^2 was directly exposed to the electrolyte. The samples were grinded down to 1200/1400 grit with silicon carbide (SiC) emery paper and polished to 1 µm prior to each electrochemical experiment. The samples were rinsed in an ultrasonic ethanol bath for 10 minutes at each stage of the grinding and polishing process before the experiment. Furthermore, the

polished samples were immediately assembled and transferred into a measurement cell filled with electrolyte. For the fretting corrosion tests, the samples were received as pins with a diameter of 9.5 mm and discs with a diameter of 38.1 mm. The pin and disc samples supplied had an average surface roughness (R_a) of 0.051 and 0.0125 µm, respectively. The discs were flat, while the pins had an out-of-roundness value of 0.014 mm. The average weight of the pins and discs was 10.74 and 117.08 g, respectively. The carbon content in the CoCrMo alloy was on average 0.05% and assumed to be uniformly distributed in the matrix and also to have no contribution to the dissolution mechanism of the alloy [97].

3.2.2 Physiological environment

The novel *sbf* used as the electrolyte is a serum based fluid that primarily consists of albumin, α1-, α2-, β- and γ-globulins, PBS, sodium hyaluronate, ethylenediaminetetra acetic acid (EDTA) and antibiotic/antimycotic (AA), with an average protein constituent of 30 g/L and clinically relevant osmolality levels and thermal stability [15]. The AA solution which contained penicillin, streptomycin and fungizone (amphotericin) was added to prevent microbial growth. A comparison of the electrochemical behavior of the CoCrMo alloy was made by using 0.14 M NaCl and PBS solutions. Unless otherwise stated, all of the experiments were performed at a pH of 7.4±0.05 which was adjusted with drops of diluted hydrochloric acid and sodium hydroxide solutions. All of the electrolytes were of analytical grade and prepared by using distilled water. All of the lubricants used were prepared in accordance with ASTM F732. The temperature of the solution was stabilized at 37^{o}C by using a temperature regulated water bath, unless otherwise stated.

3.3 Testing equipment and methods

3.3.1 Potentiostatic and potentiodynamic polarization

Potentiostatic and potentiodynamic polarization scans can be used to gather electrochemical information, such as the corrosion rate, pitting susceptibility, passivity as well as cathodic behavior of an electrochemical system. For both polarization scans in this work, the ionic conduction path was provided by using the solution (electrolyte) that separated the working and counter electrodes, while the electrical conduction path was provided by using potentiostat equipment. The potentiostat was then used to control the driving force for electrochemical reactions that took place on the working electrode (CoCrMo specimen). Potentiodynamic polarization scanning was carried out on the CoCrMo specimen to understand the electrochemical behavior from cathodic to anodic potentials.

All of the experiments were performed by using Versastudio, which is software from Princeton Applied Research. The three-electrode electrochemical set-up included the carbon rods as the counter electrodes, saturated calomel electrode (SCE) (sat'd KCl) as the reference electrode and the CoCrMo specimen as the working electrode. All of the sample specimens were left in the electrolyte for a period of 30 minutes to ensure stabilization of the OCP. All potential measurements were made with reference to the SCE. All of the experiments were repeated a minimum of two times to ascertain reproducibility of the results. The potentiodynamic potential scan rate utilized was 1 mV/s and scanning was performed from a cathodic potential of -1.5 V to an anodic potential of 1.5 V. The experiment was carried out in an aerated environment. The

corrosion potential (E_{corr}) and corrosion current density (i_{corr}) were directly extracted from the polarization plots by using the Versastudio software through Tafel slope extrapolation. The potentiodynamic polarization test was used to study the influence of passivation time and pH on the electrochemical behavior of the CoCrMo alloy in all of the corrosion media under consideration, while the potentiostatic polarization test was carried out to characterize the influence of applied potential and passivation time on the nature of the passive film formed in the clinically relevant *sbf* environment. All of the potentiostatic polarization scans were performed at static applied potentials of -0.1 V and 0.4 V respectively, depending on the specific tests, which were well within the passive potential range of the CoCrMo alloy in all of the corrosion media under consideration.

3.3.2 Electrochemical impedance spectroscopy

EIS measures the dielectric properties of a medium as a function of frequency. It is based on the interaction of an external field with the electric dipole moment of the sample. The EIS technique was used to characterize the mechanism of passive film formation on the CoCrMo implant material by measuring the impedance of the system over a range of frequencies (and therefore the frequency response of the system), energy stored, and dissipation properties. The data obtained were graphically expressed in Bode and yquist plots. The EIS was performed on prepared samples in 0.14 M NaCl, PBS and the novel sbf solution to investigate the charge-transfer kinetics at the film/electrolyte interface. All of the EIS tests were performed at OCP after an immersion time of 60 minutes to allow for stabilization of the OCP. All of the measurements were performed at 10 mHz up to 10^5 mHz, at 10 data cycles/dec with an AC amplitude of $\pm$10 mV. Attempts were not

made to fit the data into an equivalent model since the technique was mainly used to gain a qualitative understanding of the difference in the charge-transfer kinetics of the passive film layer in the three different corrosion media considered.

3.3.3 Surface and particle analysis

The electron microscope (EM) uses an electron beam to illuminate a specimen and produce a magnified image. It has greater resolving power than a light microscope and can reveal the structure of smaller objects because electrons have wavelengths about 100,000 times shorter than visible light photons. EMs find applications in a wide range of biological and inorganic specimens, including microorganisms, cells, large molecules, biopsy samples, metals, and crystals. The SEM is a type of EM which produces images of a sample through scanning with a focused beam of electrons. The electrons interact with the atoms in the sample, thus producing various signals that can be detected and contain information about the surface topography and composition of the sample.

The TEM (also a type of EM) uses a high voltage electron beam to create an image. The electron beam is produced by an electron gun, commonly fitted with a tungsten filament cathode as the electron source. The electron beam is accelerated by an anode typically at +100 keV (40 to 400 keV) with respect to the cathode, focused by electrostatic and electromagnetic lenses, and transmitted through the specimen that is in part transparent to the electrons and in part scatters them out of the beam. When it emerges from the specimen, the electron beam carries information about its structure that is magnified by the objective lens system of the microscope. An important mode of TEM utilization is the electron diffraction mode. In this study, a SEM equipped with a energy-dispersive X-ray

spectroscope and TEM are used to view sample surfaces after pure corrosion and fretting corrosion tests. For high resolution surface investigations and composition analysis, imaging was carried out by using both backscattered electron imaging (BEI) and secondary electron imaging (SEI) modes at an accelerating voltage of 20 keV. An approximate working distance of 10 mm was used throughout the measurements. For the composition analysis of the post test surfaces, an energy-dispersive X-ray (EDX) spectroscopy analysis was carried out by using INCA software. A TEM was used to characterize the wear particle shape, size, and composition. The wear particle diffraction pattern was also characterized after fretting tests by using a TEM.

3.3.4 X-ray photoelectron spectroscopy

XPS, also known as electron spectroscopy for chemical analysis (ESCA) is a surface-sensitive quantitative spectroscopic technique used to measure the elemental composition, empirical formula, and chemical and electronic states of the elements that exist within a material. XPS spectra are obtained by irradiating a material with a beam of X-rays while simultaneously measuring the kinetic energy and number of electrons that escape from the top 0 to 10 nm of the material being analyzed. This surface chemical analysis technique was used to analyze the passive film composition of the post-treated CoCrMo implant material. The CoCrMo samples used for this study are 2 mm in thickness with an exposed surface area of 0.713 sqcm. The samples were passivated at -0.1 V by potentiostatic polarization equipment in 0.14 M NaCl, PBS and *sbf*. Other samples were also passivated at -0.1 V and 0.4 V for 3 minutes and 60 minutes respectively only in the novel *sbf*. This test was performed to understand the influence of

passivation potential and time on the composition of the passive film formed on the CoCrMo alloy in the novel *sbf*.

After electrochemical preparation, the samples were carefully rinsed in doubly distilled water and dried with a jet of purified argon, before transferring them into a chamber for surface analysis. XPS analysis was carried out on an Axis Ultra ^{DLD} X-ray photoelectron spectrometer with an Al Ka (1486. eV) monochromatic source at base pressures less than 10^{-8} Torr and with a perpendicular take-off angle. A hybrid lens mode was used with the slot aperture at pass energy of 160 eV. For the survey spectra, a survey scan was executed between a binding energy of 0 and 1200 eV. For the high resolution scan, a hybrid lens mode was used with a slot aperture at pass energy of 20 eV. High resolution scans were recorded for C 1s, O1s, N 1s, Cr 2p, Co 2p and Mo 2p. The energy shift due to the surface charge was corrected with C 1s which has a binding energy of 285 eV. Peaks were fitted (Gaussian/Lorentzian curves) after background subtraction with CasaXPS® software. XPS analysis performed at different locations showed comparable results, which verified the homogeneity of the samples.

3.3.5 Augur electron spectroscopy

AES is an analytical technique that uses a primary electron beam to probe the surface of a solid material. It is based on the analysis of energetic electrons emitted from an excited atom after a series of internal relaxation events. Secondary electrons that are emitted as a result of AES are analyzed and their kinetic energy is determined. The identity and quantity of the elements are determined from the kinetic energy and intensity of the Auger peaks. A JEOL JAMP-9500F field emission Auger microscope was used for depth

profiling of the passive layer. An accelerating voltage of 10 KeV, aperture of 30 µm, start voltage of 20 eV and stop voltage of 2000 eV were used during the experiment. Additionally, the sample was titled 30° during the Auger analysis and the Auger data were processed on Auger Master Software. The passivation of the AES samples was carried out under OCP conditions by immersing the samples into the respective electrolytes for 12 hours at 37^0C.

3.3.6 Inductively coupled plasma mass spectroscopy

ICP-MS is a mass spectrometry technique capable of detecting ionic concentrations of metals (and non-metals) up to (and beyond) parts per billion. This is achieved by ionizing the sample with inductively coupled plasma and then using a mass spectrometer to separate and quantify the ions. This technique is fast, precise and sensitive, although it also has susceptibility to continuations and interference from glassware and the presence of other ions. In this work, the concentration of metallic ions released into the solution as products from corrosion are determined in ppb (µg/L) by using a Perkin Elemer ELan II inductively coupled plasma-mass spectrometer.

ICP-MS tests were carried out at the Ultra-Clean Trace Elements Laboratory (UCTEL) at the University of Manitoba. Blanks were freshly prepared daily by using a Millipore Element water purification system. Standards and blanks were acidified with trace metal grade nitric acid to 0.5% by volume. The isotopic mass numbers used were Co 59, Cr 52, and Mo 98. Similar to the potentiodynamic tests, all of the samples had a surface area of 0.713 sqcm, and a surface finish of 1 µm. The samples were washed in an ultrasonic water bath for 10 minutes at every stage of the grinding and polishing prior to the

experiment. High density polyethylene (HDPE) bottles used for the electrochemical tests were carefully cleaned with 10 vol.% concentrated HNO_3 solution and thoroughly rinsed with ultrapure de-ionized water to remove impurities. The experiments were repeated twice to ascertain reproducibility. All of the bottles were thoroughly agitated in order to homogenize the solution immediately before the ion analysis was carried out.

3.3.7 Pin-on-disc testing

The PoD tribometer can be used to measure the tribological quantities, such as coefficient of friction, friction force, and wear volume, between two surfaces in contact. The PoD simulates wear, friction and lubrication which are the objects of study in tribology. This simulation can be unidirectional or multidirectional, depending on the input settings and desired output. It consists of a stationary pin under an applied load in contact with a moving disc. The pin can have any shape to simulate a specific contact, but spherical tips are often used to simplify the contact geometry. In orthopedic applications, PoDs have been applied to closely reproduce motions and forces that occur in the hip and knee joints by performing accelerated wear tests of artificial implant products [99].

In this work, the PoD experiment was divided into two primary tasks. The first part of the PoD testing was performed dry (without the use of any lubricant), while a clinically relevant serum based novel fluid was used as the lubricant for the second part of the experiment. Testing was stopped at intermittent cycles of 0.01, 0.1, 0.5 and 1.0 Mc to take measurements and replenish the lubricant. The lubricant levels were regularly monitored for evaporation and to ensure that a minimum volume of lubricant was always present at all times during the experiment. These stops were also useful to reduce the

effect of protein degradation on wear. Gravimetric and wear rate measurements, wear appearance observation, wear surface profiles, and wear particle analysis were all performed at each intermittent stop. With focus on simulating fretting corrosion damage at the modular head/neck and neck/stem interfaces, a unidirectional wear path of 1 mm was considered. All of the experiments were performed at an applied load of 330 N, frequency of 2 Hz, temperature of 37^0C, and all of the pins and discs were mounted into the PoD wear station at the same orientation after each intermittent stop.

4 RESULTS

4.1 Electrochemical characterization

By comparing the potentiodynamic polarization plots of the CoCrMo alloy at room temperature and 37^0C, the initial stage of this experimental work justifies the need to conduct all of the other experiments at 37^0C, which corresponds to the human body environment. Figures 4.1, 4.2 and 4.3 are comparisons of the corrosion rate of the CoCrMo alloy in 0.14 M NaCl, PBS and *sbf*, under room conditions and at 37^0C respectively. The OCPs, E_{corr}, i_{corr}, i_{pass}, i_{crit}, and E_{pp} obtained from potentiodynamic polarization in these different environments are presented in Figures 4.4 and 4.5. From the results obtained, the corrosion current density (i_{corr}) increases with temperature by 59%, 49% and 16% in 0.14 M NaCl, PBS and *sbf* respectively.

Furthermore, as the temperature increases, the presence of phosphate ions, serum and protein compounds forces the OCPs to more cathodic potentials. The reverse was observed in a purely saline solution. However, for all the solution types considered, a lower critical anodic current density (i_{crit}) was recorded; this corresponded to easier passivation at room temperature, compared to 37^0C. A greater difference between the passive anodic current density (i_{pass}) and the critical anodic current density (i_{crit}) means more effective passive oxides formed [24]. At 37^0C, the passive oxides formed in all of the solution types are more effective, while the least effective passive film is formed with the CoCrMo alloy in 0.14 M NaCl at room temperature.

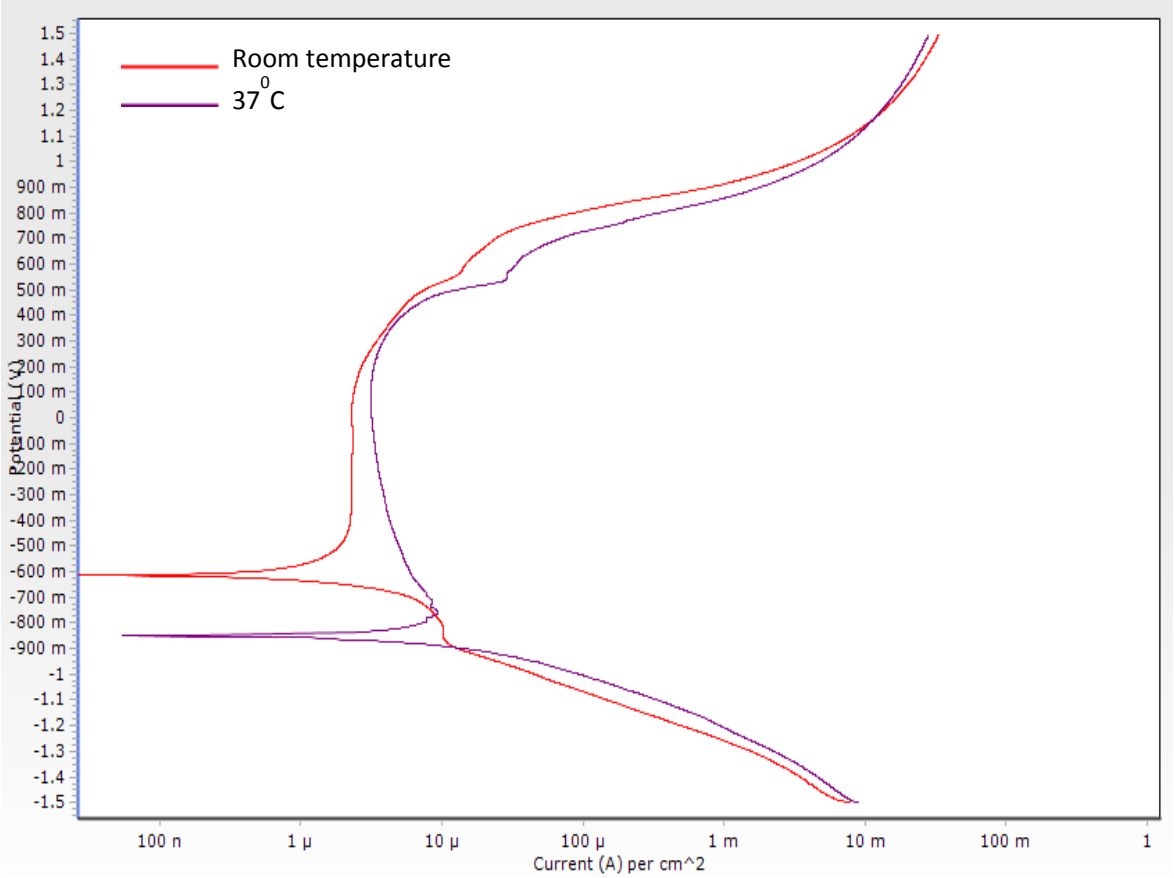

Figure 4.1: Potentiodynamic polarization plot of CoCrMo alloy in 0.14 M NaCl

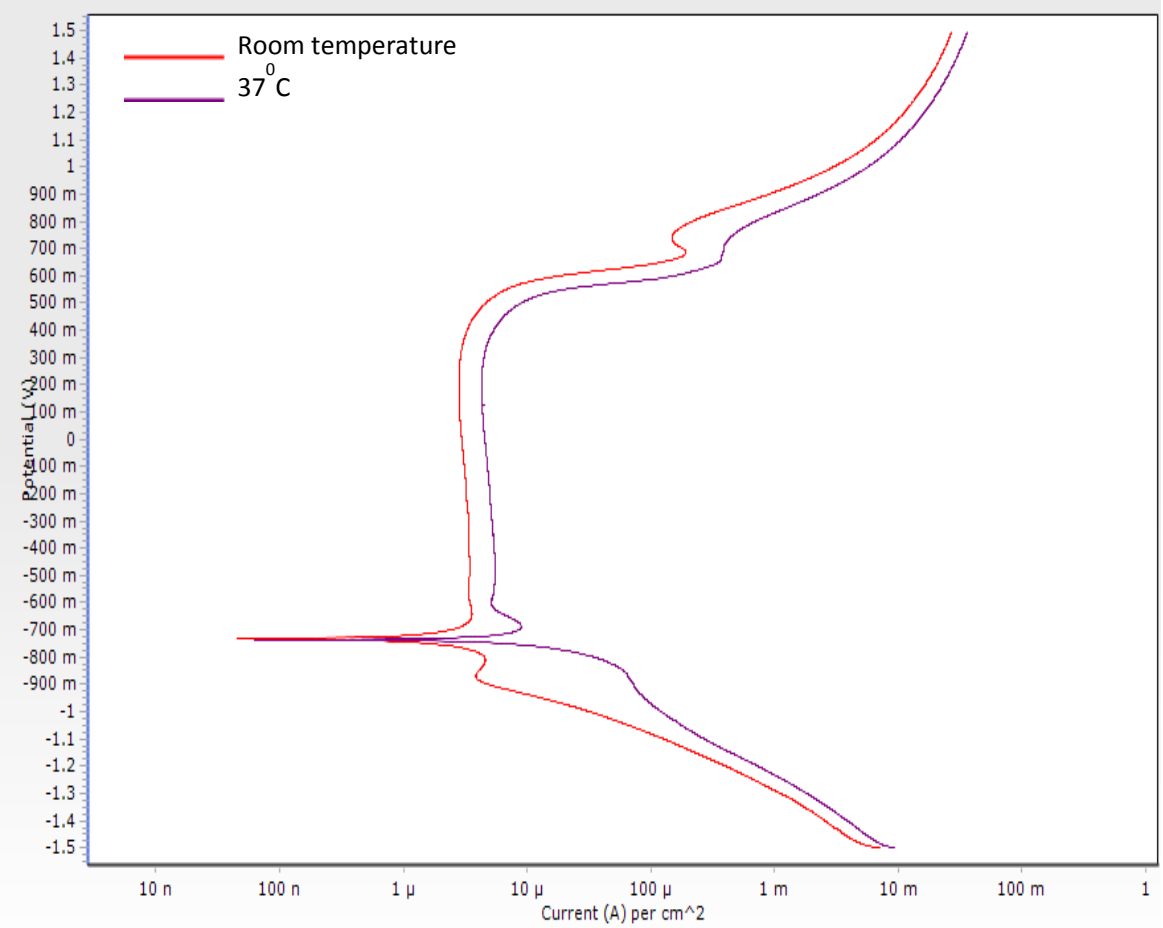

Figure 4.2: Potentiodynamic polarization plot of CoCrMo alloy in PBS

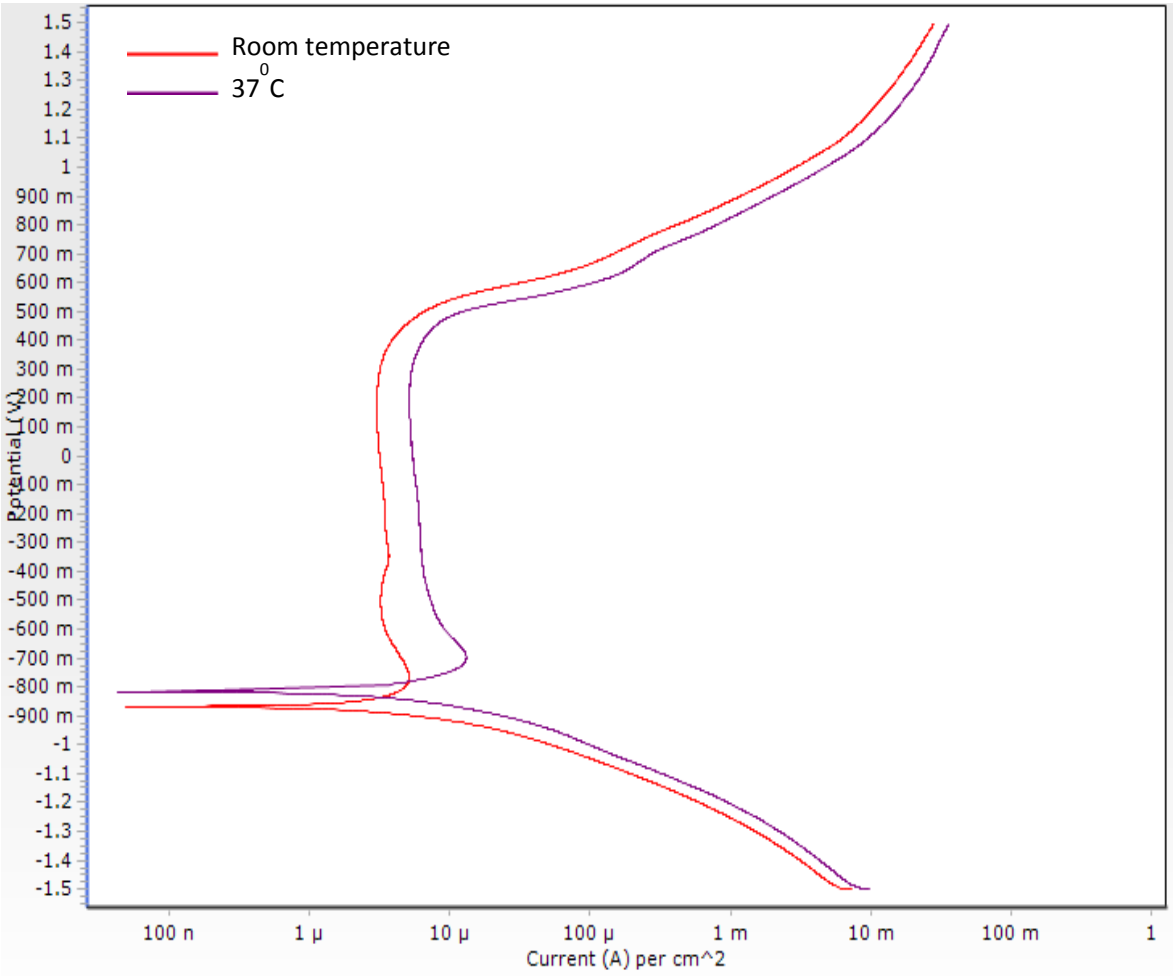

Figure 4.3: Potentiodynamic polarization plot of CoCrMo alloy in sbf

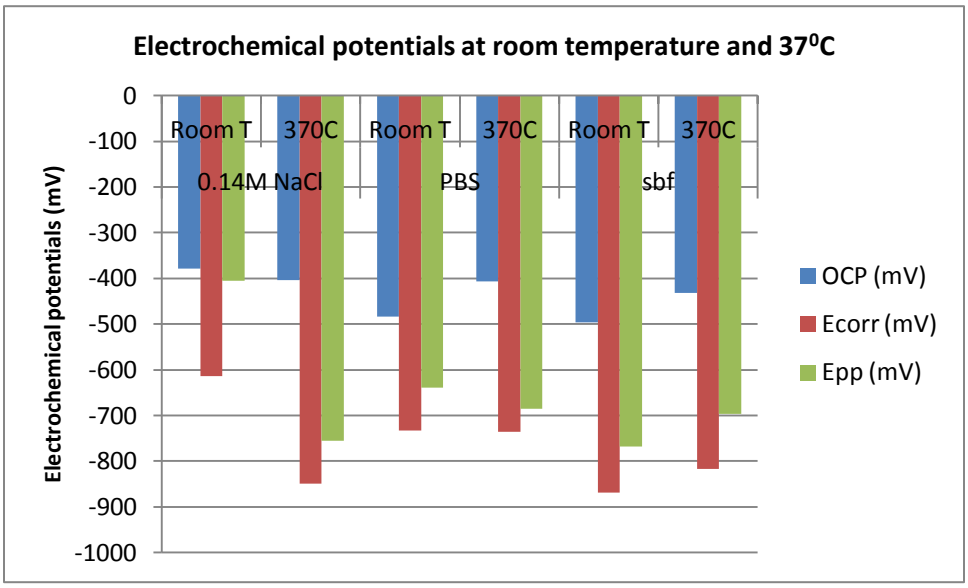

Figure 4.4: OCPs, E_{corr}, and E_{pp}, at room temperature and 37^0C in 0.14 M NaCl, PBS and *sbf*

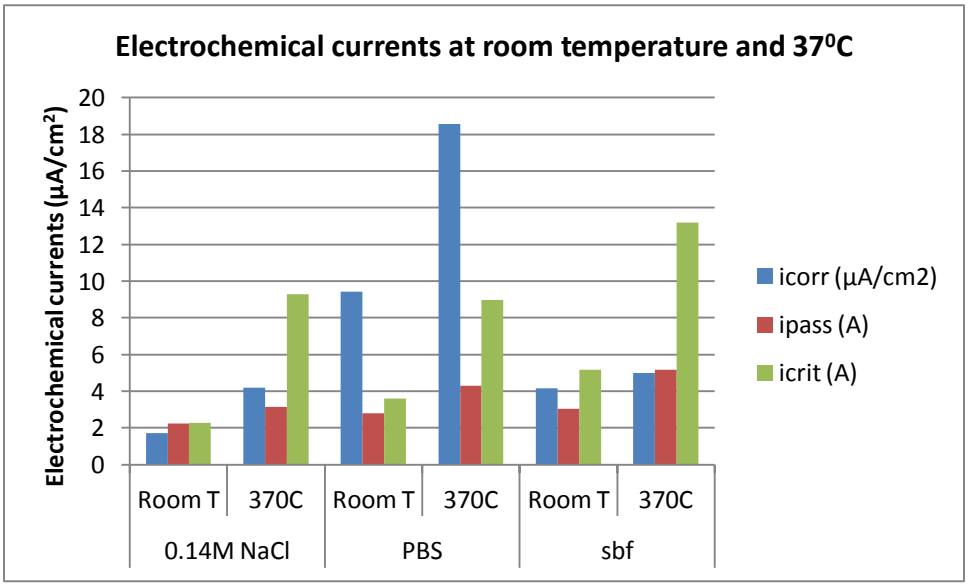

Figure 4.5: i_{corr}, i_{pass}, and i_{crit} at room temperature and 37^0C in 0.14 M NaCl, PBS and *sbf*.

There was no change in the passive potential range in all of the solution types considered with temperature, and this may have been attributed to the fact that a lower passive anodic current density (i_{pass}) was measured at room temperature. However, despite the lower passive anodic current density (i_{pass}) at room temperature and increase in the corrosion rate at 37^0C, the primary passive potential (E_{pp}) was quickly attained within an increase of 11%, 6.9% and 14.6% of the corrosion potential (E_{corr}) in 0.14 M NaCl, PBS and *sbf* solutions at 37^0C respectively. This makes the alloy more suitable for use at 37^0C, as compared to room temperature. Afterwards, all of the electrochemical experiments were conducted at 37^0C under different solution conditions.

4.1.1 Influence of solution type on electrochemical behavior

ELECTROCHEMICAL EXPERIMENTS - In all of the physiological media under study, the potentiodynamic polarization results (Figure 4.6) showed four distinct regions [5]. First, the cathodic domain included potentials below -700±10 mV for all of the solution types employed. Here, the current is determined by the reduction of water and partially dissolved oxygen [48]. Also, in the PBS solution, cathodic polarization scan showed two cathodic reactions that were inhibited by concentration polarization. Second, the transition domain was characterized by the change from cathodic to anodic potential at a corrosion potential (E_{corr}) of -850±10 mV, -820±20 mV, and -720±20 mV in 0.14 M NaCl, PBS and *sbf* solutions, respectively. Here, the current density measured that corresponded to the corrosion potential (E_{corr}) is the corrosion current density of the alloy in each media. As obtained from the Tafel extrapolation, the CoCrMo alloy in the PBS solution has the highest corrosion current density (i_{corr}) of 18.57 μA/cm^2, up to 300% times the corrosion current density (i_{corr}) observed in 0.14 M NaCl and *sbf*.

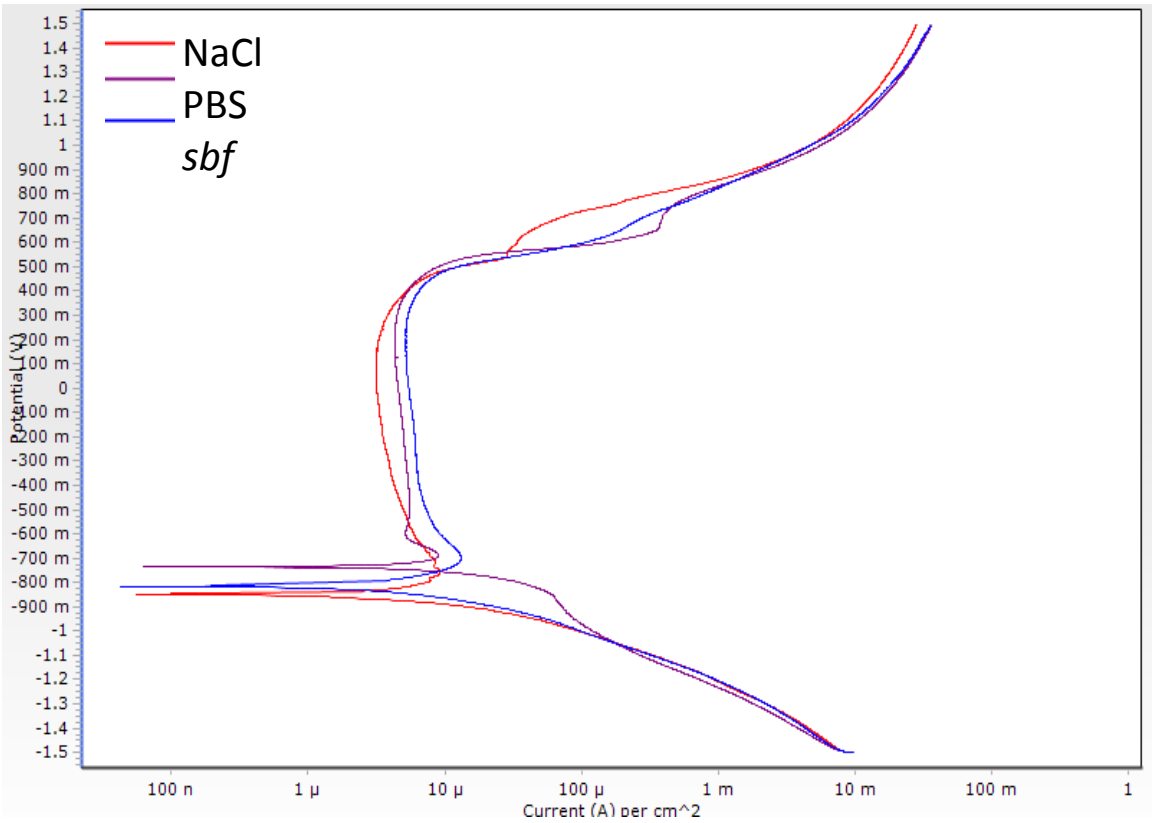

Figure 4.6: Potentiodynamic polarization scan of CoCrMo alloy in different solution types

The CoCrMo alloy in 0.14 M NaCl and *sbf* has comparably low corrosion current densities (i_{corr}) of 4.21 and 4.98 µA/cm^2 respectively. This may have been due to the high concentrations of free acid radials of $H_2PO_4^{2-}$ and HPO_4^{2-} that formed in the presence of the phosphate ions in the PBS solution, thereby catalyzing the cathodic reduction of water [7]. Third, in all of the solutions considered, a fairly constant current density (passive anodic current density, i_{pass}) was observed within a potential domain of 480±20 mV and -600±20 mV. Potentials within this range defined the passive potential that formed a passive film which protected the alloy from electrochemical degradation. Fourth, beyond the passive domain, a transpassive domain was observed at a range around and above 480±20 mV. Here, the passive oxide film breaks off and the electrode is governed by the Butler-Volmer equation, where the current exponentially rises with voltage away from the half-cell potential [34], primarily related to the breaking off of the oxide film, thus resulting in the formation of Cr^{3+} and Cr^{6+} ions [7], [48], [89].

In the PBS environment only, the peak observed in the transpassive region is attributed to the formation of Cr^{3+} and Cr^{6+}. This finding is in agreement with previous work [7], [89]. Equations 4.1-4.2 show the oxidation reaction of Cr_2O_3 into Cr_4^{2-} [7].When compared with 0.14 M NaCl, the presence of phosphate ions in PBS shifted the corrosion potential to a more anodic value and also increased the corrosion current density. However, in the novel *sbf* environment, the effect of phosphate ions was negated or palliated, perhaps by the presence of proteins and organometallic complexes in the serum based compound [100]. Similar to the findings of Muñoz and Mischler [3], the addition of albumin to the phosphate saline solution suppressed the influence of the phosphate ions and pushed the OCPs and corrosion potentials (E_{corr}) to more cathodic potentials, thereby reducing the

corrosion rate to clinically acceptable rates. Furthermore, the difference in critical anodic current density (i_{crit}) and passive anodic current density (i_{pass}) defined the effectiveness of the passive film formed. The current results show that the nature passive film formed in the *sbf* environment is more effective than that in other solution types. This is because *sbf* has the highest difference of 8.0 µA/cm^2, while 0.14 M NaCl and PBS have differences of 4.68 µA/cm^2 and 6.13 µA/cm^2 respectively. Conversely, the passive film most easily formed in 0.14 M NaCl because it has the lowest passive anodic current density (i_{pass}) of 3.145 µA/cm^2, compared to PBS and *sbf* which have passive anodic current densities (i_{pass}) of 4.292 µA/cm^2 and 5.177 µA/cm^2 respectively.

$$2Cr + 6OH^- \xrightarrow{yields} Cr_2O_3 + 3H_2O + 6e^- \quad (4.1)$$

$$Cr_2O_3 + 10OH^- \xrightarrow{yields} 2CrO_4^{2-} + 5H_2O + 6e^- \quad (4.2)$$

4.1.2 Influence of immersion time on electrochemical behavior

In 0.14 M NaCl solution: The 0.14 M NaCl solution comprises a simplified composition of the human body environment. Polarization plots obtained at different immersion times in the 0.14 M NaCl solution showed a relatively spontaneous formation of the passive film (Figure 4.7). As the immersion time increased, the OCP measured moved to more anodic potential (Figure 4.8), while the corrosion potential (E_{corr}) stabilized to -840±30 mV after 30 minutes of immersion time. Also, the corrosion current density (i_{corr}) increased with immersion time.

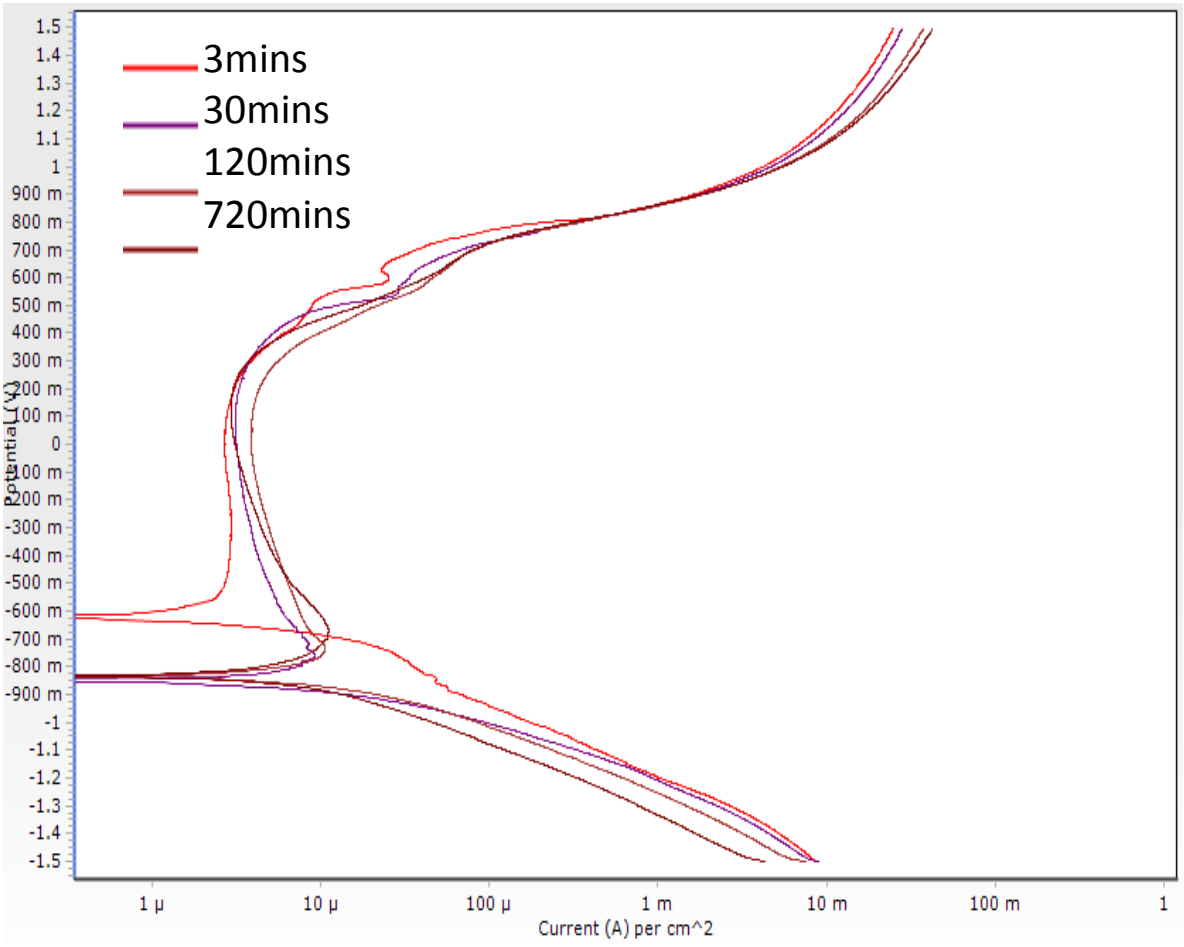

Figure 4.7: Potentiodynamic polarization plot of CoCrMo alloy in 0.14 M NaCl; effect of immersion time.

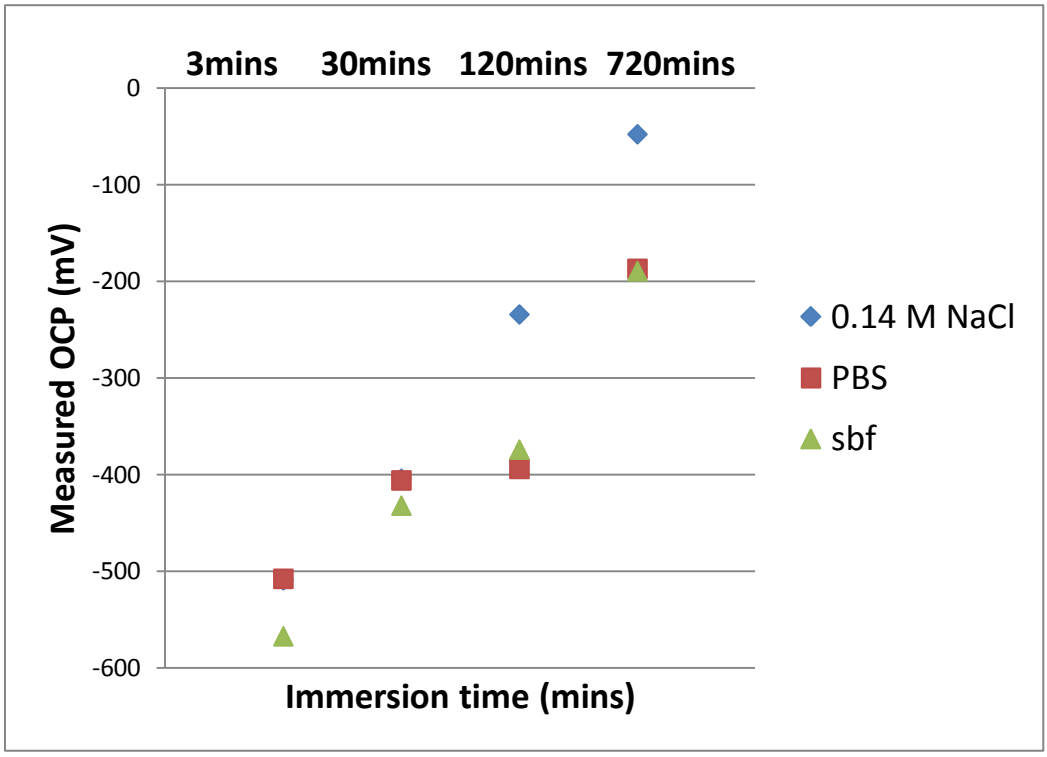

Figure 4.8: Influence of immersion time on measured OCP

For immersion times less than 30 minutes, there was an observable ease in the passivation of the CoCrMo alloy as compared to longer immersion times, although as the immersion time increased, more effective passivation of the oxide layer was observed. This is because the passive anodic current density (i_{pass}) was lower than the critical anodic current density (i_{crit}); a necessary requirement for the effective formation of passive oxide film [24].

In PBS: The potentiodynamic polarization plots of the CoCrMo alloy at different immersion times in PBS are presented in Figure 4.9. The result is in good agreement with the work of Ouerd *et al*. and Hodgson *et al*. [7], [89], who measured the corrosion current density of a CoCrMo alloy in a PBS solution. A slight increase in applied potential above the corrosion potential (E_{corr}) showed a sharp decrease in the corrosion current density, which indicates the instantaneous formation of a protective passive layer on the surface of the CoCrMo alloy upon exposure to the solution [3], [5], [11], [48], [89], [96]. This was observed for all of the immersion time. In the transpassive region, the breaking off of the passive film, which led to the formation of complex ions (e.g. $Cr^{3+}$and Cr^{6+}) in the presence of the phosphate ions was observed to be a shoulder-like nose [48], [89]. A fairly constant critical anodic current density (i_{pass}) and an increasing passive anodic current density (i_{crit}) were observed with increasing immersion time. Also, the effectiveness of the passive film formed increased with immersion time as the difference between the passive anodic current density (i_{pass}) and the critical anodic current density (i_{crit}) increased with exposure time.

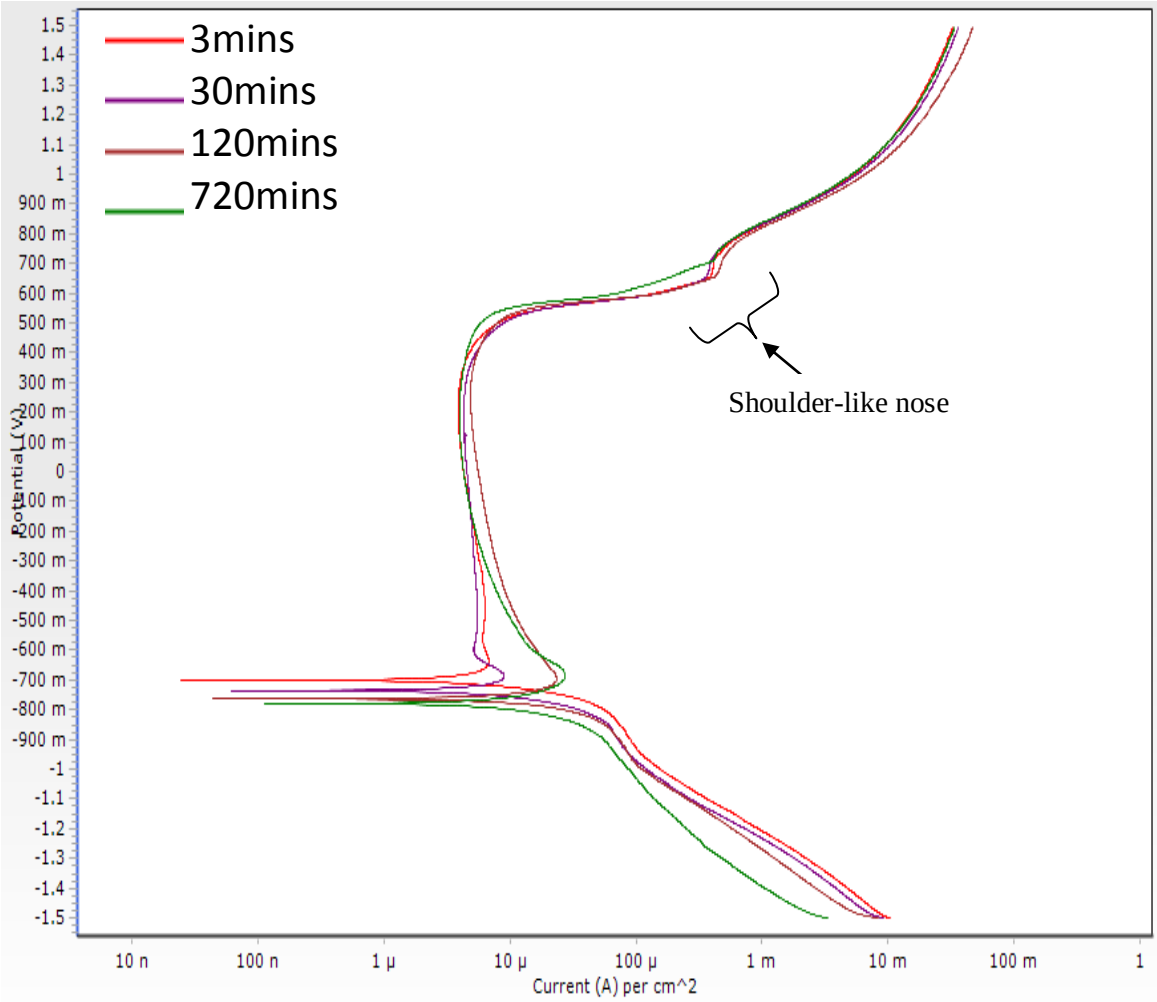

Figure 4.9: Potentiodynamic polarization plot of CoCrMo alloy in PBS; effect of immersion time.

In sbf: The potentiodynamic polarization plots of the CoCrMo alloy in *sbf* at different immersion times are presented in Figure 4.10. The computation of the corrosion current density (i_{corr}) showed a low corrosion rate; however, this corrosion rate increased with immersion time. The corrosion rates measured in the *sbf* were comparable with those measured in 0.14 M NaCl. This indicates that the presence of proteins and serum in the body environment palliates the effect of the phosphate ions in the body fluid.

However, for design, testing and validation purposes, 0.14 M NaCl may not be a good replacement because the corrosion mechanism and corrosion products formed may differ from those observed in 0.14 M NaCl. In the *sbf*, the CoCrMo alloy was easy to passivate as the critical anodic current density (i_{crit}) was just slightly higher than the passive anodic current density (i_{pass}). As the immersion time increased, the difference between the critical anodic current density (i_{crit}) and the passive anodic current density (i_{pass}) steadily increased, thus signifying that a more effective passive layer formed with immersion time. Similar to observations of 0.14 M NaCl and PBS, the measured OCP increased with immersion time (Figure 4.8) while the corrosion potential (E_{corr}) computed converged to a fairly constant value with immersion time.

4.1.3 Influence of pH on electrochemical behavior

After the electrochemical experiments were performed at a pH of 7.4, further experiments were performed at pH 4.0 to understand the influence of the pH on the electrochemical behavior of the CoCrMo alloy in 0.14 M NaCl, PBS and the novel sbf respectively.

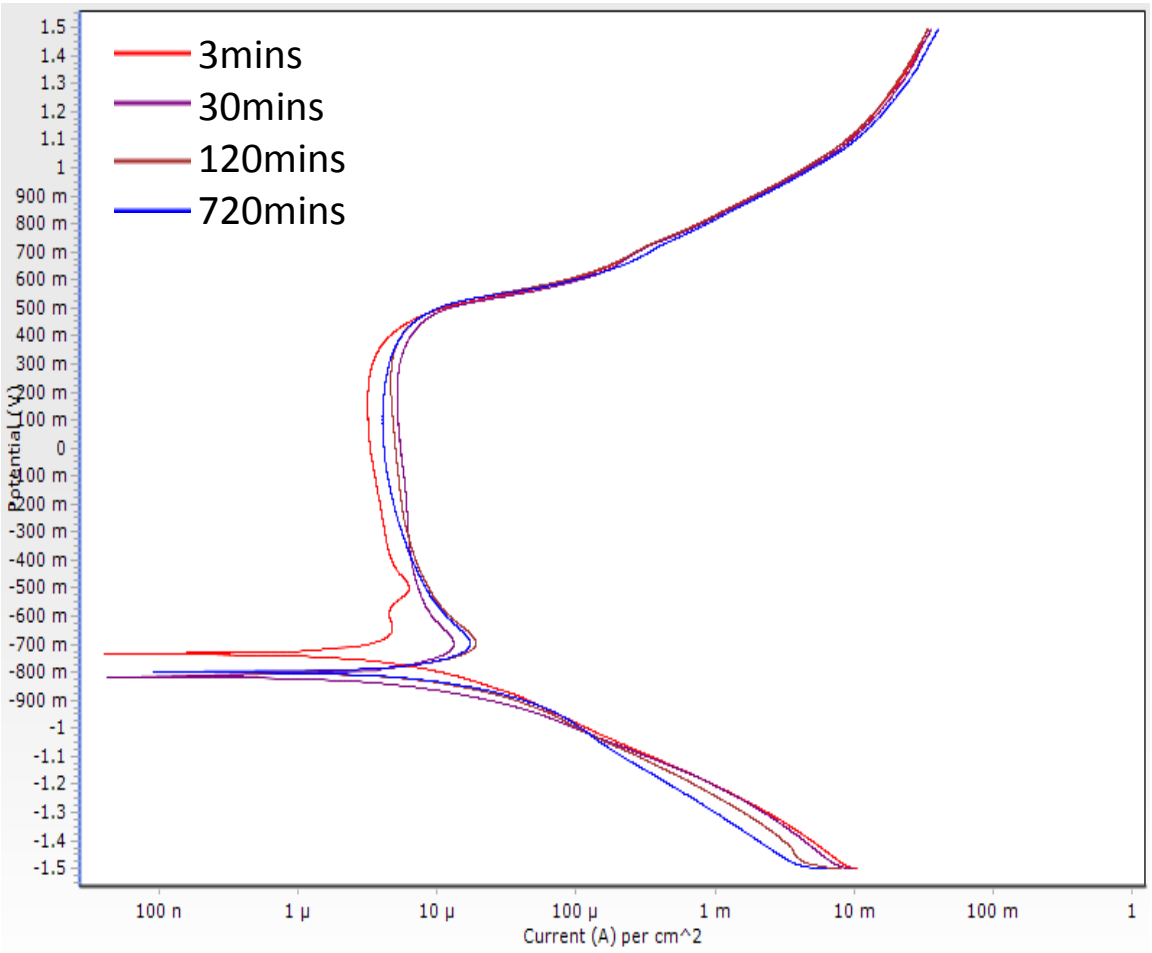

Figure 4.10: Potentiodynamic polarization plot of CoCrMo alloy in *sbf*; effect of immersion time

In 0.14 M NaCl: Figure 4.11 shows the potentiodynamic polarization plot of the CoCrMo alloy in 0.14 M NaCl at pHs of 7.4 and 4.0 respectively. The results show that the increase of hydrogen ion concentrations at pH 4.0 shifted the OCPs and corrosion potentials (E_{corr}) to more anodic potentials. Although the CoCrMo alloy exhibits a higher corrosion current density in 0.14 M NaCl at pH 7.4, a wider potential range of active dissolution of the alloy was recorded at a pH of 4.0. This means that more of the alloying element species may have gone into the solution under acidic pH conditions.

In terms of the effectiveness of the passive film formed, 0.14 M NaCl at pH 7.4 exhibits a more effective passive film due to a lower passive anodic current density (i_{pass}) and a wider passive potential range (E_{pp}) measured as compared to those at pH 4.0. The lower critical anodic current density (i_{crit}) and passive potential (E_{pp}) measured at pH 7.4 also makes it easier to form the passive film as opposed to pH 4.0. However at pH 4.0, the CoCrMo alloy has the highest active dissolution-passivity because the largest difference of 255.191 mV was shown between the measured primary passive potential (E_{pp}) and corrosion potential (E_{corr}), as compared to the CoCrMo alloy in 0.14 M NaCl at pH 7.4 which has a primary passive potential (E_{pp}) of 93.803 mV.

In PBS: Figure 4.12 shows the potentiodynamic polarization plot of the CoCrMo alloy in PBS at pHs of 7.4 and 4.0 respectively. Similar to the CoCrMo alloy in 0.14 M NaCl solution, a more acidic pH value has made the OCPs and corrosion potentials (E_{corr}) more anodic. Furthermore, a reduced corrosion current density (i_{corr}) can be observed at a more acidic pH of 4.0.

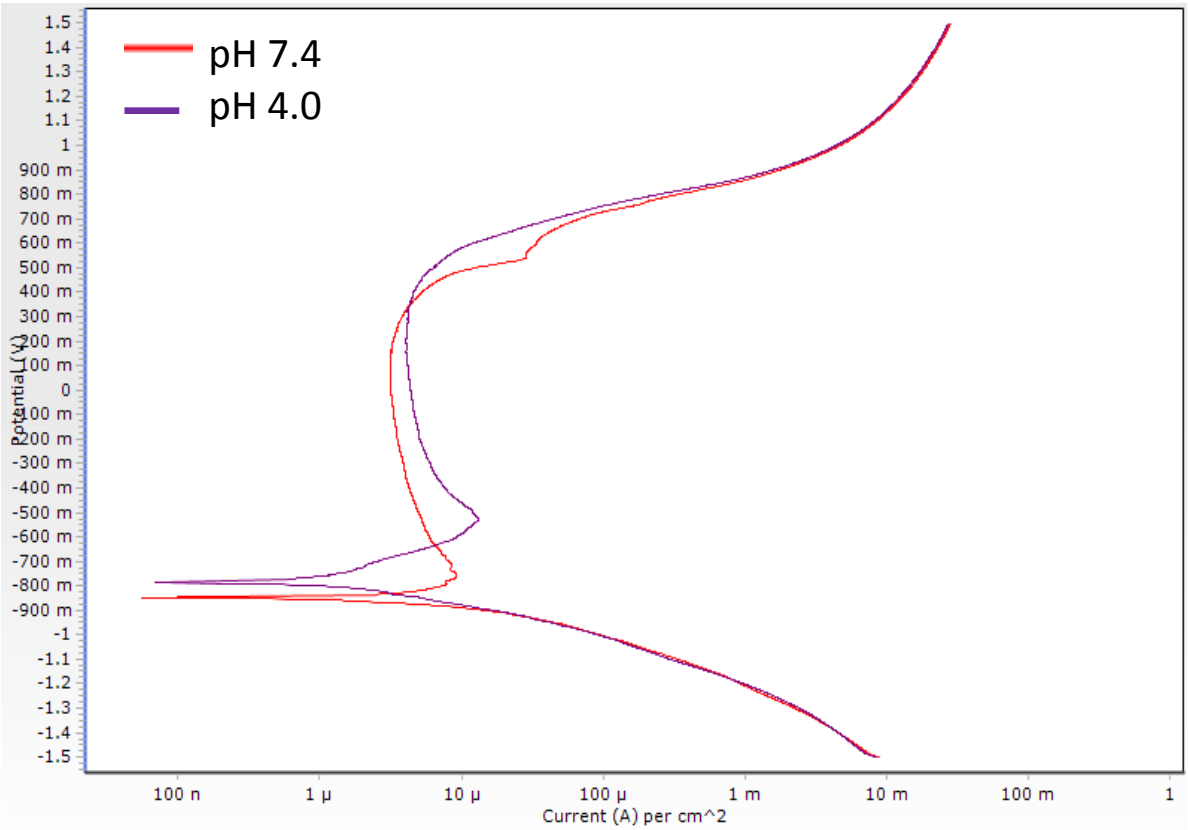

Figure 4.11: Potentiodynamic polarization plot of CoCrMo alloy in 0.14 M NaCl; effect of pH.

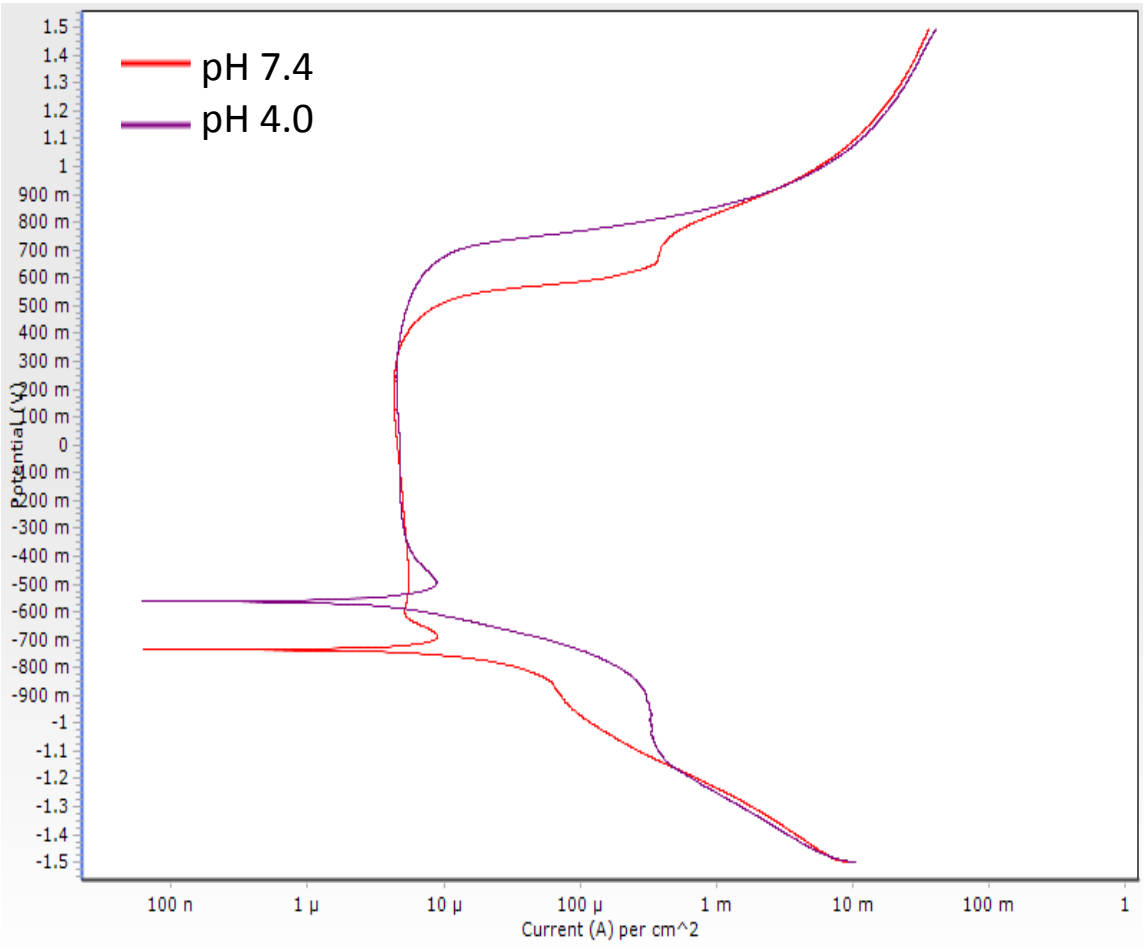

Figure 4.12: Potentiodynamic polarization plot of CoCrMo alloy in PBS; effect of pH.

The critical anodic current density (i_{crit}) and passive anodic current density (i_{pass}) recorded are fairly constant at both pH values, and this could mean that in the presence of phosphate ions, the increase in hydrogen ion concentration may not have an effect on the ease of the passive layer formation and its effectiveness. Valero Vidal and Igual Muñoz [8] reported the formation of large species of di-hydrogen phosphate ions [$H_2PO_4^-$] at pH 4.0. [$H_2PO_4^-$] is a conjugate base of phosphoric acid [H_3PO_4], a weak acid. The formation of weak acids in the PBS solution at pH 4.0 may act as a buffer which palliates the effect of a high concentration of hydrogen ions [8].

In sbf: Figure 4.13 shows the potentiodynamic polarization plot of the CoCrMo alloy in sbf at pHs of 7.4 and 4.0 respectively. Similar to the 0.14 M NaCl and PBS solutions, more acidic pH values increase the OCPs and corrosion potentials (E_{corr}) to more anodic potentials. Furthermore, a lower corrosion current density (i_{corr}) can be observed at a pH of 7.4 rather than at a pH of 4.0. At a pH of 7.4, the formation of protective organometallic complexes on the surface of the CoCrMo alloy [91] was suspected, while the denaturation of the protein complexes in *sbf* at pH 4.0 may have been responsible for the increase in the corrosion rate up to 350% [11]. This is because organometallic complexes were not seen to be adsorbed onto the surface of the CoCrMo alloy after the electrochemical tests.

In other words, in the presence of protein species, the CoCrMo alloy becomes more susceptible to increased corrosion at lower pH values. Muñoz and Mischler [3] reported that the presence of albumin shifts the corrosion potentials (E_{corr}) to more cathodic potentials.

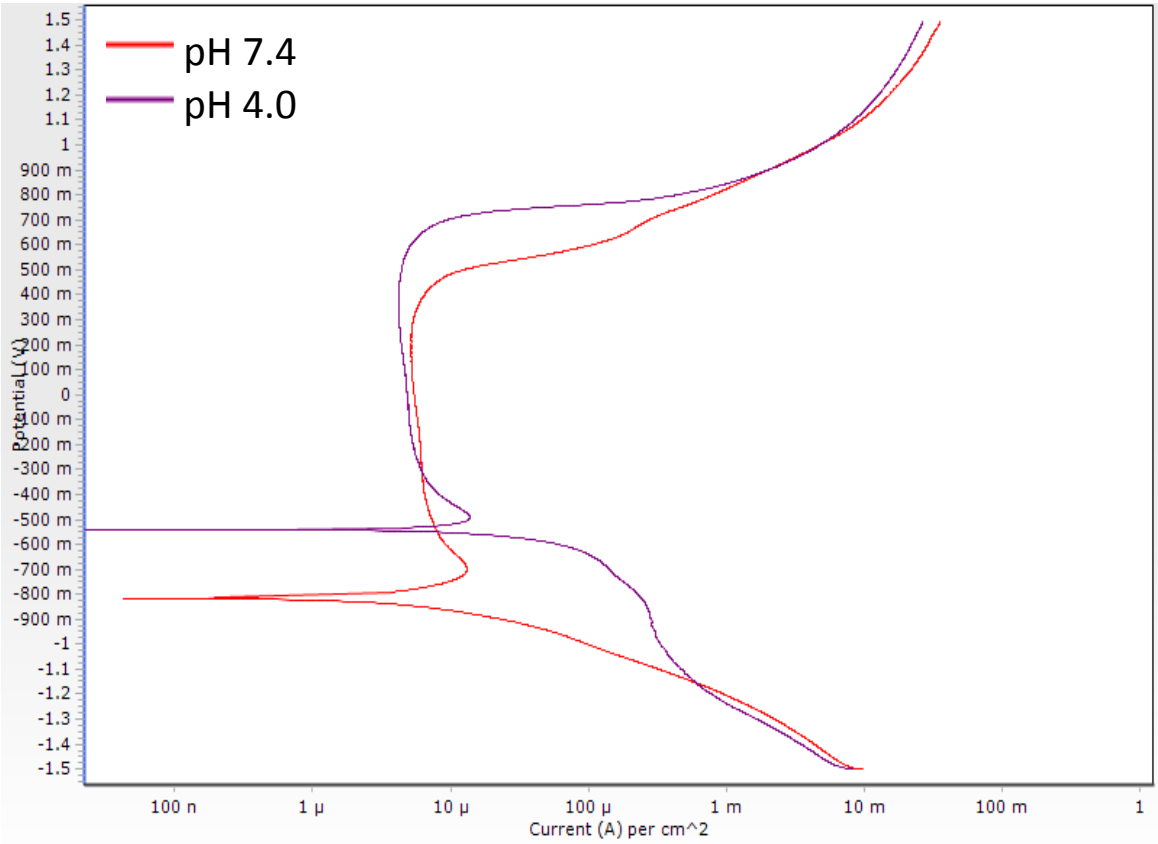

Figure 4.13: Potentiodynamic polarization plot of CoCrMo alloy in sbf; effect of pH.

Also, the critical anodic current density (i_{crit}) and passive anodic current density (i_{pass}) were fairly constant in both pHs, which means the ease of the formation of the passive layer and its effectiveness may not be altered by pH changes.

4.2 Passive film characterization

4.2.1 Film kinetics in different media

EIS was used to investigate the charge-transfer kinetics at the film/electrolyte interface on the CoCrMo alloy in 0.14 M NaCl, PBS and *sbf*. The OCP measurements recorded after stabilization were -369.27, -408.84 and -484.288 mV in 0.14 M NaCl, PBS and *sbf* respectively, which fell within the passive potential range in all cases. Bode impedance plots constructed from impedance data showed a difference in the passive film kinetics (Figure 4.14). At higher frequency perturbations, low and comparable impedance values measured in all of the solution types indicate passive layer formation controlled by charge transfer. However, at lower frequencies (as seen on the left side of the graph), higher impedance values were measured. The steeper slope observed in the 0.14 M NaCl solution at lower frequencies indicated that the passive film formed is more successful in limiting corrosion.

Generally, this means that the passive film formed even at lower frequencies in 0.14 M NaCl is still charge transfer controlled. Although a similar trend was observed in PBS and *sbf*, charge control in these two solutions seems to be less effective at lower frequency perturbation as opposed to the 0.14 M NaCl solution. Specifically, *sbf* showed a Warburg-like behavior [5], [48] at a mid to lower frequency region.

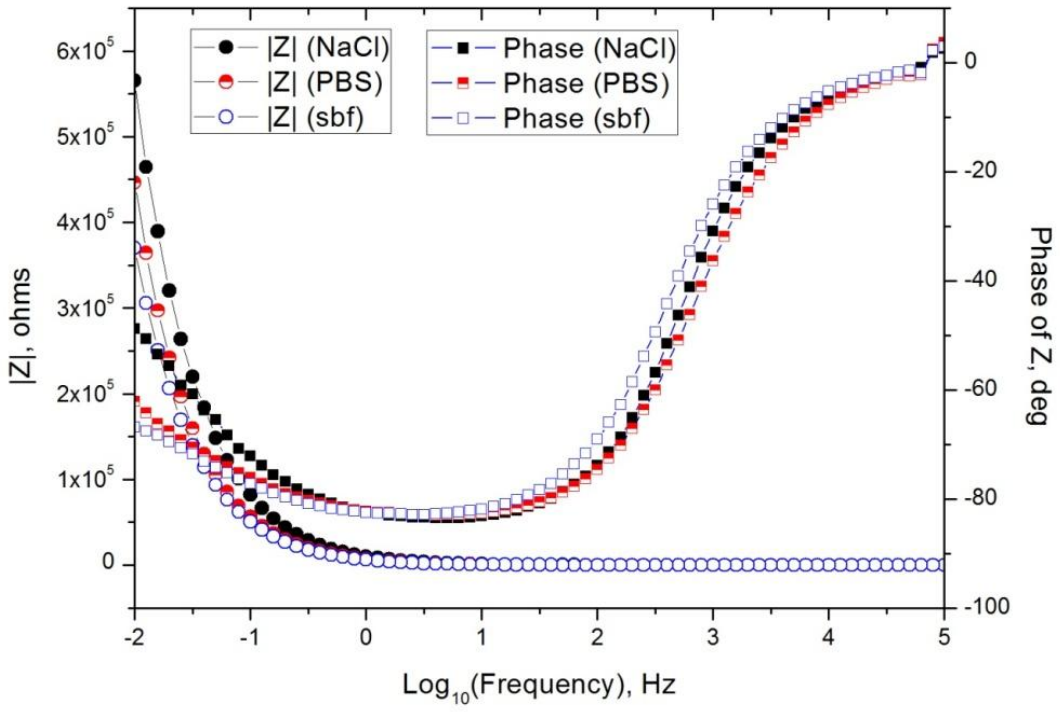

Figure 4.14: Bode impedance and phase angle plot of CoCrMo alloy in 0.14 M NaCl, PBS and sbf

This Warburg-like behavior is related to mass transport limitation by diffusion. Diffusion control appears to have influenced the behavior of the passive film formed in the *sbf*, especially at lower perturbation frequencies. In contrast, a relatively higher impedance data obtained in the PBS and 0.14 M NaCl solutions suggest that the diffusion of species in these solutions does not contribute to the passive film formation of the implant material. Mass transport limitation by diffusion of constituent ions in the *sbf* solution may be related to protein adsorption onto the CoCrMo alloy surface [52].

In line with previous work, Muñoz and Mischler reported that the presence of albumin (used to model proteins in synthesized fluids) forms a barrier that inhibits cathodic reactions in a CoCrMo alloy [3]. The phase angle of the Bode plots (Figure 4.14) was plotted to compare the passive film strength in the different solution types. The results showed that the passive film formed on the CoCrMo alloy in *sbf* may be relatively stronger than that formed in other solution types. This is because a broader range of frequencies with higher phase angles were recorded in the *sbf* environment.

Figure 4.15 is a Nyquist plot, mostly a semi circular arc, which shows the real and imaginary impedance vector spectra. Although the Nyquist plot provides no information on the perturbation frequency, it gives good information about the polarization resistance of the passive films, a quantity that defines the corrosion resistance capability of passive film. The Nyquist plot shows a capacitive passive film structure in all of the solution types under consideration.

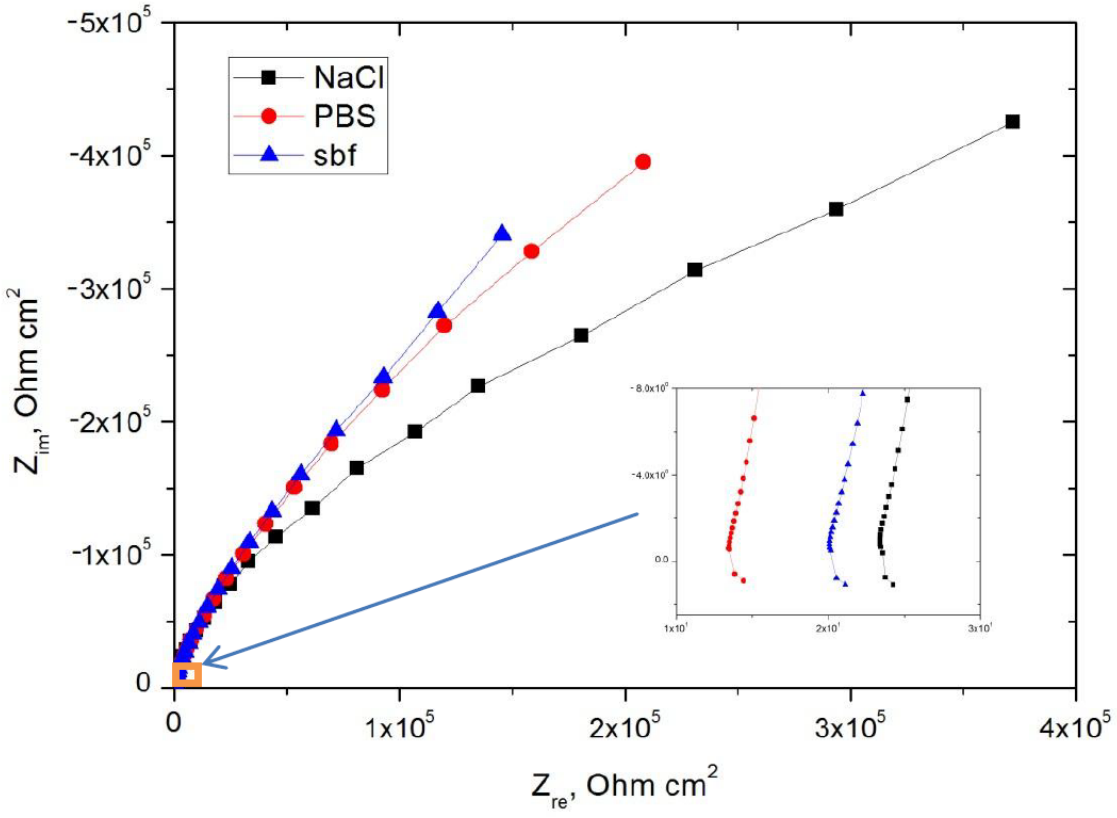

Figure 4.15: Nyquist plot of CoCrMo alloy in 0.14 M NaCl, PBS and *sbf*

The impedances obtained are contributions from electrochemical reactions that took place at the metal/film and the film/solutions interfaces, although physical phenomena and inhomogenities such as surface roughness, impurities, dislocations, grain boundaries, etc. may have accounted for the less than ideal capacitive film formed. The Nyquist plots show a typical shape of the passive state characterized by high impedance values with a largely capacitive behavior over a wide frequency range. All of the Nyquist plots are semicircle arcs with centers depressed below the x-axis (Figure 4.15 insert). The diameter of the semi-circular arc defines the polarization resistance capability at the metal/film/solution interface. Therefore, for every perturbation frequency under study, the *sbf* has the widest diametric arc which indicates a more resistant and hence better protective surface film.

4.2.2 Film composition in different media

An XPS study was performed on the CoCrMo alloy to analyze the nature and composition of the passive oxide layer developed on samples immersed into 0.14 M NaCl, PBS and *sbf*. Different locations on the samples were analyzed to confirm lateral homogeneity on the entire surface. In running a wide range scan, focus was placed on major elements, including cobalt, chromium, molybdenum, oxygen, carbon and nitrogen, as the constituent elements of interest. A high resolution scan was used to resolve the peaks of each element to gain insight into the atomic and ionic fractions of each element in the passive layer. Figures 4.16, 4.17 and 4.18 show the deconvoluted peaks of cobalt, chromium, molybdenum, oxygen, carbon and nitrogen in 0.14 M NaCl, PBS and the novel *sbf*. The atomic concentration ratio of cobalt, chromium and molybdenum in the different solution types is presented in Figure 4.19.

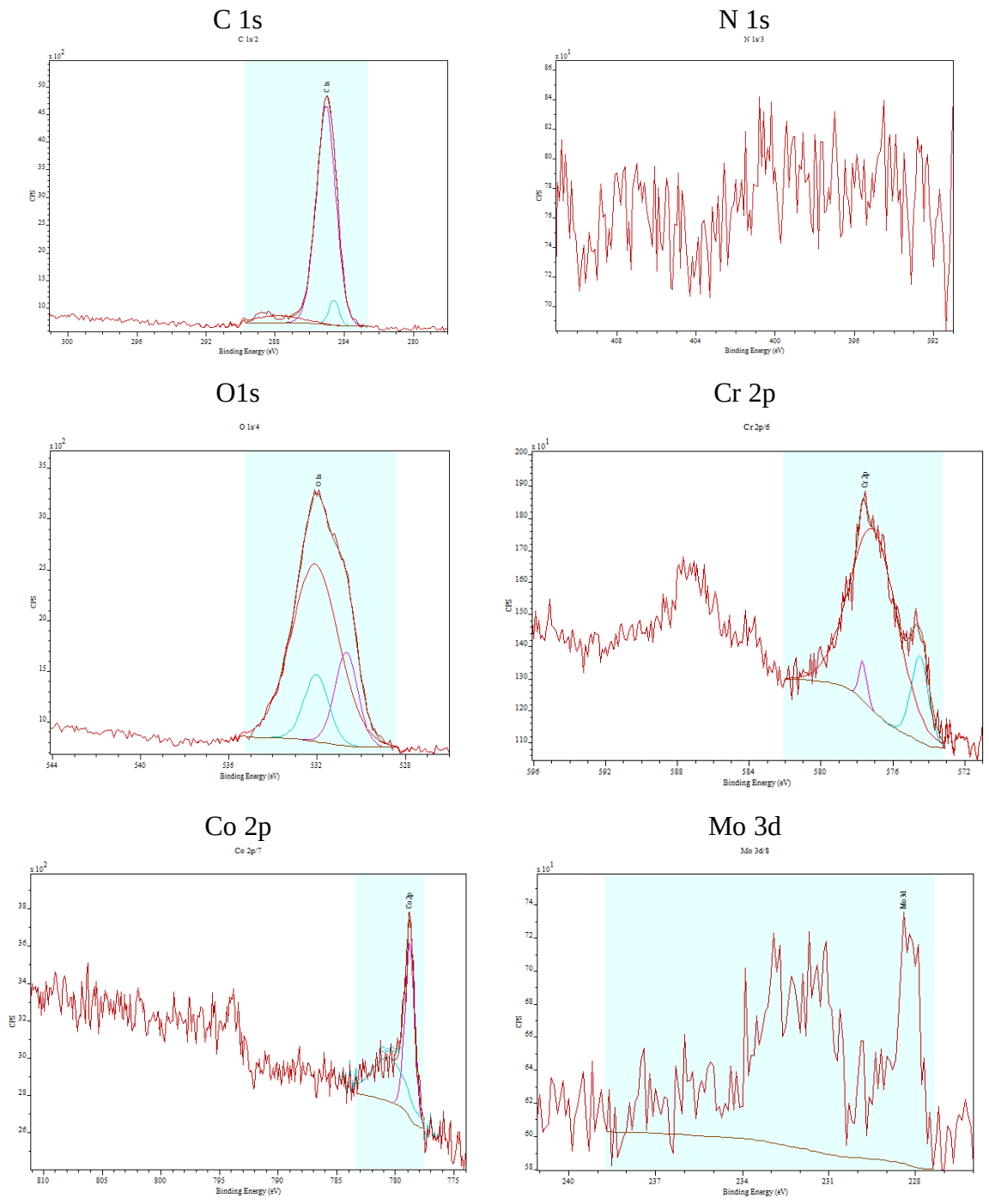

Figure 4.16: XPS results of CoCrMo alloy in 0.14 M NaCl solution at passive potential of -0.1 V for 60 minutes

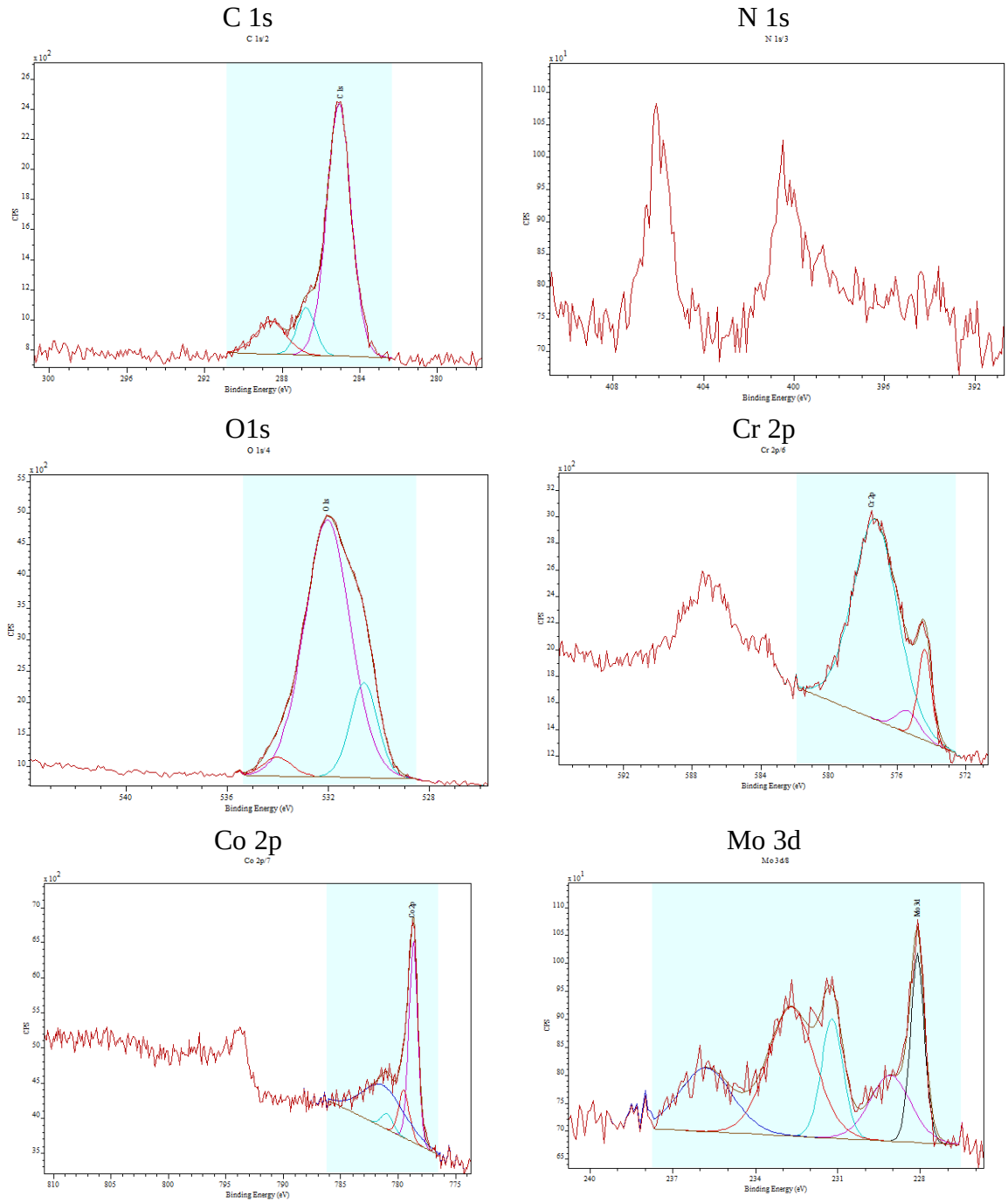

Figure 4.17: XPS results of CoCrMo alloy in PBS solution at passive potential of -0.1 V for 60 minutes

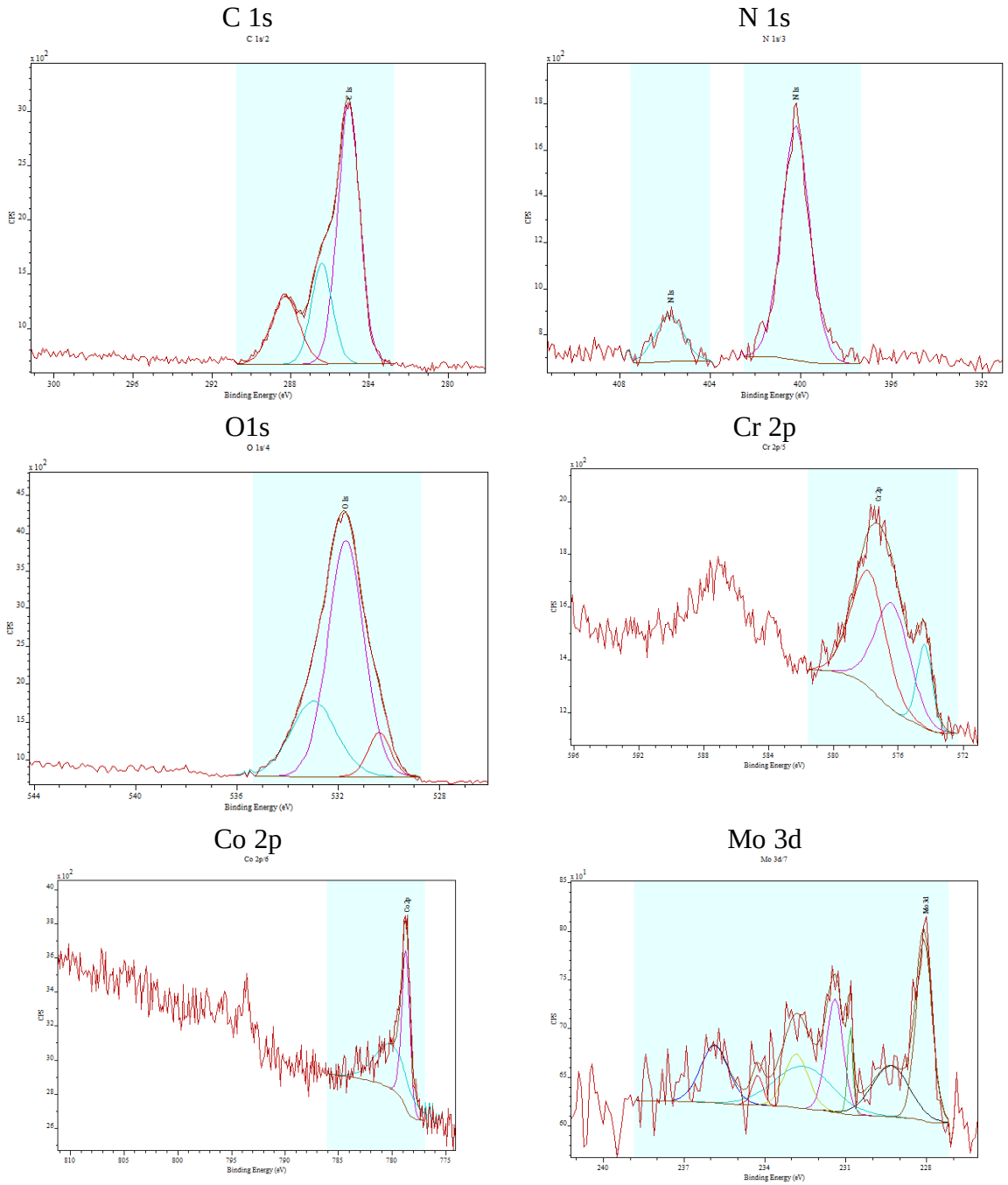

Figure 4.18: XPS results of CoCrMo alloy in *sbf* at passive potential of -0.1 V for 60 minutes

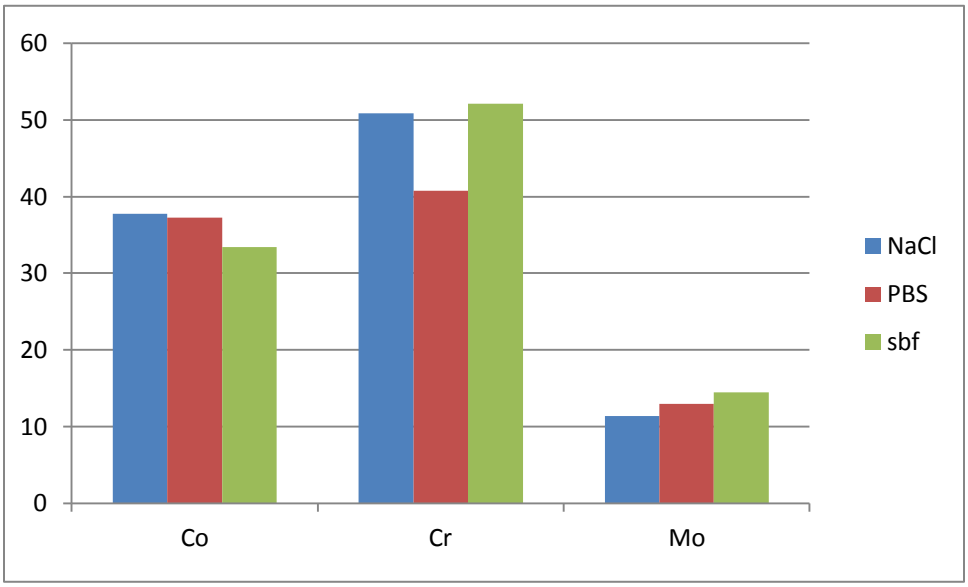

Figure 4.19: Percentage composition of Co, Cr and Mo atoms in 0.14 M NaCl, PBS and novel *sbf* environment

The results show that the passive layer formed in the *sbf* has the highest composition percentage of chromium while the least chromium is formed with PBS. Furthermore, the passive layer formed on the CoCrMo alloy in 0.14 M NaCl has the highest composition percentage of cobalt. Although the deconvoluted spectra of cobalt, chromium, molybdenum, oxygen and carbon are similar in shape, a distinct organic amine group was observed only in the N 1s spectra of the novel *sbf* (Figure 4.20). This is good confirmation of the organometallic complexes that were suspected to have been adsorbed onto the surface of the material through the EIS test result. An XPS analysis was used to characterize the cationic fraction of each oxidized species in the *sbf* environment. The results showed that up to 60% of the cationic fractions in the oxide layer are oxides of chromium; primarily the Cr (III) oxide. There was also a small amount of Co (II) oxide and Cr (III) hydroxide in the entire composition, although their ratio is not distinct enough for quantification purposes from the high resolution scan of the chromium peak. At a passive potential of -0.1 V, the cationic fraction of cobalt, which is the main alloying element of the CoCrMo alloy, is below 20%, although the presence of proteins did not have any quantifiable influence on the cationic fraction recorded. This means that in all of the cases, cobalt is oxidized into the solution, but does not contribute to the formation of the protective passive layer.

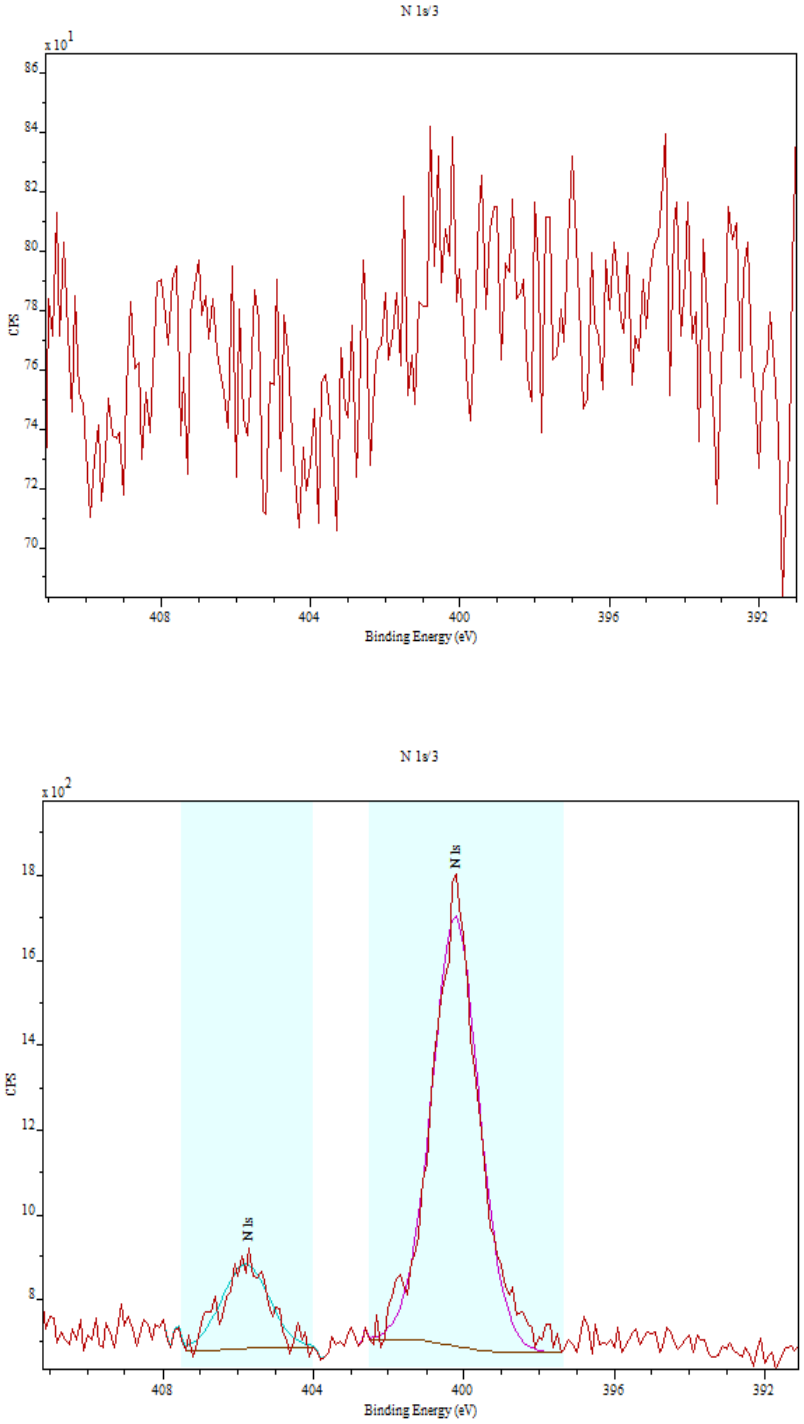

Figure 4.20: XPS peak fitting of N 1s spectrum in 0.14 M NaCl and novel sbf environment

4.2.2.1 Film composition in novel *sbf* - Influence of passivation potential

It has already been established that the potentials at the implant-environment interface can change with exposure time. In reality (and as observed earlier), when the implant stays in the implanted environment for a lengthier period of time, this will result in higher measured OCPs. Even though these potential changes still fall within the passivation potential range, it is entirely possible that these different potentials may have influence on the nature and composition of passive films formed in a synovial fluid environment. Therefore, further work was carried out to understand the effect of the passivation potential (-0.1 and 0.4 V) on the nature and composition of the passive film in the novel *sbf* environment. As observed in Figure 4.21, the result shows that as the passivation potential changes from -0.1 to 0.4 V, the composition percentage of chromium and molybdenum increases by a factor of 0.2 and 0.39 respectively. Conversely, as the passivation potential changes, the composition percentage of cobalt, the non protective component of the passive film, is reduced by a factor of 0.5. A study on the influence of passivation potentials revealed that up to 44% of the metallic chromium that formed a passive film on a CoCrMo alloy at -0.1 V was dissolved to form chromium oxides and hydroxides for better passivation at a higher potential of 0.4 V. The result showed that higher passivation potentials favor the formation of stronger and more protective passive films on CoCrMo alloys in a clinically relevant body fluid environment.

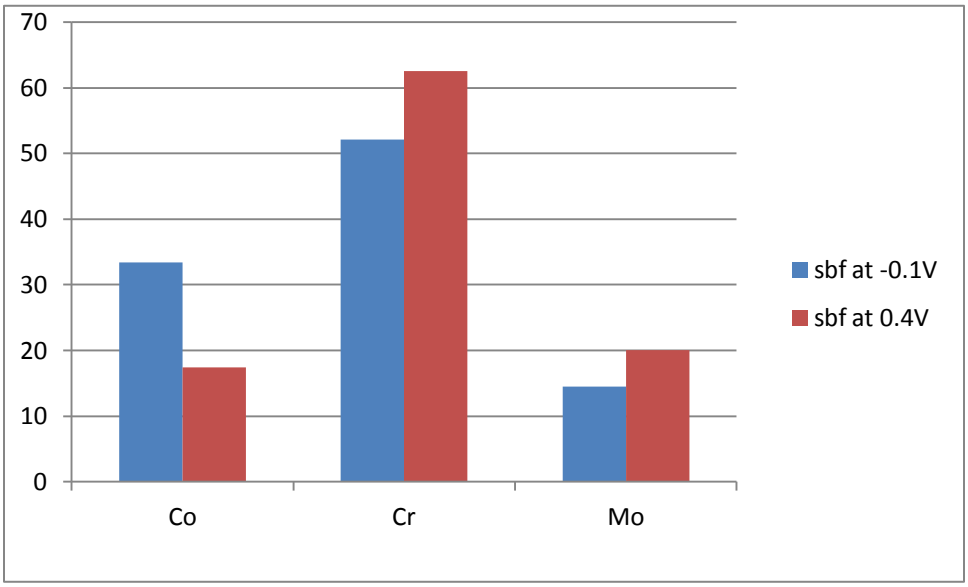

Figure 4.21: Percentage composition of Co, Cr and Mo atoms in novel *sbf* environment - influence of passivation potentials

4.2.2.2 Film composition in novel *sbf* - Influence of passivation time

It is well established that passivation spontaneously occurs on active-passive metals [101]. Although these protective films are spontaneously formed, it is entirely possible that their nature and composition may (or may not) change with exposure time in a synovial fluid environment. Therefore, further work was carried out to understand the effect of passivation time (3 and 60 minutes) on the composition of the passive film in the novel *sbf* environment. The results showed that there is no clear difference in the composition of the constituent elements of the film with passivation time (Figure 4.22). This is because at a passive potential of -0.1 V for 3 and 60 minutes respectively, only a 0.4% and 3.8% increase in chromium and molybdenum were measured respectively. Cobalt, on the other hand, had a 2% decrease with passivation time. When the cationic fractions of the constituent elements were measured, only a 7% increase in the cationic fraction of chromium oxides and hydroxides were observed. This shows that the formation of the protective passive film is spontaneous and its composition may not change with immersion time.

4.2.3 Film thickness in different media

AUGUR ELECTRON SPECTROSCOPY - The depth profile of passivated CoCrMo alloy surfaces in 0.14 M NaCl, PBS and *sbf* is provided in Figure 4.23. Attention was placed on the characteristic peaks of cobalt, chromium, nitrogen and oxygen in the spectra acquired, since they comprised the major constituents of the passive layer formed on the CoCrMo alloy. Signals from Mo were ignored for clarity of results because they were very weak.

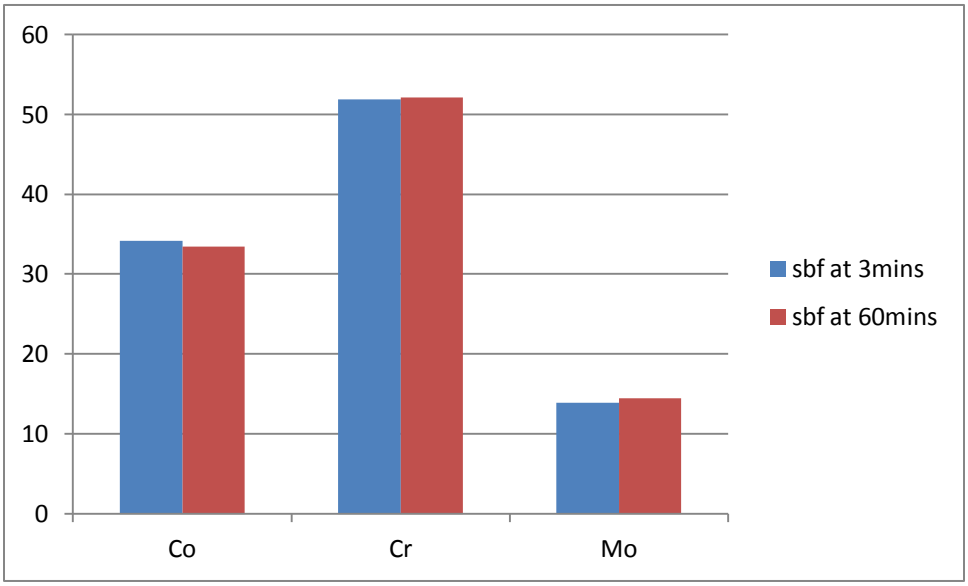

Figure 4.22: Percentage composition of Co, Cr and Mo atoms in novel *sbf* environment - influence of passivation time

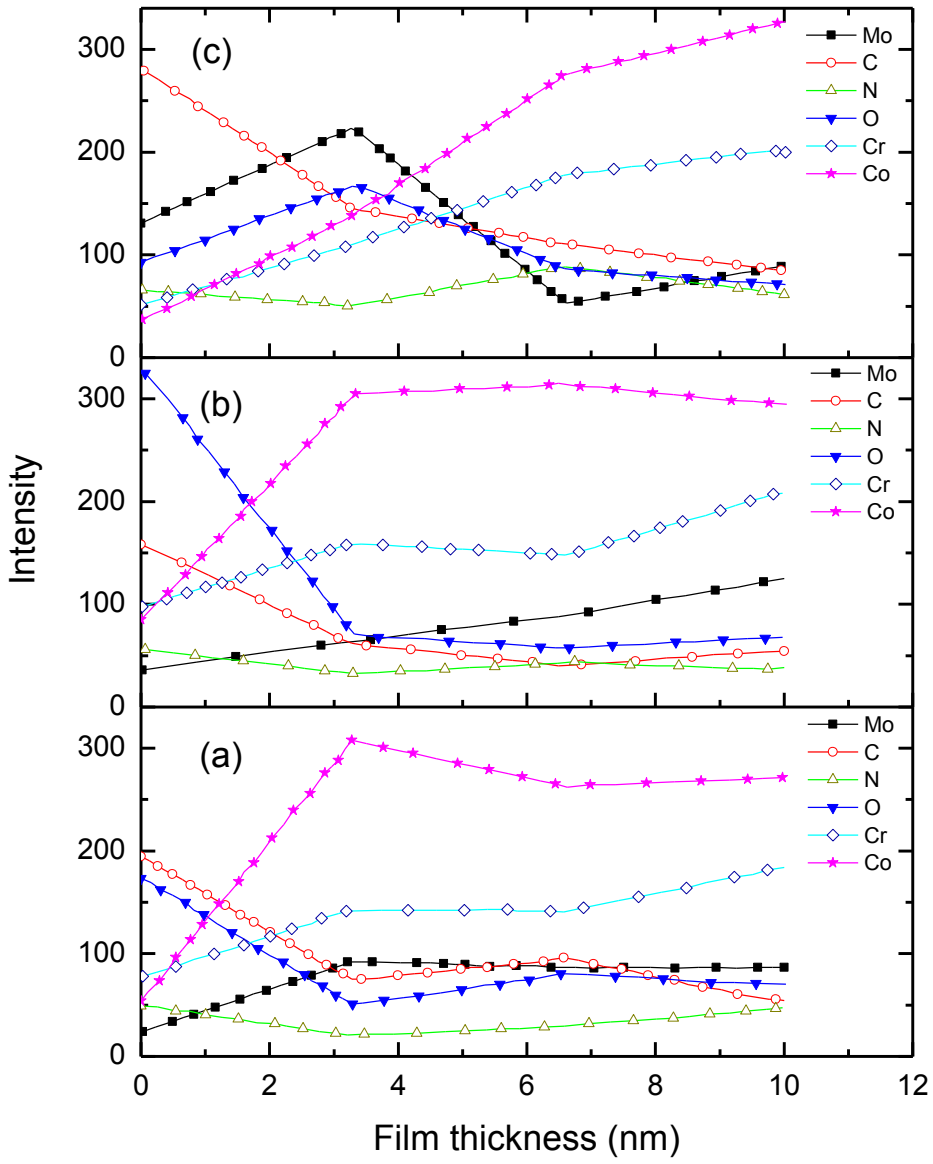

Figure 4.23: AES depth profile of passive film on CoCrMo alloy at OCP in (a) 0.14 M NaCl, (b) PBS, and (c) *sbf*

The determination of the atomic concentration of the constituent elements in the passive film and the composition of the passive film is beyond the scope of the AES study, as reflected by the XPS study reported in the previous section. As presented, the oxide film formed on the CoCrMo alloy is approximately 1.8 nm, 2.0 nm and 3.5 nm in 0.14 M NaCl, PBS and the novel *sbf* respectively

4.3 Fretting corrosion behavior

4.3.1 Dry fretting tests

The cumulative wear volume of the pins and discs measured under dry conditions with increasing number of cycles is presented in Figures 4.24 and 4.25. In all of the samples studied, the trend line shows that the cumulative wear increases with the number of cycles. Material transfer between the dry pins and discs was observed, which was more pronounced at the onset of the experiment. Both the discs and pins lost a considerable amount of weight after 0.5 Mc. The average wear rate of the dry pins and discs was 0.64 and 0.31 mg/Mc respectively. An SEM and TEM were used to study the wear path/grooves and wear particles of the dry samples. The results showed that wear asperities were produced. These asperities cracked and smeared, thus creating fine third-body wear particles that were entrapped on the mating surfaces. Wear particles generated from a dry testing procedure were analyzed for size, shape, structure and composition. The TEM revealed the formation of a nano-crystalline structure in the wear particles; it appears that the nano-crystals, evident by the electron diffraction pattern in a ring form, were generated by severe plastic deformation during fretting (see Figure 4.26). Figure 4.27 shows an image of a detached particle containing nano-sized grains.

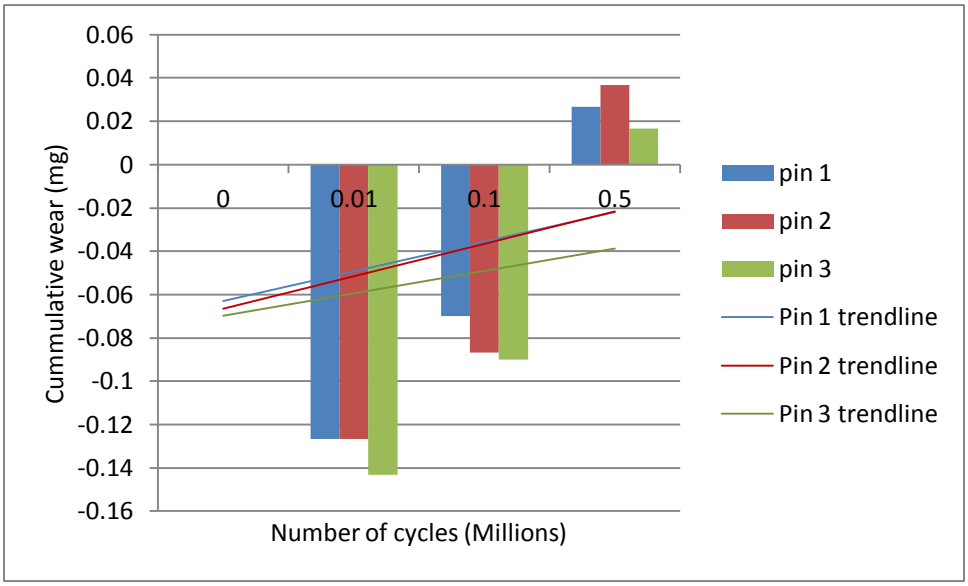

Figure 4.24: Cumulative wear of dry pins under fretting test conditions

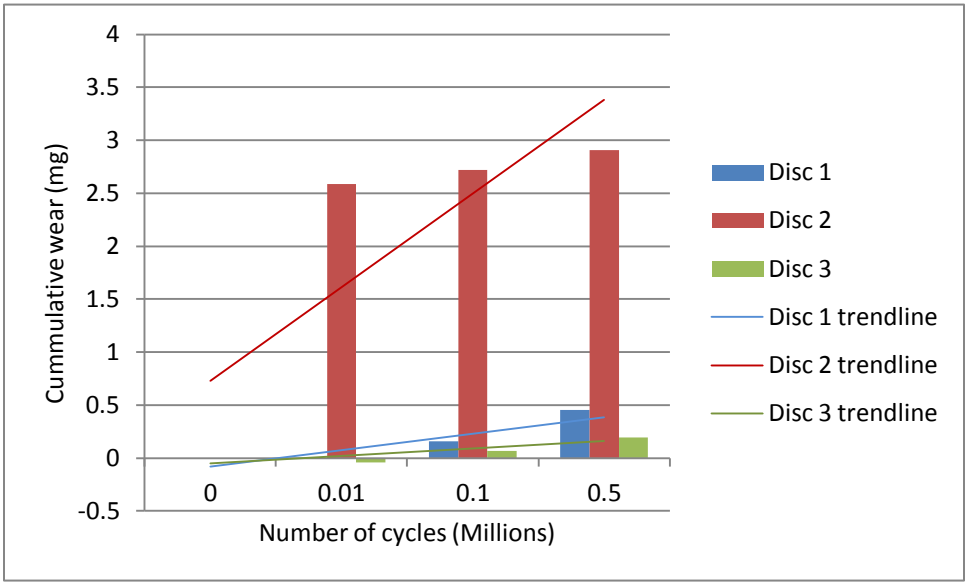

Figure 4.25: Cumulative wear of dry discs under fretting test conditions

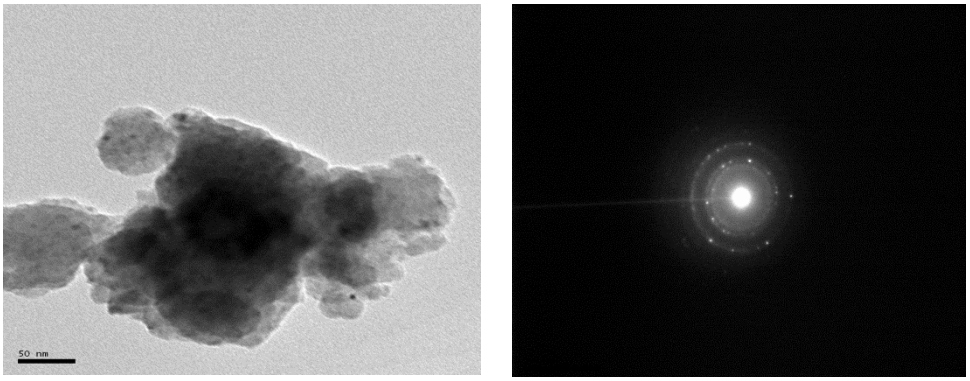

Figure 4.26: Diffraction pattern of wear particles which show polycrystalline ring pattern

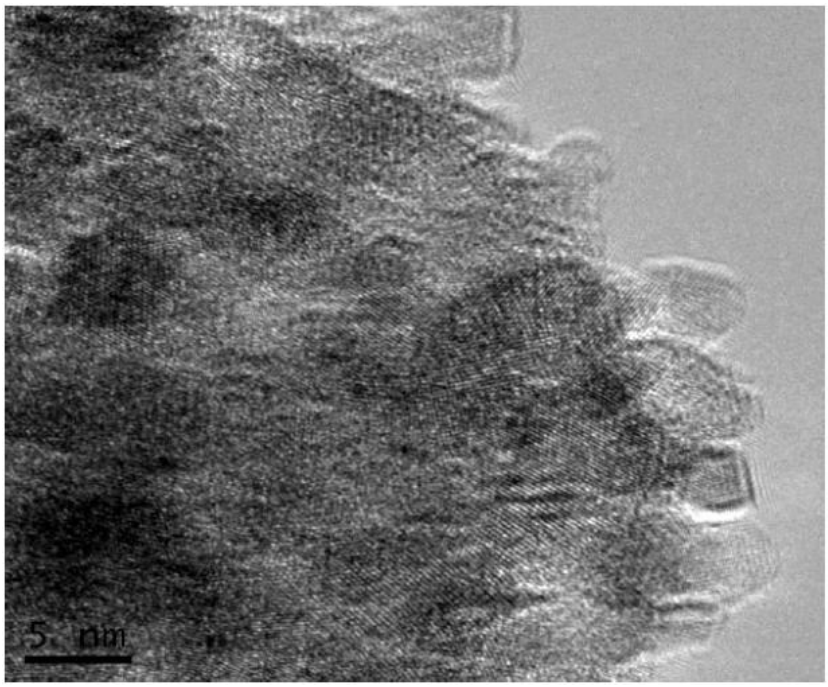

Figure 4.27: Nano-size grains in detached particles after fretting process

Also, Figure 4.28 shows detached nano-sized grain particles at low magnification with a largely oval and irregular shape, which is in good correlation with previous findings [3], [102]–[106]. The average particle size measured was less than 200 nm, while some of the particles were as small as 40 nm in size. The particle composition analysis by EDX spectroscopy clearly showed a composition close to that of the substrate alloy, which means that there is no notable oxidation reaction in dry conditions (Figure 4.29). Furthermore, the surface roughness value of the samples was measured. The average roughness value (Ra) for the dry discs and pins after 0.5 Mc was 0.25 and 0.41 µm respectively. The dry conditions provide a high surface roughness value, and the pins under this condition also had a rougher surface. This may be due to the increased wear rate and volumetric wear loss measured from the gravimetric analysis reported above.

Also, third body particles produced during fretting may have adhered to the pin and disc surfaces and affected the surface roughness values. The out-of-roundness values of the pins were used to measure the degree of deviation from an absolute circle with respect to the number of fretting cycles. Only the dry pins were measured because the discs used in this experiment were flat. After 0.5 Mc, the trend line showed varying trends in the out-of-roundness profile with number of cycles (Figure 4.30), and material transfer may have accounted for this variation. This is consistent with the values obtained from the changes in the contour analysis (Figure 4.31), where the negative values indicate material gain on the pins.

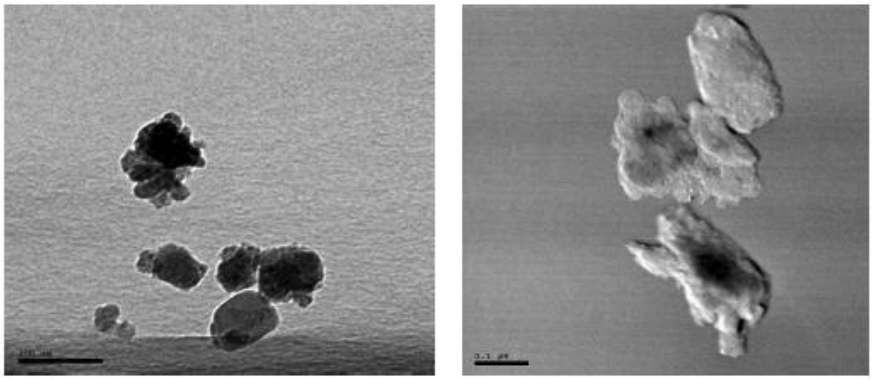

Figure 4.28: Nano sized grain particles

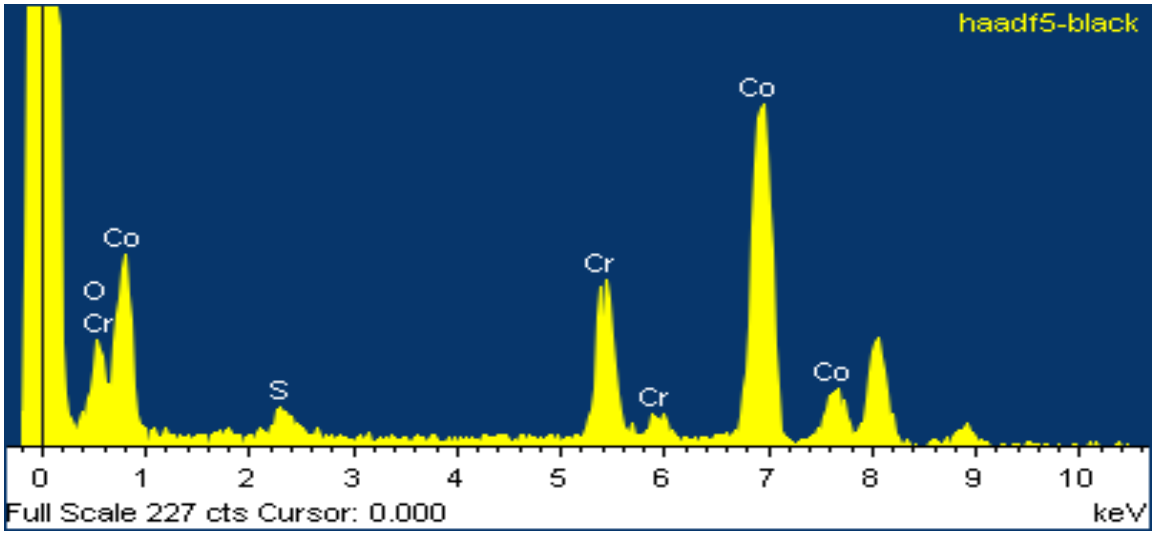

Figure 4.29: EDX spectrum of wear particles generated under dry conditions

4.3.2 Wet fretting tests

Similar to dry conditions, the cumulative wear volume trend line showed an increase in cumulative wear with the number of cycles only on the pins (Figure 4.32). Gravimetric analysis showed that there was material transfer between the pin and disc, especially in the bedding-in stage (at 0.01 Mc) of the experiment. Attempts to measure the discs for confirmatory testing under wet conditions were not successful due to the nature of the experimental set-up. Silicone was used to seal the edges of the wet discs in the PoD to avoid lubricant leakage; therefore the adhered silicone compound would have affected the accuracy of the gravimetric results of the discs only in the wet conditions. The average wear rate of the wet pins was 0.07 mg/Mc.

Clearly, the presence of a lubricant in wet conditions reduces the wear rate of the CoCrMo implant material by a factor of up to 8.6. Observation by use of a SEM of the fretted surfaces under wet conditions showed that there is no evidence of pitting or localized corrosion. This result is in line with other researchers who have also observed a similar behavior [3], [89]. The backscattered electron composition (BEC) images of the fretted samples under wet conditions showed that the wear path/grooves are not as deep as those observed in dry conditions.

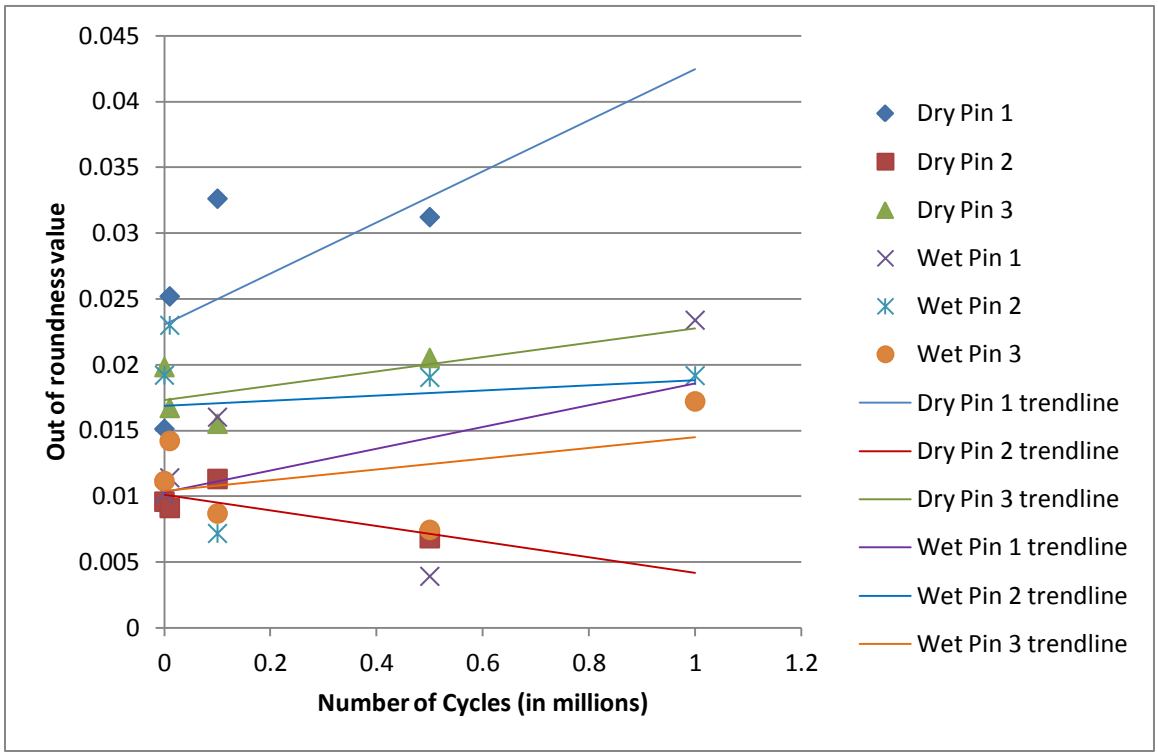

Figure 4.30: Contour analysis of fretted samples

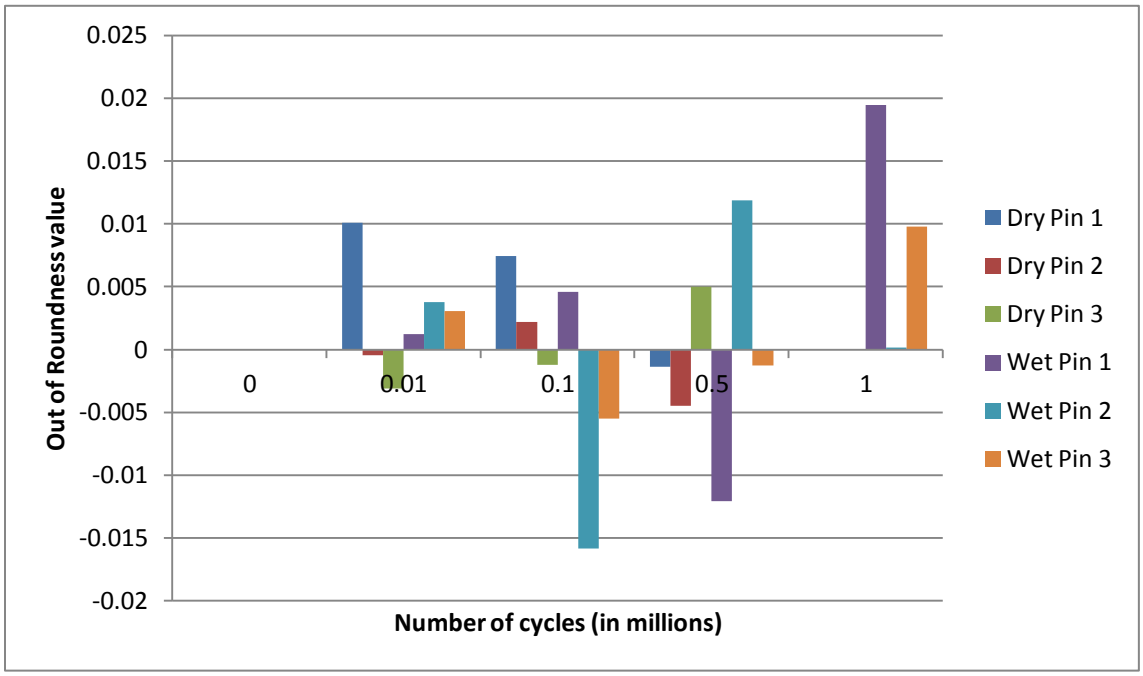

Figure 4.31: Changes in out-of-roundness values with fretting cycles

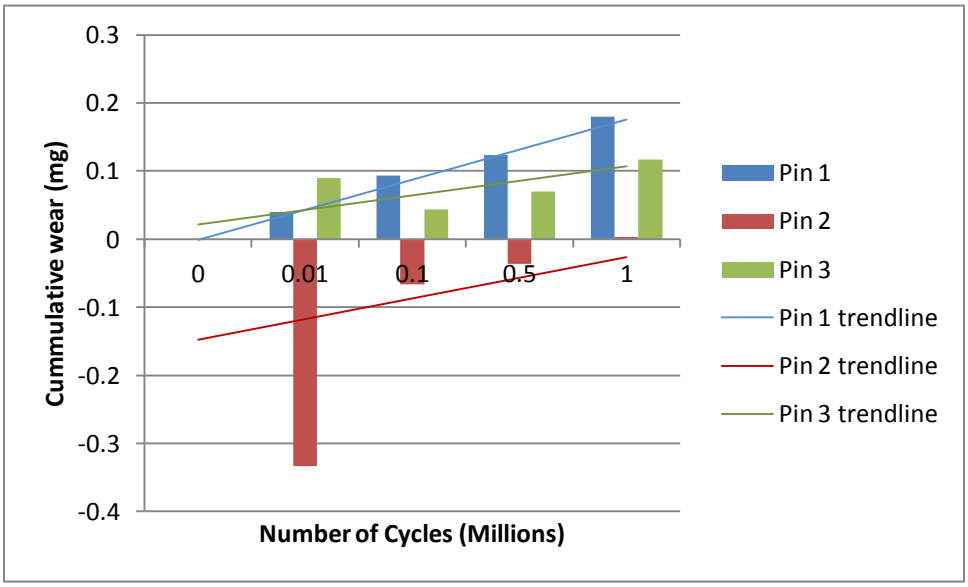

Figure 4.32: Cumulative wear of wet pins under fretting test conditions

In fact, in wet conditions, the particles were detached only from the passive layer formed, as the SEM images did not reveal deterioration beyond the passive film (Figure 4.33). Furthermore, the average roughness values (Ra) were 0.21 and 0.26 µm respectively after 0.5 Mc and 0.24 and 0.33 µm respectively after 1.0 Mc. However, after 1.0 Mc, a clear increase in the out-of-roundness value was recorded. This may be due to a steady state wear rate that was attained at this measurement time.

4.4 Ion concentration analysis

4.4.1 Ion concentration in different media

An ICP-MS analysis was performed in the different fluids (0.14 M NaCl, PBS and *sbf*) at a passivation potential of -0.1 V for 60 minutes in order to understand the concentration of the alloying elements that were in the solutions and the formed corrosion products. Table 4.1 shows the ionic concentration in $\mu g/l$ (or ppb) of the cobalt, chromium and molybdenum species. Trace amounts of other species, such as cadmium, lead, sodium, magnesium, potassium, vanadium, manganese, etc., were observed but neglected since they do not form the basis for this discussion. The highest concentration of chromium ions was measured in the *sbf* followed by 0.14 NaCl and PBS, which had the least concentration of chromium ions. The PBS environment favored the active dissolution of cobalt in the alloy. Since cobalt does not exhibit the passivity phenomenon [89], this may have accounted for the continuous anodic dissolution of the substrate alloy and high corrosion rate observed earlier in PBS. In 0.14 M NaCl and *sbf*, the molybdenum ionic concentration was below the detection limit and fewer cobalt ions went into the solutions.

Dry Disc

Wet Disc

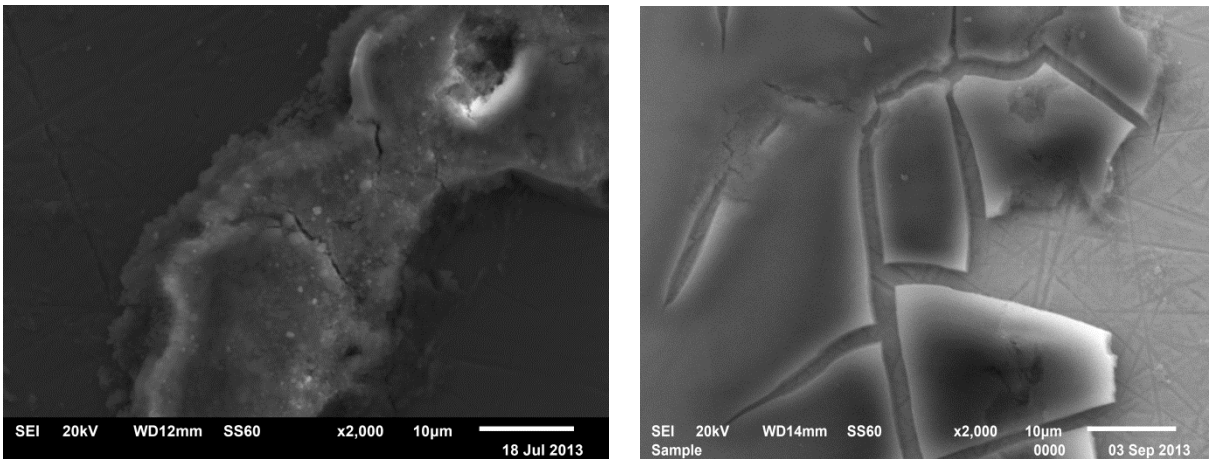

Figure 4 .33: SEM images that show wear cracks of asperities on fretted disc

Table 4.1: Ionic concentration (in µg/L) of Co, Cr and Mo

Solution type	Co	Cr	Mo
0.14 M NaCl	<DL	68.4	<DL
PBS	22.99	5.31	7.08
	26.23	5.23	7.82
sbf	17.9	74.2	<DL
	13.3	65.5	<DL
**<DL means below detection limit*			

However, the higher concentration of chromium ions in the solutions probably meant that the spontaneous formation of Cr_2O_3 was more easily attainable.

4.4.2 Role of corrosion and tribology in fretting corrosion behavior in *sbf*

In order to gain insight into the separate contributions of corrosion and mechanical interaction to the fretting corrosion damage of the CoCrMo alloy in the *sbf*, two similar experiments were performed under the same conditions (exposure time, temperature, etc.). One experiment was the isolation of the influence of fretting displacement, while the other experiment used a fretting displacement of 1 mm. An ionic concentration analysis was performed on the lubricants used in both experimental conditions. Table 4.2 shows the ionic concentration in $\mu g/l$ (or ppb) after the pure corrosion and fretting corrosion tests. From the results obtained, a greater amount of chromium is dissolved into the solution in the absence of mechanical interaction. Also, mechanical interaction has no influence on the rate at which molybdenum dissolves. Furthermore, of particular importance is the clear increase in the dissolution rate of cobalt when mechanical interaction is involved. An analysis of the result shows that there is up to 310% increase in the selective dissolution of cobalt in the CoCrMo alloy.

Table 4.2: Ionic concentration (in $\mu g/L$) in CoCrMo alloy after corrosion and fretting corrosion tests

	Co	**Cr**	**Mo**
Pure corrosion (A)	58.21	335.52	26.81
Pure corrosion (B)	71.555	227.01	<DL
Fretting corrosion (A)	164.77	152.54	<DL
Fretting corrosion (B)	238.755	252.7	16.47
**<DL means below detection limit*			

5 DISCUSSION

5.1 Electrochemical properties of CoCrMo alloy in different solution types - Effect of solution pH and immersion time

The electrochemical behavior of the CoCrMo alloy in a synovial fluid environment can be influenced by factors such as chemical composition, temperature, pH, aeration, immersion time, presence of crevices, etc. The results showed that in all of the solution types considered an increase in temperature from room temperature to 37^0C results in a corresponding increase in the corrosion current density (i_{corr}) of the CoCrMo alloy, with respect to the influence of temperature on electrochemical behavior. This may be due to the increase in excitation energy of the participating species in the electrochemical reaction with temperature. Higher excitation favors more charge and mass transfer from the substrate material to the solution, thereby increasing the corrosion rate. A similar trend was also observed when the pH of all the solutions changed from 7.4 to 4.0. In reality, factors such as joint inflammation, wound healing process after surgery and localized corrosion with crevices can reduce pH values to as low as 1 [8].

The results from this study confirm that a more acidic pH has an aggressive influence on the degradation of the implant material. The increase in the corrosion current density (i_{corr}) at lower pH values may have been accounted for by a greater tendency of protein denaturation at acidic pHs [107]. Post test physical observations of the degraded surfaces in *sbf* at pH of 7.4 and 4.0 revealed the conglomeration of degraded protein compounds (organo-metallic complexes) on the surface of the material. This conglomeration was more pronounced at more acidic pH values. Furthermore, the EIS results showed that the presence of proteins hinders the charge transfer mechanism of the ions at the metal-

electrolyte interface. Since protein compounds are negatively charged, more metallic cations may have went into the solutions to balance the charge on the surface of the CoCrMo substrate. Therefore, more cobalt ions may have went into the solutions, hence increasing the corrosion rate at lower pH values. Also, the increase in OCPs and corrosion potentials (E_{corr}) to more anodic potentials observed at a pH of 4.0 may be due to the formation of weak and free acids by hydrolysis of the metallic ions released from the metal.

A previous research [6] has reported the evolution of such reactive species (e.g. nascent hydrogen, nascent oxygen and hydrogen peroxide) which influences the biochemistry involved in the biological process. As already highlighted, a change in the solution chemistry changes the solution properties, thereby changing the OCP measured. This may have been a good reason for the increase in the corrosion rate at more acidic pH values [11]. In all of the solution types considered, the ease in passivation observed at an immersion time less than 30 minutes provided good confirmation for the spontaneous formation of passive film and use for biomedical applications. However, the effectiveness of the passive film formed increased with immersion time. This may be due to the continuous decrease in OCP with immersion time and a continuous increase in the difference between the passive anodic current density (i_{pass}) and the critical anodic current density (i_{crit}) with exposure time.

5.2 Influence of *sbf* on corrosion of CoCrMo alloy

A higher corrosion current density (i_{corr}) measured at the transition domain in PBS may have been accounted for by the presence of phosphate ions which have been reported to

adsorb onto the CoCrMo alloy [3] to produce a large species of di-hydrogen phosphate ions [$H_2PO_4^-$]. The di-hydrogen phosphate ions constitute a conjugate base of phosphoric acid [H_3PO_4], a weak acid that may have necessitated an increase in the active dissolution rate of the CoCrMo alloy [8]. In agreement with previous work [3], the ICP-MS results confirmed that the phosphate ions increase the dissolution of cobalt in the CoCrMo alloy. High concentrations of $H_2PO_4^-$ and HPO_4^{2-} ions present in PBS [7] may have contributed to this phenomenon.

Furthermore, the results from this work suggest that the presence of proteins and organo-metallic complexes effectively inhibit the influence of phosphate ions possibly by preferentially adsorbing onto the implant alloy ahead of the phosphate ions. A high resolution scan of the N 1s spectrum from the XPS results confirmed a distinctive amine group that is only present in the passivated sample immersed in the *sbf* solution. This organo-metallic complex can have a positive influence of protecting the CoCrMo alloy from electrochemical degradation by forming an organo-metallic film on the alloy as observed from the AES results of the passivated CoCrMo alloy. Therefore, despite the low and comparable corrosion current density (i_{corr}) recorded for the CoCrMo alloy in 0.14 M NaCl and the novel *sbf*, it is entirely possible that the nature of the passive films in these two solutions is different.

The EIS was used to better understand the mechanistic differences in the passive films formed in the different fluid environments. The results showed that while the charge transfer between the alloy/electrolyte interfaces is the rate determining step in the 0.14 M NaCl solution, the rate determining step is diffusion controlled, especially under low

frequency perturbations in the novel *sbf*. The absorption of protein complexes on the CoCrMo alloy caused the passive film to have Warburg-like behavior, which was observed only with the novel *sbf*. Therefore, even though the 0.14 M NaCl and *sbf* produced a low corrosion rate, the nature of the surface film which enabled the low rate of corrosion differs for both solutions. The film that contained protein complexes which may have other beneficial effects, as will be discussed in subsequent sections of this thesis, was formed only in the *sbf*.

5.3 Influence of *sbf* on fretting corrosion of CoCrMo alloy

The fretting corrosion experiment was clearly divided into two major stages. The first stage was the bedding-in stage, associated with higher material loss and material transfer, which occurred up to and above 0.1 Mc. The steady-state stage was the next stage, which occurred at cycles above 0.1 Mc. In this experiment, it is not clear exactly when the bedding-in stage stopped. Earlier work by Sinnett-Jones *et al*. [108] reported a bedding-in stage between 0.23 to 0.4 Mc. However, what is rather clear is that the steady-state stage of the cycle was attained before 0.5 Mc; this is because between 0.1 and 0.5 Mc, the wear rate may have become low and steady [66]. The gravimetric analysis carried out at intermittent stops revealed that there is more material loss under dry conditions than wet conditions.

A TEM was used to analyze the particles generated from the dry MoM tribology test. As stated earlier, the ring shape diffraction pattern observed is characteristic of nano sized polycrystalline material. In this work, the CoCrMo alloy used has an average grain size of 5 μm, and the wear particles produced under dry conditions have an average particle size

less than 0.2 μm. Therefore, the ring pattern observed indicates severe plastic deformation which leads to grain refinement even at room temperature, thus forming new and smaller grains. Other researchers [109]–[112] have reported low stacking fault energy in CoCrMo alloys, which makes cross-slip and dislocation motion difficult, thereby concentrating severe plasticity on the interfacial surface of the alloys. In line with previous findings, the SEM images of the dry fretting contact showed that an abrasive wear mechanism appears to be dominant [109]. Also, in dry conditions, the CoCrMo alloys were in direct contact and the bearing surfaces accommodated the applied load that caused plastic deformation. Clearly, a smearing effect of the fretted surface was observed in dry conditions, a characteristic of plastically deformed surfaces. This observation is corroborated with findings from the contour analysis which showed that material is transferred between the two materials.

Although other researchers have reported initiation of micro-cracks on substrates due to compressive cyclic loading [68], [113], the SEM images and metallographic analysis of the fretted surface under dry conditions only revealed micro-cracks on the third-body particles that were adhered on the discs. In the CoCrMo substrate, no evident micro-cracks were observed. This may be attributed to the fretting displacement of 1 mm and the numbers of cycles run at 0.5 Mc, which focused on the initial stages of fretting damage at the modular head/neck and neck/stem interfaces, rather than the long term effect of larger displacements at the articulating ball and socket interfaces. A greater number of cycles may be required to cause micro-cracks on the CoCrMo substrate.

In wet conditions, due to electrochemical interactions with the lubricant, the contacting surfaces developed a protective passive oxide layer which consisted largely of Cr_2O_3, an oxide that is ceramic in nature. Since the fretting corrosion experiment was carried out under OCP, the spontaneous formation of a protective passive film was favored. At the point of pin and disc contact, the relative motion and micro-motion of both surfaces caused an intermittent depassivation and repassivation of the passive film formed. The rate of depassivation and repassivation of the fretting surfaces determines the contribution of corrosion and corrosion assisted wear to volumetric wear loss and tribocorrosion synergism. In considering a fretting displacement of 1 mm, characteristic of the modular head/neck and neck/stem interfaces, the depassivated surface was very small (less than 1%) compared to the total exposed surface area. Therefore, the contribution of corrosion and corrosion related damage alone may not have been pronounced.

As confirmed from the AES results, due to the presence of proteins in the novel *sbf*, the passive film formed from the clinically relevant fluid used is bilayer in nature, with an organometallic outer layer and an inner oxide film. The presence of species such as proteins influence electrochemical kinetics under sliding conditions [66], [104], [110], [111], [114]. In fact, once the tribological process starts, the nature of the proteins may change, and turn into lubricious material, thereby influencing the friction developed between joint surfaces [66], [104]. Some researchers [109], [115], [116] have reported the influence of tribochemical reactions on the surface of CoCrMo alloys, and these reactions generate layers of denatured organic materials that cause separation on the surfaces, thereby hindering direct MoM contact. Therefore, under wet conditions, fretting

corrosion in the presence of protein containing lubricant may tribochemically produce wear particles by a phenomenon called mechanical mixing [117]–[119]. Mechanical mixing involves the incorporation of species such as proteins into the nanocrystalline wear particles [120], and this spontaneous action has been established to induce low wear rates [57], [110]. Therefore, the nano-particles produced under fretting corrosion adhere to the organic substances in the synovial fluid, and form organometallic complexes that better sustain shear strains while they roll on the bearing surfaces.

As stated earlier above, the EIS results indicate that the presence of proteins forms a kinetic barrier on the surface of the CoCrMo alloy while the XPS confirmed the adsorption of organometallic complexes onto the alloy surface. Due to the effect of the kinetic barrier of these protein complexes, the mechanically mixed nano-sized wear particles were covered by protein bearing surfaces. This reduced the further dissolution of these particles [66], [113]. This may have contributed to the lower wear rates observed from the gravimetric analysis in wet conditions.

It has been shown that by using a larger diameter for the femoral hip head and optimized clearance, iso-viscoelastic elasto-hydrodynamic lubrication can be achieved, which can reduce the total material degradation of the implant [57], [102], [104]. Although the geometric effect of the hips was not considered in the design of the experiment, it is possible that at an applied load of 330 N on the PoD tribometer, two lubrication regimes that reduced the wear of the CoCrMo alloy were at play. They are the mixed and hydrodynamic lubrication regimes. Under these conditions, a hydrodynamic lubrication regime that totally (or largely) separates the pins and discs from direct contact may have

been favored. This is because the Hertzian pressure applied at the interface may have been partly accommodated by the nano-sized wear asperity at the interface and largely by the hydrodynamic effect of the *sbf* lubricant used, which caused direct MoM separation. The SEM images that show the grooves of the fretted surface at a magnification of 2000X under wet conditions did not reveal any deformation of the substrate alloy directly under the passive layer, although the passive layer was observed to be broken at the contacting surface (Figure 4.33). Therefore, due to the load applied, the pressure on the wear asperity is large enough to break the passive layer, but not enough to cause mechanical deformation on the substrate metal exposed. This may have been due to the hydrodynamic fluid film that caused partial separation (mixed lubrication) between the two surfaces.

This result confirms that an optimized loading condition of the hips in service can favor a hydrodynamic lubrication regime that largely separates the contacting surfaces and reduces wear and corrosion related damage at the modular head/neck and neck stem interfaces. Given a passive film thickness of ~4 nm measured by AES in *sbf*, the wear nano-particle size that may have been produced under wet conditions will be smaller than that produced under dry conditions. Therefore, while nano-sized particles generated under both conditions may have rolled on the interface and served as bearing [121], [122], the larger wear particles observed under dry conditions must have detached further below (or within) the plastic shear surface zone, largely because underneath the CoCrMo alloy, a strain gradient is formed by friction induced cyclic shear stresses [121]. A smaller particle size generated means increased tendency of these third body particles to freely roll between contacting surfaces [4], thereby accommodating more shear stress from the

counter body. Studies have shown that the size of abrasives (third body particles) can have an adverse effect on the wear rate [104], [123].

In fact, smaller nano-sized particles (in wet conditions) may have favored a rolling effect which produces multiple indentations that scratch the passive film, while the larger nano-sized particles (in dry conditions) may have favored sliding which causes grooving abrasion [108]. This was observed from the BEC mode of the fretted surfaces and may have accounted for the smaller amount of material loss under wet conditions when compared to dry conditions. Therefore, the clinically relevant novel *sbf* favors the formation of a hydrodynamic lubrication film on the CoCrMo alloy with MoM implants.

5.4 Characteristics of passive film formed in *sbf* - Influence of passivation potential and passivation time

Passivation potential and passivation time have been established as influential on the nature and composition of passive films formed on active-passive metals [2]. However, in the presence of proteins and other clinically relevant synovial fluid components, their influence is still yet to be fully elucidated. The work of Hodgson *et al*. [89] showed that both passivation time and passivation potential change the composition and thickness of the film formed on a CoCrMo alloy in 0.14 M NaCl solution.

In resonance with the work of Hodgson et al., the results from this work show that in the presence of a more clinically relevant fluid environment, a higher passivation potential means stronger and more protective passive film formed. This is because the composition of chromium and molybdenum, a protective constituent of the passive film formed, is increased with passivation potential, and the composition of cobalt, a non-protective

constituent of the passive film, is reduced with passivation potential. It was also observed that even though the relative composition of the Cr (III) oxides and Cr (III) hydroxides depend on the applied potential, passivation time has no clear effect on the composition of the Cr cations measured. The similarity in composition of the cobalt, chromium and molybdenum measured at different passivation times is good confirmation of the spontaneity of the passive film formed on the CoCrMo alloy, making it suitable for use in biomedical applications.

5.5 Isolated contribution of wear and corrosion to fretting corrosion synergism in *sbf*

Optimized restoration of the hip joint has necessitated the introduction of modular hips [113]. However, the modular implants at the hips are exposed to variable loading conditions, so the issue of micro-motion at the modular head/stem and stem/neck interfaces has raised concerns related to the mechanically assisted corrosion of the CoCrMo alloy at these interfaces. Some of the previous research work have revealed that factors such as larger head size, amount of assembly force, material of the modular component, position of the center of the head to the center of the neck, etc. [113], [124]–[126] increase micro-motion which may have detrimental effects on the implant in service.

The results from the work in [127] shed more light on the extent of damage caused by the effect of micro-motion at these interfaces. The results showed that at a fretting displacement as low as 1 mm, there is up to a 300% increase in the ionic corrosion products that were released into the *sbf* lubricant. Under in-vivo conditions, the ions

released have been reported to travel into the surrounding tissues and organs within the body [127], thus causing adverse biological reactions. High concentrations of cobalt, chromium and molybdenum have been reported to lead to effects such as synovitis, periprosthetic bone loss, osteolysis and aseptic loosening of implants in the human body [128]. Clearly, the continuous increase in the active dissolution of cobalt under fretting conditions is accounted for by the continuous mechanical disruption of the passive film. In the absence of mechanical interaction, the nature of the protective passive film formed may have been more protective. This is because a higher concentration of Cr-ions may form a more protective passive film, thus allowing the formation of Cr_2O_3 to be easily attainable. Furthermore, there is no difference in the dissolution rate of molybdenum under both conditions. In fact, the measurements were below the detection limit at some of the measurement times. To this end, an increase in the ion release concentration in the presence of micro-motion makes it very important to design future implants against the causes of micro-motion.

6 CONCLUSION AND FUTURE WORK

6.1 Conclusion

Since the renewed interest of modular hip implants, the subject of corrosion and fretting corrosion at the head/neck and neck/stem interface of modular connections has been a source of concern to researchers and biomedical engineers. In CoCrMo alloy for example, ion and particle release due to micro-motion at these interfaces has been a major cause of adverse tissue reactions that leads to early revision surgery. Furthermore, a major limitation to the design of long lasting artificial hips is the proximity of the synthetic fluids used during testing and validation of these implants to the actual synovial fluid in the joint environment. However, by using a clinically relevant novel fluid, this study has made some progress towards the understanding of fundamental corrosion properties and fretting corrosion behavior of CoCrMo alloy in the human body environment.

In the approach here, a comparative study of the electrochemical behavior of the CoCrMo alloy in a more clinically relevant novel simulated body environment is made with some already existing synthesized fluids (0.14 M NaCl and PBS). The influence of implant immersion time, synovial fluid pH, and solution chemistry (composition) on the corrosion characteristics and fretting corrosion behavior of CoCrMo alloy implants in a more clinically relevant simulated body environment have been investigated and reported. Some important findings are summarized as follows.

6.1.1 Corrosion

- The presence of phosphate ions in solution increased the corrosion rate of CoCr alloy, confirming PBS as a more aggressive environment than in 0.14 M NaCl and *sbf* environments. This is because phosphate ions present in PBS adsorbed on the CoCrMo alloy and produced large species of di-hydrogen phosphate ions, a constituent conjugate base of phosphoric acid. This necessitated the increase in the active dissolution rate of the alloy. Conversely, the presence of proteins in the novel sbf impeded the effect of phosphate ions, hereby reducing the corrosion rate of CoCr alloy into more clinically relevant rates. Therefore, the presence of protein compound acted as an anodic inhibitor to the electrochemical reaction

- The formation of a passive film on CoCrMo depends on the exposure of the alloy to the lubricant environment. Although the CoCrMo alloy in *sbf* and 0.14 M NaCl shows low corrosion rates comparable to that in the human body environment, the nature of the surface film formed is different. The film composition and film formation kinetics in both solutions are different. Therefore, by using a more clinically relevant fluid, this work has experimentally characterized the most predictable passive layer comparable to the human body environment. The results from this work confirm that protein compounds and organometallic complexes in clinically relevant synovial fluids adsorb onto the surface of the material. Therefore, aside from its present value, the passive film identified will be valuable for future analysis of fretting corrosion behavior (modeling and experimental), of the CoCrMo alloy in the more clinically relevant simulated body environment,

provided the micro-motion at the modular interface is wide enough to allow exposure to the lubricant.

- As the exposure time of the CoCrMo alloy to all of the fluid environments increases, the OCPs are reduced to more stable passive potential values.

- In consideration of passivation at different applied potentials and passivation times, the nature of the passive film (film composition) formed is not different, although there is a difference in film thickness measured with passivation potentials.

- The solution chemistry modifies the passive film properties. This may have influence on the tribocorrosion behavior of the CoCrMo alloy in *sbf*s.

- In agreement with the literature, four distinct electrochemical regimes (cathodic, transition, passive and transpassive) characterize the electrochemical behavior of the CoCrMo alloy in all of the fluid environments.

- Although pH does not have serious effect on the passive potential range, the spontaneous passivation of the CoCrMo alloy is more easily attained at a pH of 7.4 than 4.0.

- The EIS studies suggest that the capacitive behavior of the passive film formed in *sbf* is different from films formed in other solution types. While all of the solutions show a capacitive nature, the *sbf* is diffusion controlled when compared

with NaCl. The XPS results confirm the EIS studies, and show different atomic and cationic factions of cobalt, chromium and molybdenum in their oxidized state.

6.1.2 Fretting corrosion

- This work shows that there is an increase in the ion release concentration during fretting, in regions where there is exposure to the synovial fluid. This finding makes it very important to focus the design of future implants against causes of micro-motion.

- Under optimized conditions in a clinically relevant fluid, a lubrication regime on the contact surface that can totally (or largely) minimize fretting damage at the head/neck and neck/stem interfaces of modular hips can be achieved in patients. This condition can reduce wear particle generation through mechanical damage. Therefore, findings from this work can be used to optimize the design of future implants, depending on the patient weight to achieve this separation.

- The size of third body particles generated influences the rate of volumetric wear loss on contacting surfaces. In dry conditions, third body particle size increases wear loss through surface abrasion and adhesion, while in wet conditions, they can be mechanically mixed with organometallic complexes, and form a solid lubricant that better freely rolls between contacting surfaces, thereby reducing damage to the implant surface. Furthermore, mechanically mixed wear nano-particles generated under wet conditions reduce the further dissolution of cobalt.

- Under dry conditions, the particles are generated by severe plastic deformation of the material surface, thus causing grain refinement and formation of smaller and finer grain sizes. The results from these findings will help to calibrate numerical models. This is because it gives a good understanding of what to expect during dry and wet fretting condition in a more clinically relevant human body environment.

- Some of the wear particles adhere between fretting surfaces. Under the dry condition, these particles flatten out and crack, thus forming smaller debris between both surfaces in contact.

- From physical observations, the contact surface suffers more damage in PoD testing under dry conditions when compared to wet conditions. Also, the wear area increases with number of cycles due to the flattening effect of the pin contact.

6.2 Future work

This work will serve as pioneer work for future tribocorrosion researchers. One major criterion for selecting a solution for the laboratory simulation of tribocorrosion experiments for biomedical application is a low corrosion rate comparable with the human body environment. However, only the use of the 'corrosion rate' can be misleading, because from this work, the CoCrMo alloy which exhibits a low corrosion rate in 0.14 M NaCl has a corrosion product (hence, nature of passive film formed) that is different from that of the CoCrMo alloy in *sbf*. Therefore, this work vividly shows that beyond the requirement of a low corrosion rate for experimental test conditions, there is

the cogent need to use a solution that will produce a more clinically relevant passive film. This is because in reality, during fretting in MoM implants, only the passive film formed is in direct contact, and not the substrate CoCrMo material itself. Therefore, by using a more clinically relevant fluid, this work has been able to confirm that the rate of corrosion of the CoCrMo alloy in the human body environment is low. The electrochemical performance of the fluid implies that this fluid can be successfully used in a simulating laboratory test environment that replicates the human body environment. Therefore, going forward, the following are recommended.

1. Modeling and simulation of fretting corrosion conditions to confirm the empirical data obtained from this experimental work can be carried out in future work.

2. Future study should focus on a design that totally eliminates or largely reduces micro-motion and head/stem and stem/neck interfaces of modular hip implants.

7 References

[1] S. R. Knight, R. Aujla, and S. P. Biswas, "Total Hip Arthroplasty - over 100 years of operative history," vol. 3, pp. 2–4, 2011.

[2] C. Valero Vidal and A. Igual Muñoz, "Electrochemical characterisation of biomedical alloys for surgical implants in simulated body fluids," *Corros. Sci.*, vol. 50, no. 7, pp. 1954–1961, Jul. 2008.

[3] A. I. Muñoz and S. Mischler, "Interactive Effects of Albumin and Phosphate Ions on the Corrosion of CoCrMo Implant Alloy," *J. Electrochem. Soc.*, vol. 154, no. 10, p. C562, 2007.

[4] R. Pourzal, I. Catelas, R. Theissmann, C. Kaddick, and a Fischer, "Characterization of Wear Particles Generated from CoCrMo Alloy under Sliding Wear Conditions.," *Wear*, vol. 271, no. 9–10, pp. 1658–1666, Jul. 2011.

[5] C. V. Vidal and A. I. Muñoz, "Effect of thermal treatment and applied potential on the electrochemical behaviour of CoCrMo biomedical alloy," *Electrochim. Acta*, vol. 54, no. 6, pp. 1798–1809, Feb. 2009.

[6] F. Contu, B. Elsener, and H. Böhni, "Corrosion behaviour of CoCrMo implant alloy during fretting in bovine serum," *Corros. Sci.*, vol. 47, no. 8, pp. 1863–1875, Aug. 2005.

[7] A. Ouerd, C. Alemany-Dumont, B. Normand, and S. Szunerits, "Reactivity of CoCrMo alloy in physiological medium: Electrochemical characterization of the

metal/protein interface," *Electrochim. Acta*, vol. 53, no. 13, pp. 4461–4469, May 2008.

[8] C. Valero Vidal and A. Igual Muñoz, "Effect of physico-chemical properties of simulated body fluids on the electrochemical behaviour of CoCrMo alloy," *Electrochim. Acta*, vol. 56, no. 24, pp. 8239–8248, Oct. 2011.

[9] Y. Yan, A. Neville, and D. Dowson, "Biotribocorrosion of CoCrMo orthopaedic implant materials—Assessing the formation and effect of the biofilm," *Tribol. Int.*, vol. 40, no. 10–12, pp. 1492–1499, Oct. 2007.

[10] I. Vucajnk and S. K. Fokter, "Modular Femoral Neck Fracture After Total Hip Arthroplasty, Recent Advances in Hip and Knee Arthroplasty," in *The Journal of arthroplasty*, vol. 28, no. 1, S. Fokter, Ed. Slovenia: InTech, 2012, pp. 196.e7–9.

[11] R. W.-W. Hsu, C.-C. Yang, C.-A. Huang, and Y.-S. Chen, "Electrochemical corrosion studies on Co–Cr–Mo implant alloy in biological solutions," *Mater. Chem. Phys.*, vol. 93, no. 2–3, pp. 531–538, Oct. 2005.

[12] L. E. S. Wong, "The Effect of Lubricant Composition on the Wear Behaviour of Polyethylene for Orthopaedic Applications By," University of Manitoba, 2013.

[13] V. K. Maskiewicz, P. A. Williams, S. J. Prates, J. G. Bowsher, and I. C. Clarke, "Characterization of protein degradation in serum-based lubricants during simulation wear testing of metal-on-metal hip prostheses.," *J. Biomed. Mater. Res. B. Appl. Biomater.*, vol. 94, no. 2, pp. 429–40, Aug. 2010.

[14] J. Brandt, "Wear and Boundary Lubrication in Modular Total Knee Replacements," University of Waterloo, 2008.

[15] J.-M. Brandt, L. K. Brière, J. Marr, S. J. MacDonald, R. B. Bourne, and J. B. Medley, "Biochemical comparisons of osteoarthritic human synovial fluid with calf sera used in knee simulator wear testing.," *J. Biomed. Mater. Res. A*, vol. 94, no. 3, pp. 961–71, Sep. 2010.

[16] M. J. Grimm, "Selection of Materials for Biomedical applications," in *Handbook of Materials Selection*, M. Kutz, Ed. John Wiley & Sons, inc., 2002, pp. 1165–1194.

[17] Y. Yan, "Corrosion and tribo-corrosion behaviour of metallic orthopaedic implant," The University of Leeds, 2006.

[18] S. M. Kurtz, E. Lau, K. Ong, K. Zhao, M. Kelly, and K. J. Bozic, "Future young patient demand for primary and revision joint replacement: national projections from 2010 to 2030.," *Clin. Orthop. Relat. Res.*, vol. 467, no. 10, pp. 2606–12, Oct. 2009.

[19] S. T. O. Brien, "Polyethylene Wear Modeling in Modular Total Knee Replacements using Finite Element," no. October, 2011.

[20] K. Vassiliou, S. C. Scholes, and A. Unsworth, "Laboratory studies on the tribology of hard bearing hip prostheses: ceramic on ceramic and metal on metal," *Proc. Inst. Mech. Eng. Part H J. Eng. Med.*, vol. 221, no. 1, pp. 11–20, Jan. 2007.

[21] P. F. Gomez and J. A. Morcuende, “Early attempts at hip arthroplasty--1700s to 1950s.,” *Iowa Orthop. J.*, vol. 25, pp. 25–9, Jan. 2005.

[22] N. Diomidis, S. Mischler, N. S. More, M. Roy, and S. N. Paul, “Fretting-corrosion behavior of β titanium alloys in simulated synovial fluid,” *Wear*, vol. 271, no. 7–8, pp. 1093–1102, Jul. 2011.

[23] C. N. Elias, J. H. C. Lima, R. Valiev, and M. A. Meyers, “Biomedical Applications of Titanium and its Alloys,” no. March, pp. 1–4, 2008.

[24] Mars G. Fontana, *corrosion engineering*, Third Edit. Singapore: McGraw-Hill Series, 1987.

[25] K. R. St John, L. D. Zardiackas, and R. A. Poggie, “Wear evaluation of cobalt-chromium alloy for use in a metal-on-metal hip prosthesis.,” *J. Biomed. Mater. Res. B. Appl. Biomater.*, vol. 68, no. 1, pp. 1–14, Jan. 2004.

[26] B. S. and B. J. D. Bolton, “production of porous sintered Co-Cr-Mo alloys for possible surgical implant applications Part 2 corrosion behaviour.pdf,” vol. 38, no. 4, p. 305, 1995.

[27] G. Bellefontaine, “The corrosion of CoCrMo alloys for biomedical applications,” University of Birmingham, 2010.

[28] B. D. Beake and T. W. Liskiewicz, “Comparison of nano-fretting and nano-scratch tests on biomedical materials,” *Tribol. Int.*, vol. 63, pp. 123–131, Jul. 2013.

[29] Y. Liao, R. Pourzal, M. A. Wimmer, J. J. Jacobs, A. Fischer, and L. D. Marks, "Graphitic tribological layers in metal-on-metal hip replacements," *Science (80-.).*, vol. 334, no. 6063, pp. 1687–1690, Dec. 2011.

[30] F. Lu, M. Royle, F. V Lali, A. J. Hart, S. Collins, J. Housden, and J. C. Shelton, "Simple isolation method for the bulk isolation of wear particles from metal on metal bearing surfaces generated in a hip simulator test.," *J. Mater. Sci. Mater. Med.*, vol. 23, no. 4, pp. 891–901, Apr. 2012.

[31] O. Sahin, A. R. Tuncdemir, H. A. Cetinkara, H. S. Guder, and E. Sahin, "Production and Mechanical Behaviour of Biomedical CoCrMo Alloy," *Chinese Phys. Lett.*, vol. 28, no. 12, p. 126201, Dec. 2011.

[32] S. Yang, "Cryogenic burnishing of Co-Cr-Mo Biomedical alloy for enhanced surface integrity and improved wear performance," University of Kentucky, 2012.

[33] J. A. Disegi, R. L. Kennedy, and R. Pilliar, "Cobalt-Base alloys for Biomedical Applications," 1999.

[34] A. M. Gilbert, Jeremy L; Sachin, *Medical Implant Corrosion : Electrochemistry at Metallic Biomaterial Surfaces*. Tel-Aviv: Springer, 2012, pp. 1–28.

[35] G. Manivasagam, D. Dhinasekaran, and A. Rajamanickam, "Biomedical Implants : Corrosion and its Prevention - A Review," no. i, pp. 40–54, 2010.

[36] D. Sun, J. A. Wharton, and R. J. K. Wood, "Effects of proteins and pH on tribocorrosion performance of cast CoCrMo – a combined electrochemical and

tribological study," *Tribol. - Mater. Surfaces Interfaces*, vol. 2, no. 3, pp. 150–160, Sep. 2008.

[37] H. Mishina and M. Kojima, "Changes in human serum albumin on arthroplasty frictional surfaces," *Wear*, vol. 265, no. 5–6, pp. 655–663, Aug. 2008.

[38] P. Schaaff, M. Dalmiglio, and U. Holzwarth, "Frequency effect in fretting wear of Co-28Cr-6Mo versus Ti-6Al-4V implant alloys.," *J. Biomed. Mater. Res. B. Appl. Biomater.*, vol. 77, no. 1, pp. 79–88, Apr. 2006.

[39] S. Virtanen, I. Milosev, E. Gomez-Barrena, R. Trebse, J. Salo, and Y. T. Konttinen, "Special modes of corrosion under physiological and simulated physiological conditions.," *Acta Biomater.*, vol. 4, no. 3, pp. 468–76, May 2008.

[40] B. Tritschler, B. Forest, and J. Rieu, "Fretting corrosion of materials for orthopaedic implants : a study of a metal / polymer contact in an artificial physiological medium," vol. 32, no. 1999, pp. 587–596, 2000.

[41] J. J. Noel, "The Electrochemistry of Titanium Corrosion," University of Manitoba, 1999.

[42] M. S. P. Sury, "Corrosion behaviour of cast and forged cobalt-based alloys for double-alloy joint endoprosthteses.pdf," *J. Biomed. Mater. Res.*, vol. 12, pp. 723–741, 1978.

[43] J. Dueck, G. Toews, S. Toth, and R. Road, "MECH 4860 Final Design Report : Modular Hip Joint Testing Apparatus," 2010.

[44] I. Garc, D. Drees, and J. P. Celis, “Corrosion-wear of passivating materials in sliding contacts based on a concept of active wear track area,” vol. 249, pp. 452–460, 2001.

[45] P. Panigrahi, “Corrosion Behavior of Solution- Annealed CoCrMo Medical Implant Alloys Corrosion Behavior of Solution-Annealed CoCrMo,” 2011.

[46] R. A. Antunes and M. C. L. de Oliveira, “Corrosion fatigue of biomedical metallic alloys: mechanisms and mitigation.,” *Acta Biomater.*, vol. 8, no. 3, pp. 937–62, Mar. 2012.

[47] E. Krasicka-Cydzik, Z. Oksiuta, and J. R. Dabrowski, “Corrosion testing of sintered samples made of the Co-Cr-Mo alloy for surgical applications.,” *J. Mater. Sci. Mater. Med.*, vol. 16, no. 3, pp. 197–202, Mar. 2005.

[48] A. Igual Muñoz and L. Casabán Julián, “Influence of electrochemical potential on the tribocorrosion behaviour of high carbon CoCrMo biomedical alloy in simulated body fluids by electrochemical impedance spectroscopy,” *Electrochim. Acta*, vol. 55, no. 19, pp. 5428–5439, Jul. 2010.

[49] F. Contu, B. Elsener, and H. Böhni, “Electrochemical Behavior of CoCrMo Alloy in the Active State in Acidic and Alkaline Buffered Solutions,” *J. Electrochem. Soc.*, vol. 150, no. 9, p. B419, 2003.

[50] Rabin Bandy, “Effect of Composition on the Electrochemical polarization behaviors and the oxide films of Orthopedic implant alloys.,” University of Manitoba, 1976.

[51] Y. Yan, A. Neville, and D. Dowson, “Tribo-corrosion properties of cobalt-based medical implant alloys in simulated biological environments,” *Wear*, vol. 263, no. 7–12, pp. 1105–1111, Sep. 2007.

[52] F. Contu, B. Elsener, and H. Böhni, “Characterization of implant materials in fetal bovine serum and sodium sulfate by electrochemical impedance spectroscopy. I. Mechanically polished samples.,” *J. Biomed. Mater. Res.*, vol. 62, no. 3, pp. 412–21, Dec. 2002.

[53] M. T. Runa, M. J. Rocha, L. A. Mathew, “Corrosion and tribocorrosion behavior of CoCrMo alloys used as hip joint implant materials under simulated body fluids: effect of proteins and noomal load,” in *1st Portuguese meeting in Bioengineering*, 2011, no. February.

[54] C. Duong, S. Park, and A. S. Preparation, “Tribological Response of Cobalt-Chromium Femoral Head under Lubrication of Bovine Serum Albumin,” pp. 243–246, 2010.

[55] M. A. Wimmer, J. Loos, R. Nassutt, M. Heitkemper, and A. Fischer, “The acting wear mechanisms on metal-on-metal hip joint bearings : in vitro results,” vol. 250, pp. 129–139, 2001.

[56] A. Sargeant and T. Goswami, “Hip implants: Paper V. Physiological effects,” *Mater. Des.*, vol. 27, no. 4, pp. 287–307, Jan. 2006.

[57] I. Leslie, S. Williams, C. Brown, G. Isaac, Z. Jin, E. Ingham, and J. Fisher, “Effect of bearing size on the long-term wear, wear debris, and ion levels of large diameter metal-on-metal hip replacements-An in vitro study.,” *J. Biomed. Mater. Res. B. Appl. Biomater.*, vol. 87, no. 1, pp. 163–72, Oct. 2008.

[58] M. Bjorling, “Friction in Elasto Hydrodynamically Lubricated contacts - The influence of speed and slide to roll ratio,” Lulea University of Technology.

[59] F. Billi, P. Benya, E. Ebramzadeh, P. Campbell, F. Chan, and H. a. McKellop, “Metal wear particles: What we know, what we do not know, and why,” *SAS J.*, vol. 3, no. 4, pp. 133–142, Dec. 2009.

[60] S. B. Goodman, T. Ma, R. Chiu, R. Ramachandran, and R. L. Smith, “Effects of orthopaedic wear particles on osteoprogenitor cells.,” *Biomaterials*, vol. 27, no. 36, pp. 6096–101, Dec. 2006.

[61] J. J. Jacobs, N. J. Hallab, R. M. Urban, and M. a Wimmer, “Wear particles.,” *J. Bone Joint Surg. Am.*, vol. 88 Suppl 2, pp. 99–102, Apr. 2006.

[62] M. T. Mathew, P. Srinivasa Pai, R. Pourzal, A. Fischer, and M. A. Wimmer, “Significance of Tribocorrosion in Biomedical Applications: Overview and Current Status,” *Adv. Tribol.*, vol. 2009, pp. 1–12, 2009.

[63] S. Mischler and A. I. Muñoz, “Wear of CoCrMo alloys used in metal-on-metal hip joints: A tribocorrosion appraisal,” *Wear*, vol. 297, no. 1–2, pp. 1081–1094, Jan. 2013.

[64] J. Jiang, M. M. Stack, and A. Neville, “Modelling the tribo-corrosion interaction in aqueous sliding conditions,” *Tribol. Int.*, vol. 35, no. 10, pp. 669–679, 2002.

[65] P. Ponthiaux, F. Wenger, D. Drees, and J. P. Celis, “Electrochemical techniques for studying tribocorrosion processes,” *Wear*, vol. 256, no. 5, pp. 459–468, Mar. 2004.

[66] M. T. Mathew, J. J. Jacobs, and M. A. Wimmer, “Wear-corrosion synergism in a CoCrMo hip bearing alloy is influenced by proteins.,” *Clin. Orthop. Relat. Res.*, vol. 470, no. 11, pp. 3109–17, Nov. 2012.

[67] M. Azzi and J. A. Szpunar, “Tribo-electrochemical technique for studying tribocorrosion behavior of biomaterials.,” *Biomol. Eng.*, vol. 24, no. 5, pp. 443–6, Nov. 2007.

[68] D. Shakhvorostov, B. Gleising, R. Büscher, W. Dudzinski, A. Fischer, and M. Scherge, “Microstructure of tribologically induced nanolayers produced at ultra-low wear rates,” *Wear*, vol. 263, no. 7–12, pp. 1259–1265, Sep. 2007.

[69] A. Salinas-Rodriguez and J. L. Rodriguez-Galicia, “Deformation behavior of low-carbon Co-Cr-Mo alloys for low-friction implant applications.,” *J. Biomed. Mater. Res.*, vol. 31, no. 3, pp. 409–19, Jul. 1996.

[70] R. J. K. Wood, D. Sun, M. R. Thakare, A. De Frutos Rozas, and J. A. Wharton, "Interpretation of electrochemical measurements made during micro-scale abrasion-corrosion," *Tribol. Int.*, vol. 43, no. 7, pp. 1218–1227, Jul. 2010.

[71] S. S. W. Barry C. Strett, "An electrochemical investigation of fretting corrosion of surgical implant materials.pdf," vol. 34, no. 11, pp. 379–386, 1978.

[72] N. Diomidis, S. Mischler, N. S. More, and M. Roy, "Tribo-electrochemical characterization of metallic biomaterials for total joint replacement.," *Acta Biomater.*, vol. 8, no. 2, pp. 852–9, Feb. 2012.

[73] E. Ingham and J. Fisher, "Biological reactions to wear debris in total joint replacement," *Proc. Inst. Mech. Eng. Part H J. Eng. Med.*, vol. 214, no. 1, pp. 21–37, Jan. 2000.

[74] I. Catelas and M. A. Wimmer, "New insights into wear and biological effects of metal-on-metal bearings.," *J. Bone Joint Surg. Am.*, vol. 93 Suppl 2, pp. 76–83, May 2011.

[75] J. H. Dumbleton and M. T. Manley, "Metal-on-Metal Total Hip Replacement," *J. Arthroplasty*, vol. 20, no. 2, pp. 174–188, Feb. 2005.

[76] M. Expression, O. F. Inducible, and N. Oxide, "ASEPTIC LOOSENING OF TOTAL HIP REPLACEMENT," pp. 467–474.

[77] R. L. S. Stuart B. Goodman, Martin Lind, Yong Song, “IN vitro, in vivo, and tissue retrieval studies on particle debris.pdf,” *Clin. Orthop. Relat. Res.*, vol. 352, pp. 25–34, 1998.

[78] K. De Smet, R. De Haan, A. Calistri, P. A. Campbell, E. Ebramzadeh, C. Pattyn, and H. S. Gill, “Metal ion measurement as a diagnostic tool to identify problems with metal-on-metal hip resurfacing.,” *J. Bone Joint Surg. Am.*, vol. 90 Suppl 4, pp. 202–8, Nov. 2008.

[79] Y. Yan, D. Dowson, and A. Neville, “In-situ electrochemical study of interaction of tribology and corrosion in artificial hip prosthesis simulators.,” *J. Mech. Behav. Biomed. Mater.*, vol. 18, pp. 191–9, Feb. 2013.

[80] D. R. Haynes, T. N. Crotti, and M. R. Haywood, “Corrosion of and changes in biological effects of cobalt chrome alloy and 316L stainless steel prosthetic particles with age.,” *J. Biomed. Mater. Res.*, vol. 49, no. 2, pp. 167–175, 2000.

[81] S. Urgery, I. Ncorporated, H. J. Cooper, C. J. Della Valle, R. A. Berger, M. Tetreault, W. G. Paprosky, S. M. Sporer, and J. J. Jacobs, “Corrosion at the Head-Neck Taper as a Cause,” pp. 1–7, 2012.

[82] B. Mathiesen, J. Urban, P. Reinholt, and A. Blomgren, “Corrosion of Modular Hip Prostheses,” vol. 73, no. 4, pp. 569–575, 1991.

[83] M. H. Huo, K. G. Stockton, M. A. Mont, and J. Parvizi, “What’s new in total hip arthroplasty.,” *J. Bone Joint Surg. Am.*, vol. 92, no. 18, pp. 2959–72, Dec. 2010.

[84] T. J. Joyce, D. J. Langton, and A. V. F. Nargol, “A study of the wear of explanted metal-on-metal resurfacing hip prostheses,” *Tribol. Int.*, vol. 44, no. 5, pp. 517–522, May 2011.

[85] A. W. Hodgson, S. Mischler, B. Von Rechenberg, and S. Virtanen, “An analysis of the in vivo deterioration of Co-Cr-Mo implants through wear and corrosion,” *Proc. Inst. Mech. Eng. Part H J. Eng. Med.*, vol. 221, no. 3, pp. 291–303, Jan. 2007.

[86] S. Mischler, A. W. Hodgson, and S. Virtanen, “In Vivo Degradation of CoCrMo Implants : Analysis of Corrosion and Wear,” pp. 1–7.

[87] A. Choubey, B. Basu, and R. Balasubramaniam, “Tribological behaviour of Ti-based alloys in simulated body fluid solution at fretting contacts,” *Mater. Sci. Eng. A*, vol. 379, no. 1–2, pp. 234–239, Aug. 2004.

[88] M. Metikos-Huković, Z. Pilić, R. Babić, and D. Omanović, “Influence of alloying elements on the corrosion stability of CoCrMo implant alloy in Hank’s solution.,” *Acta Biomater.*, vol. 2, no. 6, pp. 693–700, Nov. 2006.

[89] A. W. E. Hodgson, S. Kurz, S. Virtanen, V. Fervel, C.-O. A. Olsson, and S. Mischler, “Passive and transpassive behaviour of CoCrMo in simulated biological solutions,” *Electrochim. Acta*, vol. 49, no. 13, pp. 2167–2178, May 2004.

[90] A. C. Lewis, M. R. Kilburn, I. Papageorgiou, G. C. Allen, and C. P. Case, “Effect of synovial fluid, phosphate-buffered saline solution, and water on the dissolution and corrosion properties of CoCrMo alloys as used in orthopedic implants.,”

Journal of biomedical materials research. Part A, vol. 73, no. 4. pp. 456–67, 15-Jun-2005.

[91] Y. Yan, A. Neville, and D. Dowson, "Understanding the role of corrosion in the degradation of metal-on-metal implants," *Proc. Inst. Mech. Eng. Part H J. Eng. Med.*, vol. 220, no. 2, pp. 173–180, Jan. 2006.

[92] Y. Yan, A. Neville, and D. Dowson, "Biotribocorrosion—an appraisal of the time dependence of wear and corrosion interactions: II. Surface analysis," *J. Phys. D. Appl. Phys.*, vol. 39, no. 15, pp. 3206–3212, Aug. 2006.

[93] Y. Yan, A. Neville, and D. Dowson, "Biotribocorrosion—an appraisal of the time dependence of wear and corrosion interactions: I. The role of corrosion," *J. Phys. D. Appl. Phys.*, vol. 39, no. 15, pp. 3200–3205, Aug. 2006.

[94] C. Myant, R. Underwood, J. Fan, and P. M. Cann, "Lubrication of metal-on-metal hip joints: the effect of protein content and load on film formation and wear.," *J. Mech. Behav. Biomed. Mater.*, vol. 6, pp. 30–40, Feb. 2012.

[95] M. T. Mathew, M. J. Runa, M. Laurent, J. J. Jacobs, L. a Rocha, and M. a Wimmer, "Tribocorrosion behavior of CoCrMo alloy for hip prosthesis as a function of loads: a comparison between two testing systems.," *Wear*, vol. 271, no. 9–10, pp. 1210–1219, Jul. 2011.

[96] R. A. Gil and A. I. Muñoz, "Influence of the sliding velocity and the applied potential on the corrosion and wear behavior of HC CoCrMo biomedical alloy in

simulated body fluids.," *J. Mech. Behav. Biomed. Mater.*, vol. 4, no. 8, pp. 2090–102, Nov. 2011.

[97] A. C. Lewis and P. J. Heard, "The effects of calcium phosphate deposition upon corrosion of CoCr alloys and the potential for implant failure.," *J. Biomed. Mater. Res. A*, vol. 75, no. 2, pp. 365–73, Nov. 2005.

[98] R. Dyrkacz, J. Brandt, O. Ojo, T. Turgeon, and U. Wyss, "The Influence of Head Size on Corrosion and Fretting Behavior at the Head-Neck Interface of Artificial Hip Joints," 2012.

[99] C. G. Figueiredo-Pina, A. A. M. Neves, and B. M. B. Das Neves, "Corrosion-wear evaluation of a UHMWPE/Co–Cr couple in sliding contact under relatively low contact stress in physiological saline solution," *Wear*, vol. 271, no. 5–6, pp. 665–670, Jun. 2011.

[100] C. Valero Vidal and A. Igual Muñoz, "Study of the adsorption process of bovine serum albumin on passivated surfaces of CoCrMo biomedical alloy," *Electrochim. Acta*, vol. 55, no. 28, pp. 8445–8452, Dec. 2010.

[101] Y. Yan, A. Neville, D. Dowson, and S. Williams, "Tribocorrosion in implants—assessing high carbon and low carbon Co–Cr–Mo alloys by in situ electrochemical measurements," *Tribol. Int.*, vol. 39, no. 12, pp. 1509–1517, Dec. 2006.

[102] D. Dowson and Z.-M. Jin, "Metal-on-metal hip joint tribology," *Proc. Inst. Mech. Eng. Part H J. Eng. Med.*, vol. 220, no. 2, pp. 107–118, Jan. 2006.

[103] J. Hesketh, X. Hu, Y. Yan, D. Dowson, and A. Neville, “Biotribocorrosion: Some electrochemical observations from an instrumented hip joint simulator,” *Tribol. Int.*, vol. 59, pp. 332–338, Mar. 2013.

[104] Y. Yan, a. Neville, D. Dowson, S. Williams, and J. Fisher, “Effect of metallic nanoparticles on the biotribocorrosion behaviour of Metal-on-Metal hip prostheses,” *Wear*, vol. 267, no. 5–8, pp. 683–688, Jun. 2009.

[105] C. Brown, S. Williams, J. L. Tipper, J. Fisher, and E. Ingham, “Characterisation of wear particles produced by metal on metal and ceramic on metal hip prostheses under standard and microseparation simulation.,” *J. Mater. Sci. Mater. Med.*, vol. 18, no. 5, pp. 819–27, May 2007.

[106] I. Catelas, J. B. Medley, P. A. Campbell, O. L. Huk, and J. D. Bobyn, “Comparison of in vitro with in vivo characteristics of wear particles from metal-metal hip implants.,” *J. Biomed. Mater. Res. B. Appl. Biomater.*, vol. 70, no. 2, pp. 167–78, Aug. 2004.

[107] S. Dan, “Abrasion-corrosion of Cast CoCrMo in simulted Hip Joint Environments,” University of Southampton, 2009.

[108] P. E. Sinnett-Jones, J. A. Wharton, and R. J. K. Wood, “Micro-abrasion–corrosion of a CoCrMo alloy in simulated artificial hip joint environments,” *Wear*, vol. 259, no. 7–12, pp. 898–909, Jul. 2005.

[109] R. Büscher and A. Fischer, “The pathways of dynamic recrystallization in all-metal hip joints,” *Wear*, vol. 259, no. 7–12, pp. 887–897, Jul. 2005.

[110] R. Pourzal, R. Theissmann, S. Williams, B. Gleising, J. Fisher, and A. Fischer, “Subsurface changes of a MoM hip implant below different contact zones.,” *J. Mech. Behav. Biomed. Mater.*, vol. 2, no. 2, pp. 186–91, Apr. 2009.

[111] R. Pourzal, R. Theissmann, M. Morlock, and A. Fischer, “Micro-structural alterations within different areas of articulating surfaces of a metal-on-metal hip resurfacing system,” vol. 267, pp. 689–694, 2009.

[112] D. Sun, J. A. Wharton, and R. J. K. Wood, “Micro- and Nano-scale Tribo-Corrosion of Cast CoCrMo,” *Tribol. Lett.*, vol. 41, no. 3, pp. 525–533, Feb. 2011.

[113] M. Baxmann, S. Y. Jauch, C. Schilling, W. Blömer, T. M. Grupp, and M. M. Morlock, “The influence of contact conditions and micromotions on the fretting behavior of modular titanium alloy taper connections.,” *Med. Eng. Phys.*, vol. 35, no. 5, pp. 676–83; discussion 676, May 2013.

[114] Y. Yan, A. Neville, D. Dowson, S. Williams, and J. Fisher, “The influence of swing phase load on the electrochemical response, friction, and ion release of metal-on-metal hip prostheses in a friction simulator,” *Proc. Inst. Mech. Eng. Part J J. Eng. Tribol.*, vol. 223, no. 3, pp. 303–309, May 2009.

[115] A. Fischer, “Subsurface microstructural alterations during sliding wear of biomedical metals. Modelling and experimental results,” *Comput. Mater. Sci.*, vol. 46, no. 3, pp. 586–590, Sep. 2009.

[116] M. A. Wimmer, C. Sprecher, R. Hauert, G. Täger, and A. Fischer, “Tribochemical reaction on metal-on-metal hip joint bearings,” *Wear*, vol. 255, no. 7–12, pp. 1007–1014, Aug. 2003.

[117] M. Scherge, J. M. Martin, and K. Pöhlmann, “Characterization of wear debris of systems operated under low wear-rate conditions,” *Wear*, vol. 260, no. 4–5, pp. 458–461, Feb. 2006.

[118] M. Scherge, “Structure and mechanical properties of tribologically induced nanolayers,” vol. 260, pp. 433–437, 2006.

[119] Y. Liao, E. Hoffman, M. Wimmer, A. Fischer, J. Jacobs, and L. Marks, “CoCrMo metal-on-metal hip replacements.,” *Phys. Chem. Chem. Phys.*, vol. 15, no. 3, pp. 746–56, Jan. 2013.

[120] F. Billi, S. N. Sangiorgio, S. Aust, and E. Ebramzadeh, “Material and surface factors influencing backside fretting wear in total knee replacement tibial components.,” *J. Biomech.*, vol. 43, no. 7, pp. 1310–5, May 2010.

[121] A. Fischer, S. Weiss, and M. A. Wimmer, “The tribological difference between biomedical steels and CoCrMo-alloys.,” *J. Mech. Behav. Biomed. Mater.*, vol. 9, pp. 50–62, May 2012.

[122] D. Sun, J. A. Wharton, and R. J. K. Wood, “Micro-abrasion mechanisms of cast CoCrMo in simulated body fluids,” *Wear*, vol. 267, no. 11, pp. 1845–1855, Oct. 2009.

[123] D. Sun, J. A. Wharton, and R. J. K. Wood, “Micro-abrasion–corrosion of cast CoCrMo—Effects of micron and sub-micron sized abrasives,” *Wear*, vol. 267, no. 1–4, pp. 52–60, Jun. 2009.

[124] D. J. Langton, R. Sidaginamale, J. K. Lord, A. V. F. Nargol, and T. J. Joyce, “Taper junction failure in large-diameter metal-on-metal bearings.,” *Bone Joint Res.*, vol. 1, no. 4, pp. 56–63, Apr. 2012.

[125] J. S. Kawalec, S. A. Brown, J. H. Payer, and K. Merritt, “Mixed-metal fretting corrosion of Ti6Al4V and wrought cobalt alloy.,” *Journal of biomedical materials research*, vol. 29, no. 7. pp. 867–73, Jul-1995.

[126] V. Swaminathan and J. L. Gilbert, “Fretting corrosion of CoCrMo and Ti6Al4V interfaces.,” *Biomaterials*, vol. 33, no. 22, pp. 5487–503, Aug. 2012.

[127] B. W. Cunningham, “Basic scientific considerations in total disc arthroplasty.,” *Spine J.*, vol. 4, no. 6 Suppl, p. 219S–230S, 2004.

[128] S. C. Scholes and A. Unsworth, “The tribology of metal-on-metal total hip replacements,” *Proc. Inst. Mech. Eng. Part H J. Eng. Med.*, vol. 220, no. 2, pp. 183–194, Jan. 2006.